Università degli Studi di Cagliari

DOTTORATO DI RICERCA

INGEGNERIA ELETTRONICA ED INFORMATICA

Ciclo XXVII

TITOLO TESI

WIDEBAND DIGITAL INSTRUMENTATION FOR THE ITALIAN RADIO TELESCOPES

Settore/i scientifico disciplinari di afferenza

ING-INF/01 ELETTRONICA

Presentata da: ANDREA MELIS

Coordinatore Dottorato FABIO ROLI

Tutor MASSIMO BARBARO

Esame finale anno accademico 2014 – 2015

Ph.D. in Electronic and Computer Engineering
Dept. of Electrical and Electronic Engineering
University of Cagliari

Wideband digital instrumentation for the Italian radio telescopes

Andrea Melis

Advisor: Prof. Massimo Barbaro
Curriculum: ING-INF/01 Elettronica

XXVII Cycle
March 2016

Ph.D. in Electronic and Computer Engineering
Dept. of Electrical and Electronic Engineering
University of Cagliari

Wideband digital instrumentation for the Italian radio telescopes

Andrea Melis

Advisor: Prof. Massimo Barbaro
Curriculum: ING-INF/01 Elettronica

XXVII Cycle
March 2016

Dedicated to My Family

Abstract

Italy has a key role in the radio astronomical international context thanks to large collaborations like the VLBI (Very Long Baseline Interferometry) in which all three radio telescopes (Sardinia, Medicina, Noto) are deeply involved.

However, also the single dish activity represents a great opportunity to understand the fundamental laws of nature in the Universe.

Usually, in the past, ad-hoc digital backends were developed for each particular scientific goal; however, although highly optimised, they very often do not keep up with the times. In addition to the absent versatility even if based on reconfigurable FPGA-based hardware, the major issue why digital backends are often obsolete - even before they can be fully exploited - is the very long time necessary to make them integrated into the software controlling the radio telescope.

In this thesis, a different approach - both regarding hardware and software - has been developed to overcome aforementioned drawbacks and is described here. The unprecedented achieved scientific results are presented in different fields (imaging, polarimetry, spectroscopy, pulsars), and confirm the forcefulness of the adopted solution. The versatility of the proposed infrastructure also allows us the development of innovative spectrometers, which are able to meet the main requirements astronomers asking us: wide-bandwidth, high-spectral resolution and an uniform passband response (namely, no spectral "holes"). Finally, we describe an innovative infrastructure for the SETI (Search for ExtraTerrestrial Intelligence) international program. In particular, the KLT (Kahrunen-Loeve Transform) has been investigated together with the FFT approach usually adopted.

Acknowledgements

First of all I wish to thank Massimo Barbaro for giving me this important opportunity. Several people helped me during these years: a big thank you to Raimondo for the priceless collaboration during each step of this thesis. More generally, I say thanks to all people that, in one form or another, have made this possible: all of my colleagues (technological, scientific and admin people) in particular and, above all, Andrea Possenti for the trust given to me.

A special thanks to the Autonomous Region of Sardinia (RAS) that have been funded the project - on which this thesis is based - "High resolution sampling of the Universe in the radio band: an unprecedented instrument to understand the fundamental laws of nature" - P. I. of the project Andrea Possenti - in the context of the research project CRP-49231 (year 2011).

Contents

List of Figures

List of Tables

The development of the SARDARA back-end has been funded by the Autonomous Region of Sardinia (RAS) using resources from the Regional Law 7/2007 "Promotion of the scientific research and technological innovation in Sardinia" in the context of the research project CRP-49231 (year 2011): "High resolution sampling of the Universe in the radio band: an unprecedented instrument to understand the fundamental laws of nature"

P.I. of the project: Dr. Andrea Possenti

Chapter 1

Introduction

1.1 Radio astronomy

Radio astronomy is a science that studies the electromagnetic radiation emitted by celestial objects. Galaxies, quasars, stars - both at the beginning and at the end of their lives - as well as gaseous nebulae, could emit radio waves due to various natural processes. Radio waves of cosmic origin were detected for the first time in the 1930's by Karl Jansky, an engineer of the Bell Telephone Co., who, while studying the reason for radio interferences present in transatlantic radiophone transmissions, noticed a weak signal coming from the Milky Way: radio astronomy was then born.

The radio band is arbitrarily defined in the following frequency range: 30 KHz - 2 THz. However, only a portion of that spectrum is able to go through the Earth's atmosphere, so that only the interval 3 MHz - 900 GHz can be studied with instrumentation placed on the ground. Besides, by getting up close to the millimeter emission (approximately 100 GHz), dry days are imperative due to CO_2 and water vapor present in the atmosphere; indeed, they both absorb electromagnetic radiation in different quantities. This is why, in order to observe at this frequency interval, new telescopes are placed at high altitudes, in deserts or arid areas.

Astronomical sources emit radiation closely related to the physical mechanism in place. The emitted radiation can be quantified using the concept of brightness. The brightness $B(\nu, T)$ is defined as the received power per unit of frequency, of receiving surface and of solid angle subtended by the source. In the case of thermal emission, the brightness depends on the temperature of the material that emits via the Planck law. In the Rayleigh-Jeans approximation ($h\nu << K_B T$), the temperature T is directly proportional to the brightness:

$$B(\nu, T) = \frac{(2k_B T \nu^2)}{(c^2)} \tag{1.1}$$

Equation (1.1) is used as a convention to express the source's radiation in terms of temperature. Indeed, in all physical processes that rule the radiation's emission and the frequencies at work is, the emitted energy is provided in terms of brightness's temperature T_B:

$$T_B = \frac{(c^2 B)}{(2K_B \nu^2)} \tag{1.2}$$

Generally speaking, T_B is not the physical temperature of the emitting source, unless it is a black body that satisfies the Rayleigh-Jeans approxymation. The brightness over the entire solid angle, once integrated, provides the flux density. The unit of measure of brightness is the Jansky (Jy). For of a generic source with brightness $B(\nu, T)$, an antenna that subtends a solid angle Ω_A, with effective area A_e and bandwidth Δ_ν, receives the following power:

$$W_r = \frac{1}{2A_e B \Delta_\nu \omega_A} \tag{1.3}$$

The same power, in terms of antenna temperature T_A ,is defined as follows:

$$W_r = K_B T_A \Delta_\nu \tag{1.4}$$

Hence, the equivalent antenna temperature T_A emitted by a source is:

$$T_A = \frac{1}{2K_B} A_e B \Omega_A \tag{1.5}$$

Likewise, we can define the antenna temperature T'_A as the unwanted power produced by both the ground and the atmosphere, and the noise temperature of the receiver T_R as the signal equivalent to the noise of the entire receiver generated by electronic devices (active and passive) without any source. Since the two noises are uncorrelated, the sum of the two temperatures T'_A and T_R provides the total power measured in absence of astronomical signals, i. e. the so called "Temperature of the System", often abreviated as "Tsys".

1.2 Radio telescopes

The instrument necessary for studying the weak radio waves coming from the universe is called a radio telescope. Radio telescopes can be placed on the ground or, much alternately, can be sent into space. Clearly, the latter must be much smaller and have unavoidable limitations concerning sensibility and longevity; however, they are able to overcome the aforementioned effects due to the atmosphere; therefore, they can be employed for highest frequency observations. In this thesis, we are only dealing with radio telescopes on the ground, the Sardinia Radio Telescope in particular, thus we focus on them.

Almost always, a radio telescope is a paraboloid that differs from a traditional domestic satellite antenna in its largest dimension. A radio telescope, simplifying as much as possible, is made of three main parts: antenna, front end and back end. Figure 1.1 illustrates all three.

1.2.1 Antenna

The antenna collects the radio waves coming from the cosmos and converts them into an electrical signal. The paraboloid, made of reflectors metal, is named "primary mirror" or main dish. It is composed of several panels that are properly aligned; this is a crucial issue, especially for high-frequency observations. Furthermore, the greater the dish, the greater the inevitable deformation due to its weight, to gravitational effects, to thermal expansion as well as wind effects. We can mitigate these issues by building larger radio telescopes with an "active" surface, where the panels can be properly moved by electromechanical actuators so as to correct the aforementioned effects in real time. Radio telescope must be as big as possible because the angular resolution that can be reached by a single antenna depends

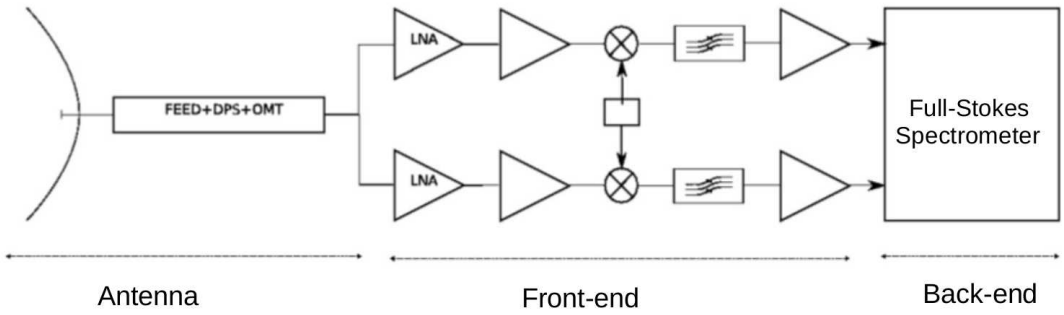

Figure 1.1: *Block diagram of a telescope.*

on it. We can define θ as the minimum angular separation between two sources that can be distinguished by the telescope; in accordance with the ondulatory theory, θ is defined as follows:

$$\theta = 1.22\frac{\lambda}{D} \tag{1.6}$$

The diameter of the dish D is limited from a technical point of view (for instance, the largest fully steerable radio telescope in the world has a diameter of 101 meters) therefore, to obtain a better angular resolution, an interferometric system is needed. Another important parameter is the antenna gain G defined as follows:

$$G = 10^{-26} m\eta_A \frac{A_g}{K_B} \tag{1.7}$$

where K_B is the Boltzman constant, A_g is the collecting area of the antenna (also called geometric aperture), η_A is the aperture's efficiency defined as the ratio between A_e and A_g. m has a value of 0.5 because we are considering only a single polarization. The signal goes through three different components: the $Feed$, the DPS (Differential Phase Shifter) and the OMT (OrthoMode Transducer). The feed is a transducer from the electromagnetic wave propagating in space to a guided wave that passes through a waveguide. One of the most common configurations uses a furrowed, highly-directive circular horn, with a very symmetrical main lobe and the capability of receiving two states of orthogonal polarization with a low cross-talk. The DPS is a component that transforms a circular polarization state into a linear one by introducing a $\lambda/4$ delay compared to the other one. As a consequence, the output of the device (see fig. 1.2) consists of two linear components along N and P, phased between them along the two device's diagonals, L and R respectively.

Finally, the OMT separates the two orthogonal components provided by the DPS and sends them into two different waveguides L and R, as shown in fig. 1.3:

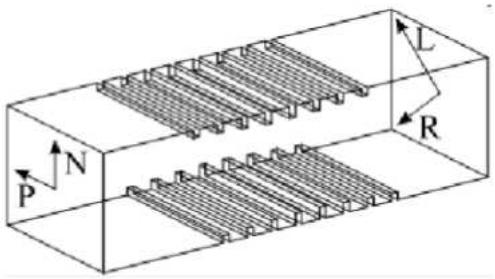

Figure 1.2: *Diffential Phase Shifter.*

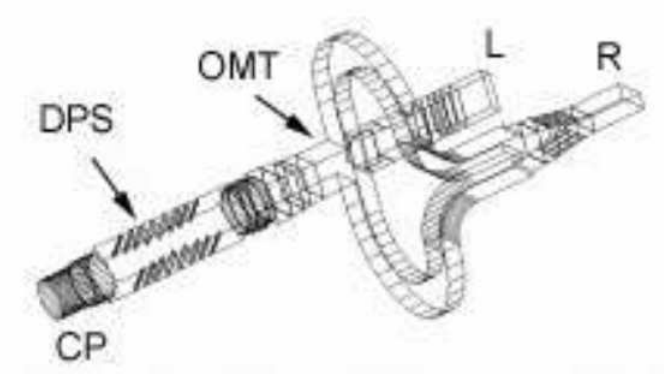

Figure 1.3: *Orthogonal Mode Transducer.*

1.2.2 Front-end

The front-end block has the role of amplifying, moving in frequency and then filtering two electrical signals provided by the OMT. Figure 1.4 shows a standard front-end:

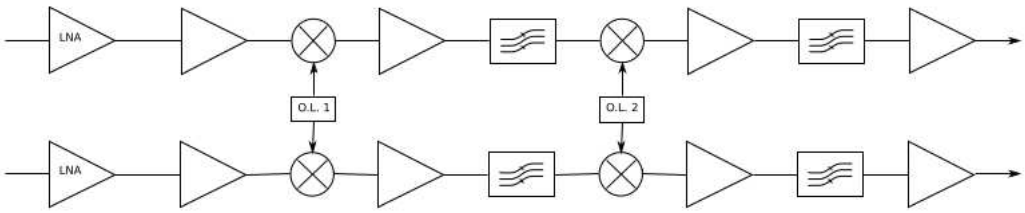

Figure 1.4: *Front-end.*

The first stage is a Low Noise Amplifier (LNA), namely an element with high gain and low noise in the passband: it is undoubtedly the most important component of the entire receiving chain. Other amplifiers (white triangles in fig. 1.4) are placed in the chain. In the modern receivers, both the components in waveguide and the LNAs are cryogenically cooled at roughly 10 Kelvin. As a consequence, receiver temperatures have usually levels up to ten times the quantistical level defined as $T_q = h\nu/k_B$, which indicates a high sensibility. One or

more synthesizers are used as local oscillators (O.L. 1 and O.L. 2 in figure 1.4); the signal can be beaten with a proper sinusoidal tone so as to move it up to base-band, i. e. the spectrum's portion from 0 (DC component) and the maximum desired frequency.

1.2.3 Back-end

Finally, once properly conditioned by previous blocks, the signal can be converted into digital format and then processed in order to provide the data in a convenient format for later studies. Depending on the nature of the received radiation, different backends allow the measurements of the received power as function of time, frequency and the eventual polarization's state. The first "spectral" instrument adopted in radio astronomy was the analog filter bank; it consists in a set of adjacents analog pass-band filters. Although the functioning may appears simple, such a system is complicated especially for the required accuracy of each filter; moreover, the major drawback is the fixed passband and resolution. In order to improve the latter ones, we use digital autocorrelators: in this case, both bandwidth and resolution can vary with the sampling time of the signal. The autocorrelation of a generic radio signal $v(t)$ is defined as follows:

$$R_v(\tau) = \int_{-\infty}^{+\infty} v(t-\tau)v(\tau)dt \tag{1.8}$$

and the Fourier Transform of the (1.8) provides the power spectrum. According to the Wiener-Khinchin theorem, the power spectrum is defined as follows:

$$S_v(\tau) = \int_{-\infty}^{+\infty} R_v(\tau)e^{-2\pi i v\tau}d\tau \tag{1.9}$$

With the advent of digital circuits and in particular reconfigurable devices like FPGAs (Field Programmable Gate Arrays), the Fourier Transform can be directly calculated implementing spectrometers based on the FFT (Fast Fourier Transform) on segments of the signal $v(t)$:

$$V(v) = \int_0^T v(t)e^{-2\pi i v\tau}dt \tag{1.10}$$

The (1.10) allows the proper calculation of the spectral density:

$$S(v) = V(v)V(v)^* \tag{1.11}$$

Moreover, if we also calculate the cross-correlation between orthogonally-polarized signals, we achieve a complete reconstruction of the signal's polarization as a function of the frequency.

Depending on the emission mechanism and on the type of observation the astronomer wishes to do, dedicated signal processing systems are required. In a very general way, observations made with a radio telescope are for studying emission in continuum, spectral line, spectropolarimetry and pulsars. The continuum studies regarding broadband emission are used to characterize the physical condition of the emitting region. Such an emission can be either due to thermal sources (thermal motion of source's particles) or nonthermal ones; the most probable, in this latter case, is the so called "synchrotron emission". Spectral lines studies regard narrow-band emission, in most cases when a particular molecule changes

its energy level. In this case, the molecule emits in a specific narrow portion of the bandwidth: for instance, MASER (Microwave Amplification by Stimulated Emission of Radiation) emission. We can study the temperature, magnetic fields, ionisations etc. by analyzing the emission of the (up to a few hundreds known) molecules.

As said earlier, we can also make polarimetric observations by calculating the cross-correlations of the two orthogonal signals provided by the OMT. These studies are very important for analyzing the cosmic magnetic field. Celestial sources emit different radiation in a certain polarization state, and the vectorial sum of the electromagnetic waves can be studied by calculating the Stokes parameters. Auto-correlations and cross-correlations provide all of the information necessary to get Stokes parameters.

Pulsars are highly-magnetized and rapidly-rotating neutron stars, whose detected signal appears as a periodic sequence of pulses. Their observations require wide frequency bands (some hundreds of MHz), but the frequency-dependent signal's dispersion effect (due to the interstellar medium) imposes the subdivision of the frequency band into narrow frequency channels (fraction of MHz). Moreover, since the period of the most interesting pulsars is of the order of milliseconds, sampling times of the order of few tens of microseconds are mandatory. The computational resources for pulsars are dramatically higher than the ones required for other celestial objects; hence, astronomers often need to use ad-hoc digital backends.

Basically, an instrument called a full-Stokes spectrometer is necessary for satisfying all of the requirements listed above. A full-Stokes spectrometer is a platform that must be able to split up the radio astronomical bandwidth into a sufficient number of channels, as well as capable of calculating the auto and cross-correlations of the double-polarization acquired signal. Concerning continuum, a total power machine would be sufficient, i. e. a system that simply takes the digital samples, square and integrate them so as to provide the entire power received. Nonetheless, the total power concept is fairly out of date because of radio interferences that come together with the celestial signals. In fact, the total power is nothing more than the sum of the power contained in every single spectrum's channel; therefore, we can use a spectrometer with a few thousand channels in order to "kill" a certain narrowband RFI (Radio Frequency Interference). Chapter three describes a specific project for this matter; clearly, in case of wideband RFI distributed over the entire received bandwidth, this approach is not adequate. In order to avoid the latter scenario, receivers containing an array of antennas must be employed and, with a technique named "beamforming", the RFIs coming from a certain direction can be killed by implementing a proper spatial filtering. This scenario represents the future of radio astronomy, and in particular with the SKA (Square Kilometer Array) project.

Chapter 2

State of the art

In this chapter we describe current available instrumentation regarding Italian radio astronomy. First, we present radio telescopes, especially the newest 64-m diameter Sardinia Radio Telescope (SRT). We will discuss in particular the available digital platforms since this thesis focuses on innovative ideas concerning digital backends for single dish science.

2.1 Italian radio telescopes

Italy is very active in the context of radio astronomical instrumentation, with three telescopes located in Medicina (Bologna), Noto (Siracusa) and, finally, San Basilio (Cagliari); figure 2.1 shows the telescope's locations. The following sections describe all of them.

Figure 2.1: *Radio telescopes in Italy.*

Up until now, Italian telescopes have been mainly employed as stations in the EVN (Eu-

ropean VLBI Network) [1] international collaboration; moreover, the SRT is part of the LEAP (Large European Array for Pulsars) project [2] since 2013. In this thesis, we have made an effort to make them more appealing also for single dish uses, with a particular emphasis on SRT because of its greater dimension as well as its active surface: these features make SRT more sensitive than the other telescopes and, consequently, the most important antenna in Italy.

2.1.1 Medicina Radio Telescope

Medicina is a little town near Bologna. A few kilometers from the city a radio astronomical station [3] is located; it includes the older Italian 32-m single dish and the Northern Cross. Figure 2.2 shows a picture of the entire radio astronomical station.

Figure 2.2: *Radio astronomical station at Medicina.*

The Northern Cross Radio Telescope is one of the largest transit radio telescopes around the world. It was conceived to receive radio waves with a central frequency of 408 MHz. The telescope is composed of two series of antennas: the first one is oriented from East to West (E-W), and the second one from North to South (N-S) direction. The system was developed as a transit telescope, therefore it is steerable only in declination, namely it is able to observe only when the celestial body crosses the local meridian.

The single dish antenna was built in 1983, with a frequency range of 1.4 - 26.5 GHz. It was thought mainly to be part of the EVN consortium, both for astronomy and geodesy; the latter allow us to measure, with incredible precision, minimal movements of the crustal plates. This is possible by observing, with at least two antennas, the same far celestial source like quasars, namely objects at the boundaries of the Universe. Indeed, at those distances,

quasars appear fixed by observing the same source at different moments, in case the correlation between antennas changes, the reason can be only due to a movement of the crustal plates in which the antennas are placed.

For single dish activities, the telescope allows total power measurements, spectroscopy and polarimetry focusing, and in particular spectrometry of water and methanol maser, sky surveys, observations of Galaxy regions, planetary studies, and so on. The telescope has a Cassegrain configuration with a parabolic mirror and a hyperbolic secondary one. Table 2.1 indicates current available receivers.

Table 2.1: *Available receivers at the 32-m Medicina telescope.*

Receiver	Number of feeds	Frequency Interval (GHz)	Focus
L band	1	1.35 - 1.45	Primary
L band	1	1.595 - 1.795	Primary
S band	1	2.2 - 2.36	Primary
C band	1	4.3 - 5.8	Cassegrain
C band	1	5.9 - 7.1	Cassegrain
X band	1	8.18 - 8.98	Primary
K band	2	18 - 26.5	Cassegrain

2.1.2 Noto Radio Telescope

Noto is a little town near Siracusa; fig. 2.3 shows the Noto section [4]. The radio telescope was completed in 1988 and since then has performed astronomical, geodetic and space science observations. The radio telescope of 32m in diameter is designed to work within the International VLBI networks for both astronomy and geodesy. One of the major capability of the antenna, within Europe, is the primary mirror equipped with an active surface, i.e. 256 computer-controlled panels that can be adjusted to compensate surface deformations. Moreover, it is equipped with a high velocity fiber optics connection, which allows for data transfer in real time (eVLBI).

The telescope, which is basically identical to the Medicina one except for its active surface, has a Cassegrain configuration with a parabolic mirror and a hyperbolic secondary mirror. From a scientific viewpoint, the active surface allows us to observe at higher frequencies than the Medicina antenna. Table 2 indicates current available receivers. A very notable receiver is the Q-band, which is able to work very efficiently at up to 43 GHz.

The Noto's section is well-known for the development of the Digital Base Band Converter (DBBC), i.e. a digital platform that is replacing obsolete analog terminals named Mark4 for all of the EVN stations. One of the next section describes the DBBC, and in particular its use as a backend for a radio frequency interference monitoring system.

Figure 2.3: *Noto radio astronomical station.*

Table 2.2: *Available receivers at the Noto 32-m.*

Receiver	Number of feeds	Frequency Interval (GHz)	Focus
P band	1	0.317 - 0.332	Primary
L band	1	1.40 - 1.72	Cassegrain
S band	1	2.2 - 2.36	Primary
C band	1	4.70 - 5.05	Cassegrain
X band	1	8.18 - 8.58	Primary
Ku band	1	11.70 - 12.75	Cassegrain
Ku band	1	11.70 - 12.75	Primary
K band	1	22.18 - 22.46	Cassegrain
Q band	1	39.0 - 43.5	Cassegrain

2.1.3 Sardinia Radio Telescope

The Sardinia Radio Telescope [5] is a new general purpose, fully-steerable 64-m diameter parabolic radio telescope capable of operating with high efficiency in the 0.3-116 GHz frequency range. Figure 2.4 shows a picture of the telescope.

The instrument is the result of a scientific[6] and technical[7] collaboration among three structures of the Italian National Institute for Astrophysics (INAF): the Institute of Radio Astronomy of Bologna, the Cagliari Astronomy Observatory, and the Arcetri Astrophysical Observatory in Florence. Main funding agencies are the Italian Ministry of Education and Scientific Research, the Sardinia Regional Government, the Italian Space Agency (ASI), and

Figure 2.4: *Sardinia Radio Telescope.*

INAF itself.

SRT is located in the plain of Pranu Sanguni, 35 km north of Cagliari, in the municipality of San Basilio. The manufacturing of its mechanical parts and their on-site assembly was commissioned in 2003 and completed in mid 2012. The antenna was officially opened on September 30th 2013, upon completion of the technical commissioning phase. The Astronomical Validation (AV) is now over and early science/shared risk observations have started in early 2016. The SRT is planned to be used for astronomy, geodesy and space science, both as a single dish and as part of the European and International networks.

After the first successful VLBI data correlation - obtained between the SRT and Medicina stations in January 2014 - SRT has regularly been participating in EVN test observations[8], and since 2015 the telescope is offered as an additional EVN station in shared-risk mode for all of its three first-light observing bands (L-[9], C- and K-[10] bands). In addition, the LEAP (Large European Array for Pulsars) project has been successfully implemented, and in particular all of the necessary hardware and software are now well-tested and operative. SRT participates in monthly LEAP runs, and data acquisition is now fully automated.

The antenna design, whose schematic view is shown in Fig. 2.5, is based on a wheel-and-track configuration.

The main reflector (M1) consists of a back-structure that supports - through actuators - the mirror surface, itself composed of rings of reflecting panels. A quadrupod, connected to the back-structure, supports the sub-reflector (M2) and the primary focus positioner and instrumentation. The main and secondary mirrors and the quadrupod lie on the alidade, which is a welded steel structure standing on a large concrete tower that forms the bulk of the antenna foundation. Three large rooms were built behind the primary mirror to contain the secondary focus receivers, the beam-waveguide mirrors and several electronic instrumen-

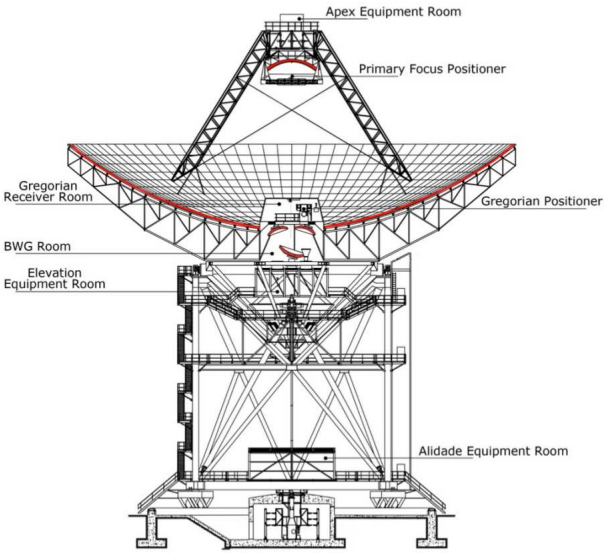

Figure 2.5: *SRT mechanical structure. The radio-frequency reflecting surfaces are highlighted in red..*

tation and cable distributions, respectively. A fourth room is located in the lower part of the alidade, where the power drivers for the motors, the antenna control unit and the cryogenic compressors are installed. The alidade also supports the elevation wheel, which is a conical truss anchored to the reflector back-structure through a massive pyramidal structure. The radio telescope is supported by a reinforced-concrete foundation excavated into rock; an outer ring beam sustains the azimuth track, while a central building accommodates the azimuth pintle bearing support, the azimuth cable wrap and the encoder system. The wheel-and-track structure consists of 16 wheels lying on the rail, which is a continuous welded ring 40 m in diameter. This is connected to the foundation by 260 pairs of anchor bolts and by a fiber-reinforced grout. The overall structure of the antenna weighs approximately 3300 tons. The antenna is steerable around the azimuth and elevation axes. The rotation around the two axes is managed by a servo control system, consisting in 29-bit absolute encoders (peak-to-peak position error 0.8 arcsec), 12 brushless asynchronous motors (eight in azimuth and four in elevation) and an ACU available on a BECKHOFF hardware platform employing an IRIG-B generator. A proper torque bias is applied to the motors to overcome the gearbox backlash and to improve the antenna pointing accuracy. The primary reflector surface consists of 1008 individual aluminum panels divided into 14 rows of identical panel types. Each panel has an area ranging from 2.4 m^2 to 5.3 m^2. It is built using aluminum sheets glued, by means of a layer of epoxy resin, to both longitudinal and transversal Z-shaped aluminum stiffeners. The basic back- structure is composed of 96 radial trusses and 14 circumferential trussed hoops supported by a large center hub ring. The sub-reflector surface consists of 49 individual aluminum panels with an average area of about 1 m^2, whereas its back-structure

is formed by 12 radial trusses and 3 circumferential trussed hoops supported by a center hub ring. Three of these trusses are directly connected to a triangular steel frame, which has the function of a transitional structure to the six sub-reflector actuators. These actuators define the sub-reflector position, and provide for sub-reflector motion with five degrees of freedom. Further mirrors beneath the Gregorian focus, arranged in a Beam WaveGuide configuration, allow the addition of four more focal points with magnified and de-magnified F/D ratio in the intermediate frequency bands. Two of the four designed BWG layouts have already been constructed. They use three mirrors: M3 as a shared mirror, M4 for the first layout and M5 for the second one. The re-imaging optics for BWG layout I were designed for maximum focal ratio reduction, whereas BWG layout II was designed so that the output focal point F4 lies beneath the elevation axis of the antenna. By an opportune rotation of M3, which takes 1.5 minutes, the desired BWG layout is selected. The two missing BWG layouts will be added in a later stage to the present configuration using two more mirrors and an appropriate rotation of M3; they will be dedicated to Space Science applications. A rotating turret (Gregorian positioner assembly) is mounted eccentrically on the focal plane of the antenna dish, and can house eight separate cryogenic receiving systems and the associated feed horns for operating up to 115 GHz. A drive system can rotate the turret (within 2 minutes for a complete rotation of 340 degrees) so that any of the feed horns can be positioned on the focal plane. The servo control system consists of two brushless servo motors with drivers and a position-control computer.

All of the available receivers are listed in table 2.3.

Table 2.3: *Available receivers at the 64-m SRT.*

Receiver	Number of feeds	Frequency Interval (GHz)	Focus
L-P band	2	0.305 - 410; 1300 - 1800	Primary
C band	1	5.7 - 7.7	BWG
K band	7	18 - 26.5	Gregorian

2.2 Digital Backends at Italian radio telescopes

Against the background of these antennas, the major hindrance to their use as single dish stations is largely due to the absence of “attractive” digital backends. In this section, we give an overview of this scenario, i.e. a “photograph” of digital instruments that are currently operative.

2.2.1 Total Power

The Total Power (TP) is a digital platform developed by the Institute of Radio Astronomy (IRA) and Medicina. It has a dual function: “focus selector” mode (fig. 2.6) and continuum back-end (fig. 2.7). The TP is available at all three Italian telescopes, and in the case of SRT, the overall system is made up of 14 boards. Each board can manage up to three IFs from

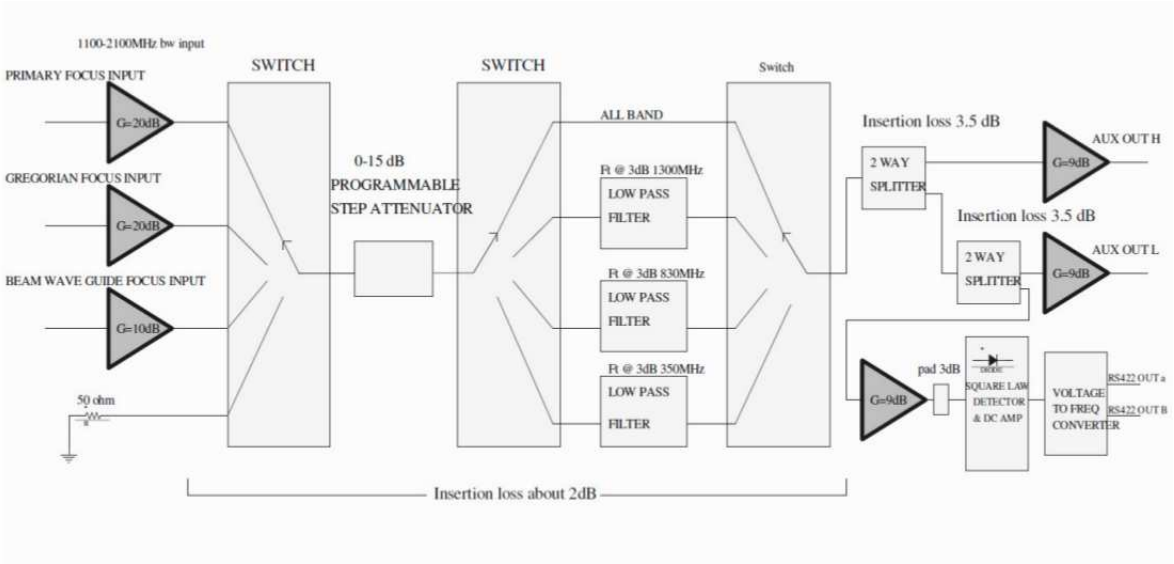

Figure 2.6: *Focus Selector.*

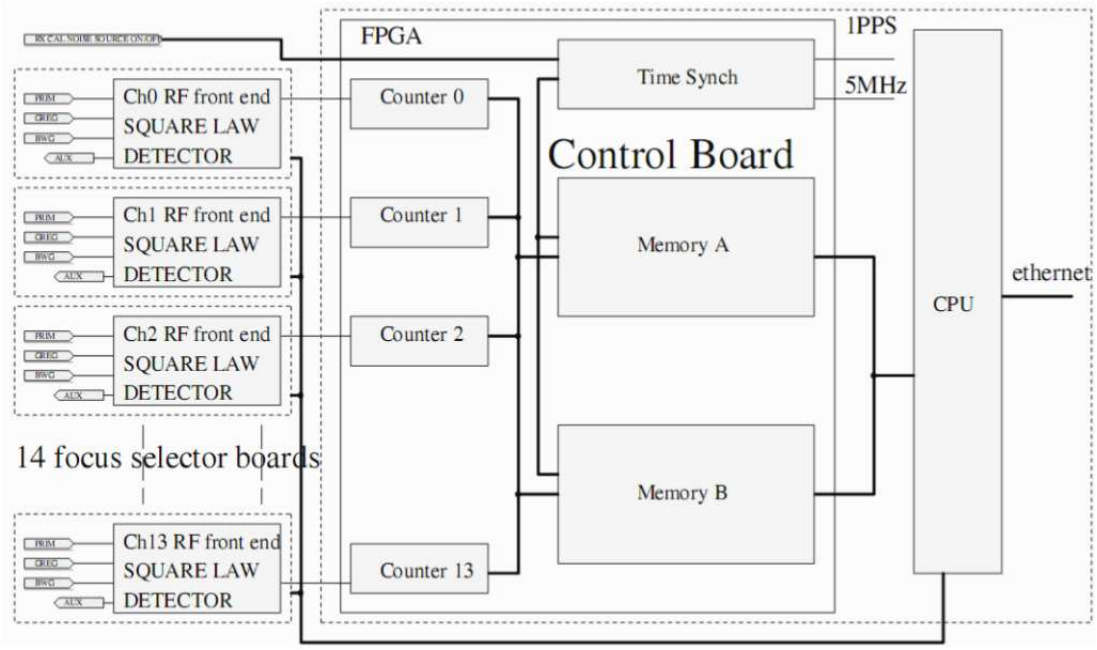

Figure 2.7: *Total Power.*

all three foci (Primary, Beem Wave Guide, Gregorian). The selected signal can be attenuated (range 0-15 dB) and then filtered by selecting one of the low pass filters (with cut-off frequency of 350, 830, 1300 MHz respectively or all band). Some splitters are used to provide three copies of the conditioned signal in order to employ them with the other available back-ends; another output is instead used internally for the total power back-end. Signals go through square law detectors, and are converted into digital format by voltage to frequency converters. An Actel FPGA-based controller contains a few digital counters that count the

pulses generated by the corresponding voltage-to-frequency converter. Memory A and B are interchangeable: while one of them accumulates counts, the CPU reads the previous acquisition data set from the other one, then memories exchange their roles. The integration time is programmable by user from 1 ms to 0.5 sec. The back-end is fully integrated in the control software of the Sardinia and Medicina radio telescopes; moreover, it is going to be installed at Noto telescope as well. Despite inevitable limitations of a system that is unable to break the radio astronomical bandwidth into smaller pieces, the Total Power is currently the only backend capable to perform on-the-fly (OTF) mapping for all seven-feed K-band receiver. For receivers at lower frequencies, the use of the TP is quite impractical due to strong radio interferences that can degrade the observed data.

2.2.2 ARCOS

ARCOS (ARcetri COrrelation Spectrometer)[11] is a digital spectrometer developed by the Astrophysical Observatory of Arcetri. ARCOS can be connected to the Mark IV (i.e. the analog terminal with which VLBI sessions were performed at Medicina and Noto for many years), and receives 2x16 MHz inputs from videoconverters. The system can handle two signal 20 MHz of bandwidth each. The system is mainly composed of two correlation boards (2048 channels in total) and two analog-to-digital samplers (each channel is represented with 2 bit, therefore it allows four levels). The system is available at both the Medicina and Noto stations. However, as reported in the official website, ARCOS is not officially offered. Observers who interested to use it must contact people working at the telescope so as to receive information and proper assistance.

2.2.3 MSpec0

MSpec0[12] is a high-resolution digital spectrometer installed in 1994 at Medicina. MSpec0 offers a number of channels that are selectable in the interval 512 - 131072 channels; the maximum bandwidth can be chosen in the interval 125 kHz - 16 MHz. The spectrometer receives only a single analog band from the Mark IV, digitizes it and applies a high efficient FFT algorithm. Major components are: an Ultra ADC A/D board, a VT-524 board and two UltraDSP/1128 boards equipped with two LH9124 processors. Processors run in a parallel way and operate the FFT engine with the following characteristics: 24 bit, 256,000 spectral points. Resulting spectra are integrated on the VT-524 board. DSP boards are completely programmable through the VME bus. The VT-524 board also allows us to show results in real time. The spectrometer is connected to an external PC equipped with the "Spett" software, which provides a user interface to control the system (channels number, sampling frequency, number of spectra to be averaged, number of On-Off cycles). Just like ARCOS, MSpec0 is not officially offered.

2.2.4 XARCOS

XARCOS[13] is a full-Stokes spectrometer developed by the electronics group of the Astrophysical Observatory of Arcetri. The system is equipped with four boards and contains a total of fourty FPGAs. The system is capable of acquiring and processing up to sixteen intermediate frequency signals 125 MHz bandwidth each, and to provide total power and spectro-

polarimetric information. Figure 2.8 shows the back-end installed and cabled[14] at SRT, while figure 2.9 shows a simplified block diagram (with just four input signals).

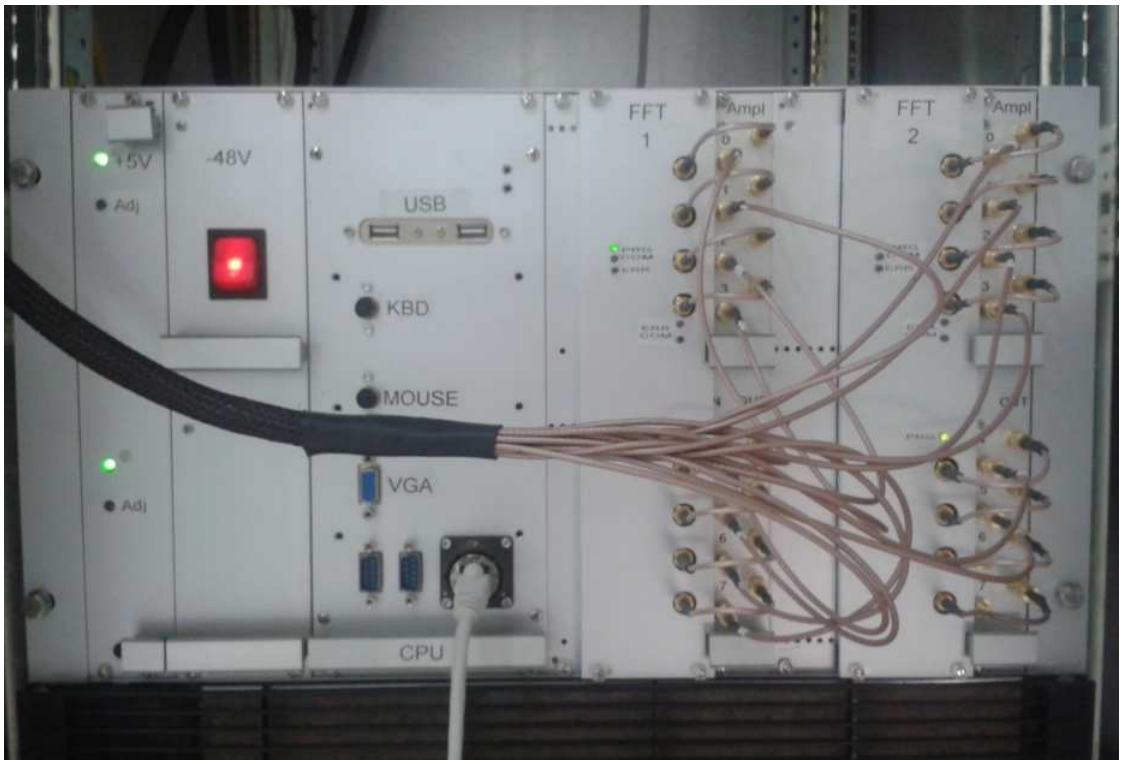

Figure 2.8: *XARCOS.*

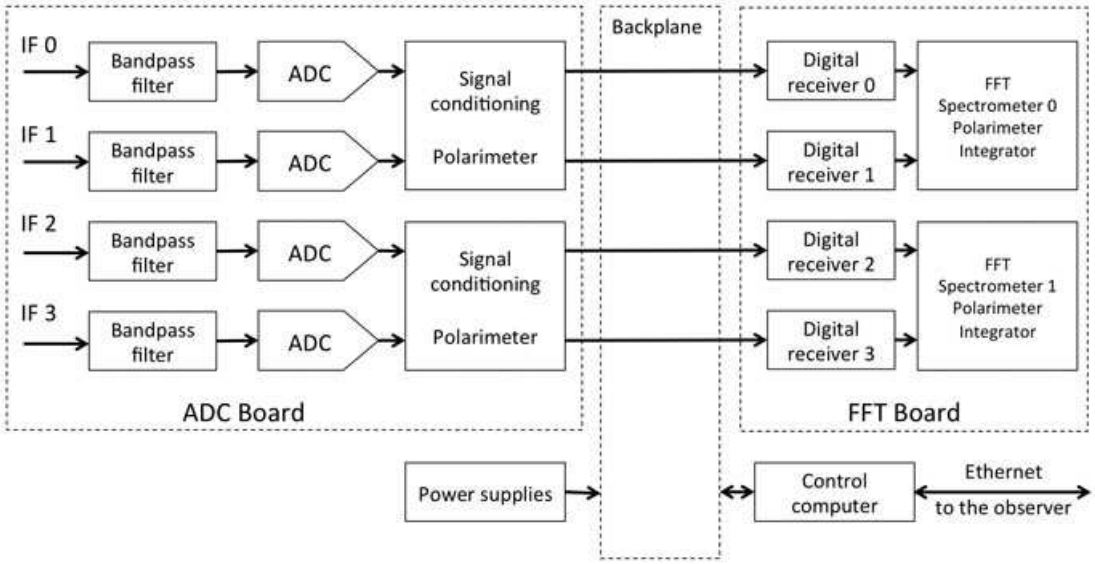

Figure 2.9: *XARCOS simplified block diagram (with 4 inputs instead of 14).*

The processing chain starts with the amplification of the signal coming from the front-end system and, after a pass-band filtering that operates in 125 - 250 MHz the range, a conversion of the data from analog to digital format is performed by two ADC boards. Each ADC board contains eight analog-to-digital converters operating in their second Nyquist window, down-converting the input signal to base-band (between 0 and 125 MHz). Once the data (with a resolution of 6 or 8 bits) are in digital format, four Xilinx FPGAs contained in the ADC boards convert the data into complex-valued samples at a frequency of 125 MSample/s. The signal then goes through a backplane toward the FFT boards containing Altera FPGAs in which several variable decimating filters are available. They enable us to select different values for the input bandwidth for each IF, starting from a bandwidth of 125 MHz halving until a bandwidth of 0.488 MHz. Thus, a chain composed of an FFT spectrometer followed by a polarimeter provides both spectral auto- and cross-correlation of the left and right polarization of the corresponding double-polarization input signal. Finally, four parallel output signals (LL, RR, LR, RL) from the polarimeter are integrated for a programmable time. Peculiar characteristics of the back-end are the capability to zoom in until four sub-bands contemporaneously. The system was tested on very bright spectral line astronomical sources. The back-end, available both at Medicina and SRT, is fully integrated[15] in the control software of the telescopes.

2.2.5 Digital Base Band Converter

The Digital Base Band Converter (DBBC)[16] is a project developed in the last decade within the European VLBI community. The DBBC consists of a generic, modular radio astronomical data acquisition architecture; fig. 2.10 shows a block diagram of the architecture.

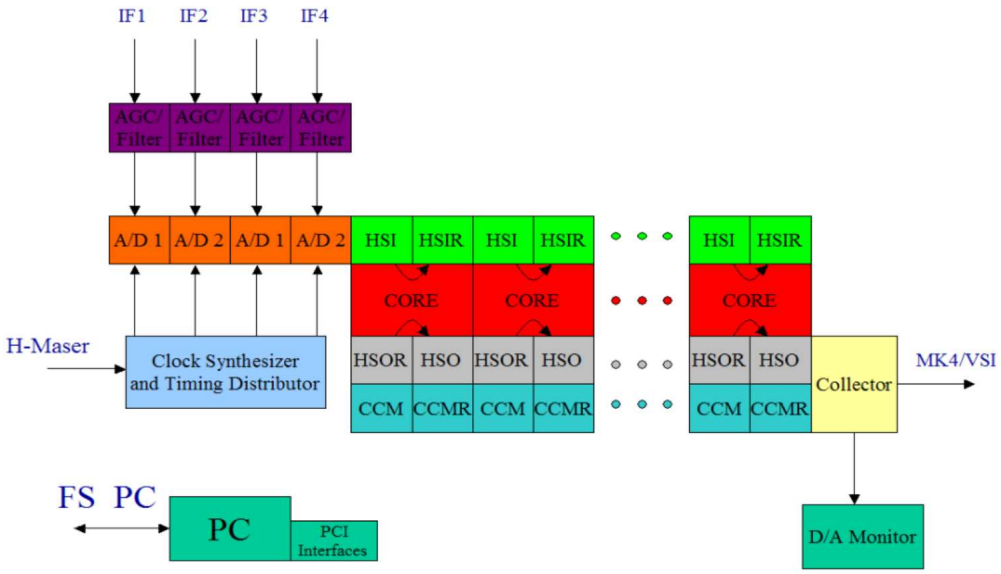

Figure 2.10: *DBBC architecture.*

The DBBC includes a class of boards, firmware and software, that gives the possibility of building a general purpose back-end system for VLBI or single-dish observational activities. The instrument is composed of a base box, containing power supply, a control computer, clock distribution and JTAG interface, as well as a stack of small, modular boards that can be composed according to the user needs. The First and Last modules in the system (FILA boards) provide control signal distribution, a DAC (Digital-to-Analog Converter) for monitoring, and an electric interface to the standard VSI bus for the VLBI data recorder. An optional FILA10G provides one SFP+ optical transceiver cage for 10G Ethernet.

Between the two FILA boards, up to 4 ADC boards and up to sixteen CORE (processing) boards can be stacked, in almost any order. ADC modules contain a single high speed ADC, and CORE modules have a single FPGA. Modules can be upgraded without changing the rest of the system. Each ADC module receives its input from an analog conditioning module. The module basically contains a set of filters, thus we can set one of its possible Nyquist sampling bands, an isolation amplifier and a programmable attenuator. Modules are interconnected using stackable surface mount differential connectors. Signals enter from one side of the board, are regenerated inside the FPGA, and exit on the other side of the board. Three data buses are used. The fast data bus is generated by the ADC and contains unprocessed data samples. It is structured as 8 LVDS buses at a sample rate of 512 MS/s, and may be used for up to 2 data streams at 2 GS/s or up to 4 at 1 GS/s. A clock at 512 MHz is associated with each data stream. High Speed Output (HSO) bus is generated by the CORE boards, with each board passing on the signals that are generated by the previous boards. It is a single differential 64 bit wide bus, with a maximum data rate of 128 Mb/s. The Control, Command and Monitor (CCM) bus is a low speed bus containing various signals used for system control. A 32 bit bidirectional bus, with an associated strobe signal, is generated by a parallel interface in the control computer, and is used to address, read and write generic registers inside the CORE modules. A JTAG interface is used to program FPGAs. A 12 bit bus is used to send tests and debug signals (e.g. partially processed signals inside the FPGAs) to a monitor DAC in the last FILA. The typical minimum configuration includes one ADC and one CORE module, with the CORE hosting one of the applications described here. For example, it can implement a mini-VLBI terminal, with up to 4 equivalent broadband converters. The maximum configuration includes 4 units, each composed of an ADC board followed by 4 CORE2 boards. It can implement 16 BBC per ADC, with up to 4 input signals, or a multichannel wideband spectrometer with four 1 GHz input signals. The control node is a standard industrial computer, under Windows operating system. Porting of the necessary hardware drivers under Linux is in progress. The processor uses a standard Xilinx JTAG interface to program the CORE2 stack, and a commercial 32 bit parallel interface to control both conditioning modules and any logic instantiated in the CORE2 FPGAs. A generic framework has been developed to control the instantiated logic. Basically, the application in the FPGA is controlled by a number of 16 bit write registers (up to 1024 per FPGA), and its status (or the observation results) is read using a set of 32 bit read registers. The 32 bit output of the parallel interface is split into a 16 bit address, used to identify the register, and 16 bit of data. The read bus is completely used for the data. The address is divided into a 5 bit portion identifying the module (often comparing it to a physical address serial by a switch), a bit discriminating between the read and write address space, and a 10 bit address space per FPGA. A standard addressing scheme has been consistently used in the system, with some dedicated registers reserved for commonly used functions like DDS reset. Absolute timing is maintained using an external peak-per-second (PPS) signal. As signals are regenerated inside each module, a

propagation delay is present across different modules in the stack. This is accounted for by adding a programmable offset to the internal PPS signal.

2.2.6 Pulsar Digital Filter Bank

The Pulsar Digital Filter Bank (PDFB)[17] is a digital platform developed by the ATNF (Australian National Telescope Facility). Fig. 2.11 shows a block diagram of the system, while fig. 2.12 shows a picture of the platform.

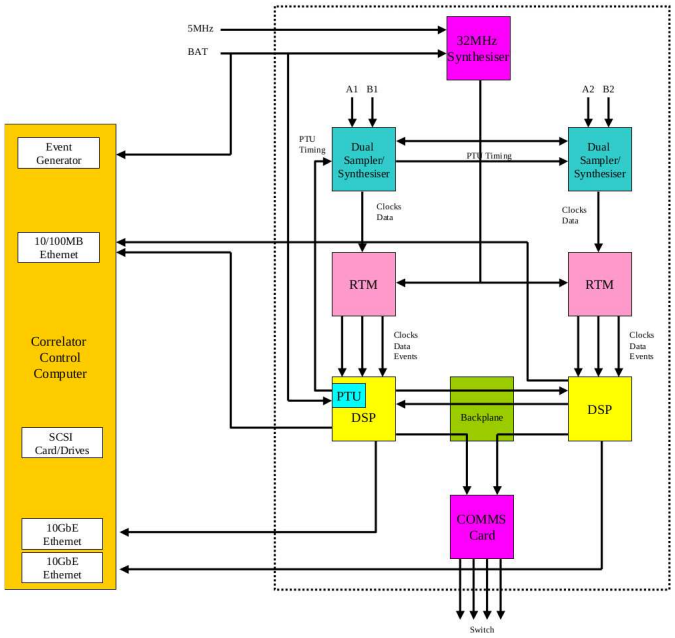

Figure 2.11: *Block diagram of the PDFB.*

As the name implies, the PDFB is primarily used for pulsar science in all modes of observations: in particular folding, search and base band mode. The PDFB system is composed of two main components, a high-speed dual input sampler and a Digital Signal Processing (DSP) card capable of pulsar processing. These two components are surrounded by a significant amount of hardware to provide power, communication, control and data acquisition. There is one frequency reference for the system at 5 MHz that gets multiplied up to various frequencies, the highest being 2048 MHz for the sampling clock. An additional BAT (Binary Atomic Time) signal generated from an ATDC (Australian Telescope Distributed Clock) is required to synchronise the system and provide absolute time. The sampler module contains two 10-bit ADCs, of which only 9-bits is output in a serial fashion. The serialiser requires a 640 MHz reference - which is also sent to the RTM module - that contains a deserialiser. The sampler module contains a synthesizer, which generates 2048 MHz, 640 MHz and 256 MHz (used for the DSP module.) Data is transmitted serially at a rate of 10.24 Gbps. A Pulsar Timing Unit (PTU), included on the DSP cards, generates three signals: bin, period and bank; they control the pulsar folding engine on the DSP module. The PTU is directly controlled from the DSP card computer with its time reference generated from the ATDC's BAT.

Figure 2.12: *PDFB.*

The Rear Transition Module (RTM) is an acronym used for describing a board located in an AdvancedTCA rack. The RTM is based on this standard, as well as the board called DSP. The RTM accepts the serial data from the sampler and converts it to a parallel format. Other signals input into the RTM include several clocks, as well as the physical 10/100/1000M Ethernet connections (although in the diagram they are shown connected to the DSP card). All of these signals are connected to the DSP board. The DSP board contains many large high speed FPGAs and DDR2 memory to perform pulsar operations required. Here, two digital filter banks are implemented as well as the PPU. Data processing is shared between two DSP cards across a backplane using serial data communications at 3.125Gbps. The data sharing between the two DSP cards is allowed to implement many different configurations. Data out of the DSP board can vary tremendously in bandwidth, thus there are three possible methods of data transport: a 10/100M Ethernet link, a 1Gb Ethernet link and three 10Gb Ethernet links. In general, the 10/100/1000 network is suitable for folding, however for search mode or base band processing the 10Gb links provide higher bandwidths.

The back-end is equipped with four ADC boards with a sampling frequency of 2.048 MS/s, therefore up to four IFs 1 GHz bandwidth each one can be processed. These features particularly fit the dual-frequency L-P receiver for the SRT. The FPGAs contained in the boards, being reconfigurable, allow spectro-polarimetric mode as well. The spectropolarimetric mode can provide up to 8192 spectral channels. Pulsar observations have specific features, thus a new observing tool called Srt Expanded Data Acquisition System (SEADAS)[18] is under development for managing pulsar observing sessions and, more specifically, the data acquisition by multiple pulsar back-ends in parallel.

2.2.7 Reconfigurable Open Architecture and Computing Hardware

The Reconfigurable Open Architecture and Computing Hardware (ROACH)[19] is a digital board developed by CASPER (Collaboration for Astronomy Signal Processing and Electronic Research). The centerpiece of the board is a Xilinx FPGA Virtex 5, while Z-DOK connectors,

CX4 connectors and further features allow us to acquire, process and then send data for radio astronomical applications. A minimal PowerPC runs Linux and is used to interact with the FPGA and external devices through Ethernet. These boards have had great success due primarily to CASPER's efforts in simplifying the design flow of radio astronomical instrumentation; the open source philosoph (both hardware and software) has always been the CASPER motto.

The ROACH board for SRT is equipped with an ADC 1024 Msample/s that allow either the processing of two IFs 512 MHz bandwidth each or a single IF 1 GHz bandwidth. As shown in figure 2.13, SRT has a ROACH board mainly employed for the LEAP (Large European Array for Pulsars) project. However, the same configuration can be used for other purposes: indeed, a lot of different personalities are being developed for every kind of scientific request. At present, the back-end is not fully integrated in the control software of SRT. For pulsar observations, this backend can be controlled by SEADAS.

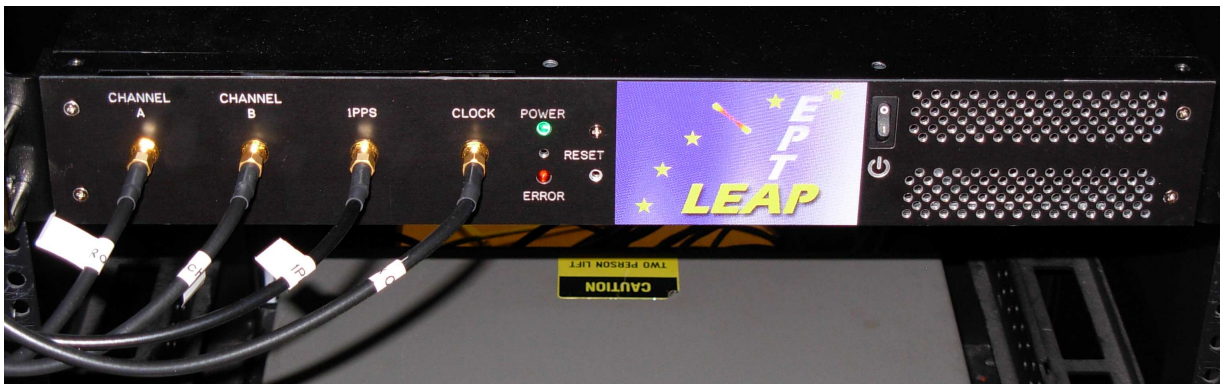

Figure 2.13: *ROACH at SRT.*

Large European Array for Pulsar

The Large European Array for Pulsars (LEAP)[20] project performs simultaneous observations of millisecond pulsars at 5 large European radio telescopes: the Lovell telescope at Jodrell Bank Observatory (UK), the Westerbork Synthesis Radio Telescope (Netherlands), the Effelsberg Telescope (Germany), the Nancay Radio Telescope (France) and the Sardinia Radio Telescope (Italy). This project is part of the European Pulsar Timing Array (EPTA)'s effort to directly detect gravitational waves from supermassive black hole binaries using an array of millisecond pulsars. Pulsars are observed simultaneously, thus baseband data from each telescope can be added coherently in phase, which leads to a greater increase in the signal-to-noise of the observed pulsars. Observations with LEAP are equivalent to observing with a single dish of 196 meters in diameter, which is similar to the illuminated area of the Arecibo dish, but with a larger range of observable declinations.

The Sardinia Radio Telescope is the latest telescope to join the LEAP effort. LEAP observations started in early 2012 with the Effelsberg and Westerbork telescopes, and were joined later that year by the Lovell and Nancay telescopes. Observations are performed monthly and are 25 hours long. The participation of SRT in LEAP was made possible once the dual-band L/P receiver was installed at the primary focus of the telescope (June 2013) and the ROACH backend was installed on-site (July 2013). The first ever LEAP session was conducted

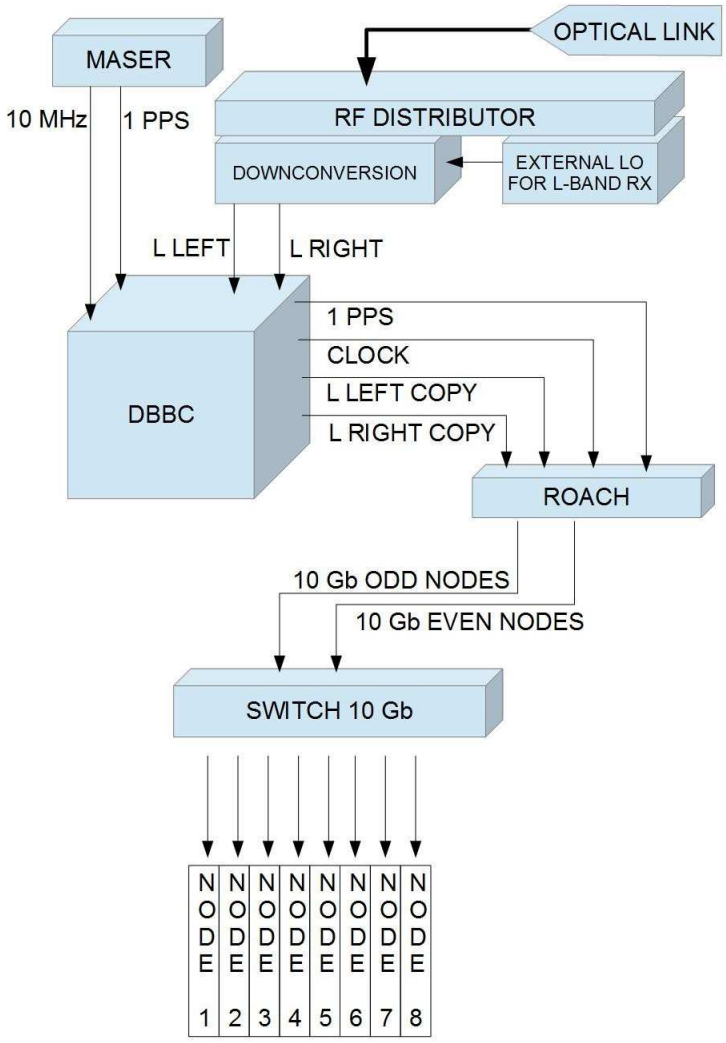

Figure 2.14: *General setup (radio astronomical signal from antenna to computer cluster).*

on July 27, 2013 for one pulsar (PSR J1022+1001), which was observed simultaneously at all 5 telescopes. The observation at SRT was limited to one 16 MHz band (we chose the band centered at 1436 MHz) due to hardware limitations. Indeed, the ROACH backend was controlled by a computer that only allowed data acquisition in one 16 MHz sub-band. In subsequent months, SRT participated in LEAP in the 1436 MHz sub-band (September, November, December, January). The August 2013 and February 2014 sessions were skipped because of the antenna's unavailability. In February 2014, a computer cluster with eight nodes was installed at SRT. Data acquisition and pulsar analysis software were installed on the cluster, and first tests were performed to record baseband data in 8 x 16-MHz sub-bands, covering the full 128 MHz LEAP bandwidth (1332-1460 MHz). We were successful in observing the bright pulsar B0329+54 and the bright millisecond pulsar B1937+21 in all eight bands. This paved the way for the participation of SRT in the full LEAP bandwidth. On March 23, SRT participated in LEAP for the first time using the full 128 MHz bandwidth, joining for part of the 25-hour

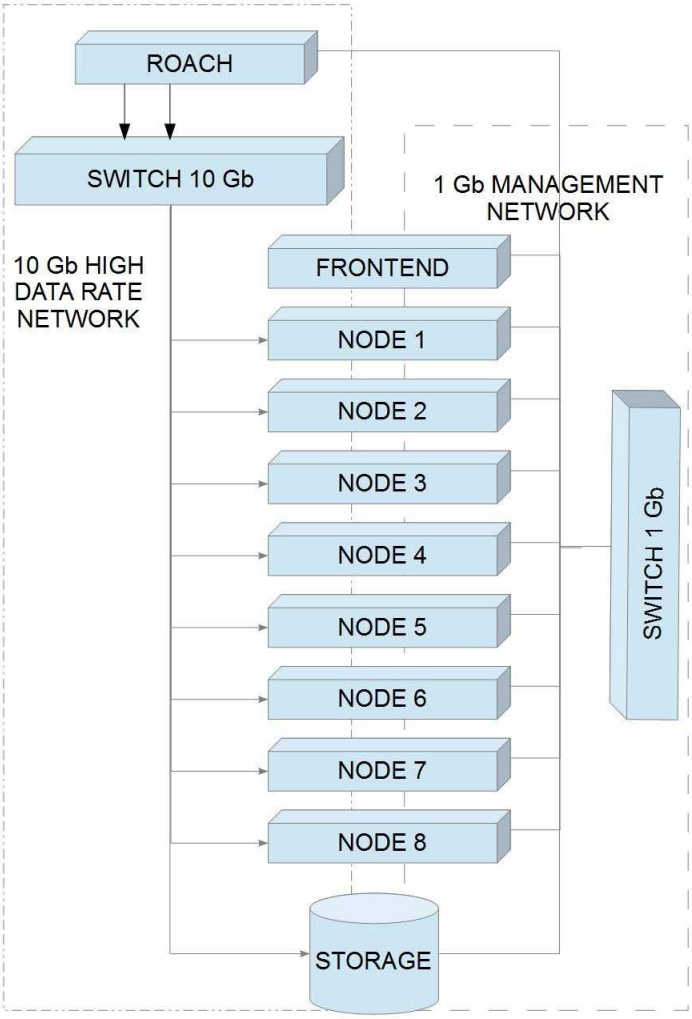

Figure 2.15: *ROACH/cluster/storage system.*

run. SRT joined for the April 12-13 LEAP run as well. Because of the high volume of data (64 MB/sec for each 16 MHz sub-band), one 25- hour run needs about 40 TB of space for the full bandwidth at each telescope. The SRT cluster can accommodate 7 TB per node, or 56 TB in total. The routine performing of 25-hour runs and the recording of many TB of data at SRT was however not possible until a storage system was installed on-site (April 2014). In April 2014, a storage system with a capacity of 96 TB was shipped alongside 32 x 3 TB disks by the LEAP project in Manchester. Previous data were copied onto disk and the cluster was made ready for the first-ever 25-hour LEAP run at SRT on May 21-22, 2014. LEAP observations are made in L-band. The L-band receiver is located at the primary focus of the telescope and requires the use of a âparabolicâ shape for SRT's active surface. The L-band receiver detects the two linear polarizations of the incoming electromagnetic waves in the 1,300-1,800 MHz frequency range, which are then transferred to the apparatus box, where they are mixed with a monochromatic signal (set at a frequency of 2,316 MHz) generated by a synthesizer, and

are thus down-converted to the adequate backend frequency range. The signal is then sent to the DBBC backend and, exploiting a few power splitters contained in the DBBC, to the ROACH backend as well. This enables the RFI monitoring of the L-band while recording data with the ROACH. The 10 MHz clock and 1 PPS provided by a maser allow synchronization of the synthesizer contained in the DBBC; it provides the 1,024 MHz sampling clock necessary for the analog-to-digital converters (ADCs) of both the DBBC and the ROACH. The clock used for VLBI (with the DBBC) and LEAP (with the ROACH) is therefore identical.

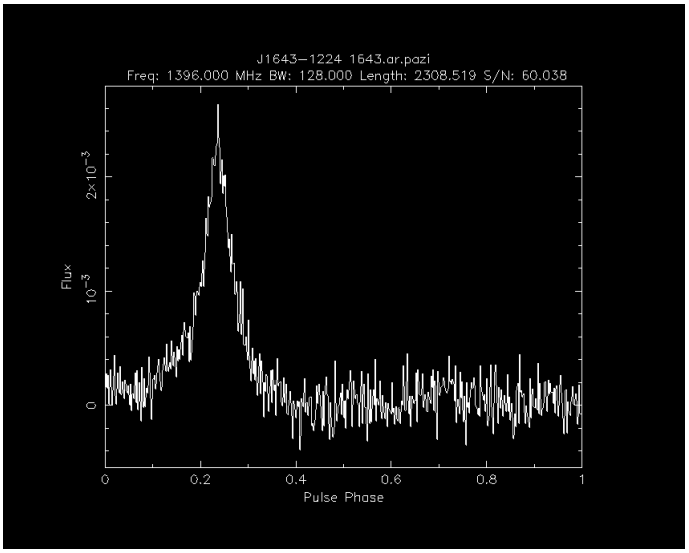

Figure 2.16: *Pulsar observed by the 5 telescopes of LEAP. From the left, Plot of power vs. phase; plot of time vs. phase; plot of frequency vs. phase.*

The employed ROACH backend is identical to the ones used at Effelsberg and Jodrell Bank for LEAP. As said earlier, the analog-to-digital converters work at a sampling frequency of 1,024 MS/s with an 8-bit representation, providing 512 MHz of bandwidth for each polarization. At SRT, the ADCs operate in the second Nyquist zone (512 - 1024 MHz). The ROACH produces 32 complex channels of 16 MHz each; the desired sub-bands can be chosen by modifying an IP table. The acquired cluster is composed of 8 servers/nodes + 1 management server (frontend or head node), with a dual-socket motherboard (G34). Each node is equipped with: 1) 2 x 8 core 2.5 GHz CPUs (16 cores in total for each node) 2) 64 GB of RAM (DDR3-1600) 3) RAID: Adaptec 6805 SAS/SATA 4) HDD: 4 x 2 TB 5) LAN: 4 x 1 Gbe ports + 1 port dedicated to IPMI In order to send the data from the ROACH to the cluster, a 10 Gbe switch equipped with four CX4 connectors (paid for and shipped by the LEAP team at Manchester) was installed. Finally, the system is complemented by a storage unit with a capacity of 32 disks of 3 TB = 96 TB. Each node is directly linked to 4 disks, where baseband data is copied to after a LEAP run. Once completely full, the disks are shipped to Manchester. The general setup of the observing system (astronomical signal from antenna to ROACH and cluster) is illustrated in Figure 2.14, while the ROACH/cluster/storage system is illustrated in more detail in Figure 2.15. Figure 2.16 shows the plots of power vs. phase for the millisecond pulsar J1643-1224.

Chapter 3

Radio Frequency Interference

Radio Frequency Interferences (RFI) represent one of the major issues in single-dish, low-frequency radio-astronomical observations. A traditional RFI approach consists of a monitoring station placed near the radio telescope in order to monitor the RF environment. However, its antennas do not have enough telescope sensibility, unlike systems like wide-band digital spectrometers operating in piggy-back mode on radio astronomical signals. In this chapter, we discuss an innovative RFI monitoring system based on a two-stage polyphase filter bank spectrometer. Firstly, we describe the polyphase filter bank theory, and in particular a two-stage implementation. Secondly, we present an innovative infrastructure for the SRT, as well as how we can exploit it for dynamic scheduling both before and during an observation. Finally, we describe a hybrid approach combining this solution and the one that uses a traditional RFI station.

3.1 Wideband digital spectrometer approach

Radio astronomical observations have to take into account different variables. Usually, in order to ascertain that the telescope is working properly, one or more Tsys are calculated. However, real-time spectral information of the observed bandwidth represents the best way to make sure this is the case. The idea of implementing an infrastructure that is able to check the observed signal - especially for RFI monitoring purposes - has motivated this work.

3.1.1 Polyphase Filter Bank

Radio astronomical signals usually have a very large instantaneous bandwidth (up to several GHz), while currently available digital signal processing hardware - especially Field Programmable Gate Array (FPGA) - have maximum clock rates of the order of a few hundred MHz. Thus, a certain type of multiplexing technique is necessary for processing the acquired data at a reduced clock frequency. The most efficient way to perform this function is to use a filterbank, in order to split the incoming wideband signal into separate sub-bands of reduced bandwidth and sample rate. A very efficient way to perform this function is the polyphase filterbank (PFB), a multi-rate filter structure followed by a Fast Fourier Transform (FFT)[21] engine. The filter is a low-pass finite impulse response (FIR), and its bandshape

is translated in frequency by the FFT algorithm. In its simplest form, the PFB implements a filterbank with adjacent bands; however, due to the finite transition region at the end of the FIR passband, it produces small holes between the sub-channels, as shown in figure 3.1:

Figure 3.1: *Non-Overlapping filterbank response.*

Algorithm description and mathematical formulation

As mentioned above, a PFB is basically an N-point FFT performed by a narrow polyphase filter, followed by a small FFT engine, as shown in figure 3.2. The signal is deserialized into N streams at 1/N the original data rate, and each stream is preprocessed by a short filter leg. Tap coefficients of each filter leg correspond to the taps of the original low-pass filter, spaced by N taps: the first leg processes taps (0, N, 2N, ...); the second leg taps (1, N+1, 2N+1...) and so on. The original filter shape is translated in frequency by the N-point FFT engine producing N adjacent replicas, as shown in figure 3.1. For a real-valued signal (as our case), only outputs 0 to N/2 of the FFT engine are used (N/2 + 1 in total); the others only produce the complex conjugate (frequency mirrored) version of the same bands.

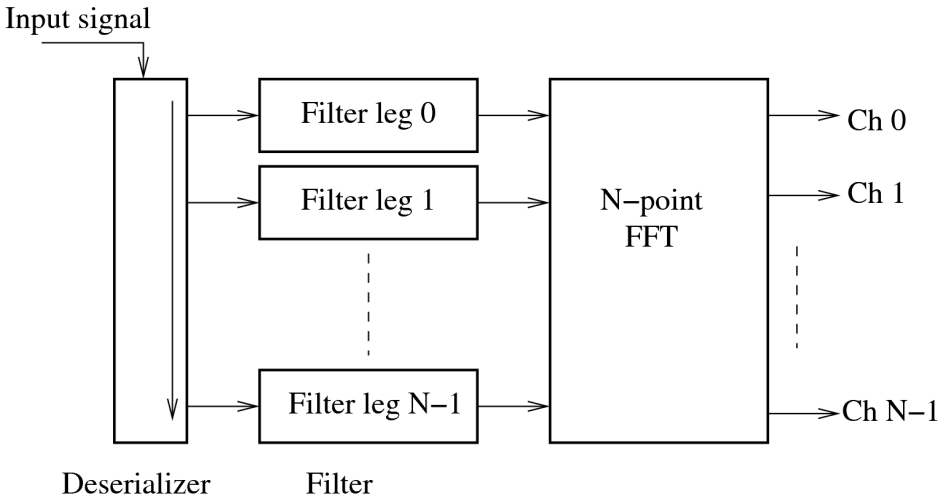

Figure 3.2: *Typical block diagram of a PFB.*

The input signal, represented by the discrete sample time series x(i) sampled at a clock frequency fc , is processed by the polyphase filterbank to provide a number N of output signals, $X'_k(l)$, sampled at a data rate fc/N . The processing is basically a convolution by a

low pass filter, whose finite impulse response is $t(p)$, and is frequency shifted by an amount of $kfc/(2N)$. The resulting $x'(l)$ is then converted to a real quantity by up-shifting it by half a band and k, taking the real part of the result.

Mathematically [22], this corresponds to:

$$X_k(l) = Re\left[\exp(\frac{\pi}{2} i\, l) x'_k(l)\right] \tag{3.1}$$

$$x'_k(i) = \sum_p x(Nl-p)\, t(p) \exp\left(-2\pi i \frac{(Nl-p)k}{2N}\right) \tag{3.2}$$

The input signal is represented, at each cycle j of the output clock, as a set of N parallel samples, x(Nl-p), p = 1 . . . (N - 1). The process can be further decomposed as a set of N convolutions and a Fourier transform of length 2N . The filtered signal is computed only one time with j = N l, i.e. is decimated by a factor N , and the index p for the tap is decomposed as p = q + 2N r, with q = 0, . . . 2N . This gives the well known polyphase filter structure:

$$x'_k(i) = (-1)^{lk} \sum_{q=0}^{2N-1} y_q(l) \exp\left(2\pi i \frac{qk}{2N}\right) \tag{3.3}$$

$$y_q(l) = \sum_r x(Nl-q-2Nr)\, t(q+2Nr) \tag{3.4}$$

The alternating sign in equation 3.4 corresponds to a frequency reversal in odd numbered output channels, and is removed in the conversion to real process. The Fourier transform is performed using the division in time FFT algorithm. The last stage of the algorithm is left out explicitly, as it will be combined in the conversion to real process, i.e. odd and even samples are processed separately by two half length transforms, and then combined together:

$$x'_k(l) = (-1)^{lk} \sum_{q=0}^{N-1} y_{2q}(l) \exp\left(2\pi i \frac{qk}{N}\right) + \sum_{q=0}^{N-1} y_{2q+1}(l) \exp\left(2\pi i \frac{(q+1/2)k}{N}\right) \tag{3.5}$$

$$= z_e^q(l) + \exp\left(2\pi i \frac{k}{2N}\right) z_k^o(l) \tag{3.6}$$

$$z_k^e(l) = \sum_{q=0}^{N-1} y_{2q}(l) \exp\left(2\pi i \frac{qk}{N}\right) \tag{3.7}$$

$$z_k^o(l) = \sum_{q=0}^{N-1} y_{2q+1}(l) \exp\left(2\pi i \frac{qk}{N}\right) \tag{3.8}$$

Only values of $k \leq N$ must be computed, so only one leg of the "butterfly computation" (that with the + sign) needs to be computed, as described in the above equation. As y_q is real, the quantities z_k^e and z_k^o are hermitian, i.e. $z_{N-k} = z_k^*$, where the asterisk denotes the complex conjugate. z_0 and z_N are real. The FFT processor takes N real inputs, and delivers N - 1 complex plus 2 real outputs. From the two complex quantities z_k^e and z_k^o , the equation 3.2 can be written - to compute the two real output signals X_k and X_{N-k} - by considering that $z_{N-k} = z_k^*$.

$$X_k(l) = (-1)^{lk} Re\left(\exp\left(\frac{\pi}{2} i\, l\right)\left[z_k^e(l) + \exp\left(2\pi i \frac{k}{N}\right) z_k^o(l)\right]\right) \tag{3.9}$$

$$X_{N-k}(l) = (-1)^{lk} Re\left(\exp\left(\frac{\pi}{2} i l\right)\left[z_k^{e*}(l) - \exp\left(-2\pi i \frac{k}{N}\right) z_k^{o*}(l)\right]\right) \tag{3.10}$$

In the second relation, we assume that N is even, for simplicity. The first exponential assumes only the values ± 1 and $\pm i$, and the sign can be absorbed in the first factor. The second exponential corresponds to a linear combination of the twiddle factors, $W_k^r = \cos(\pi i k/N)$ and $W_k^i = \sin(\pi i k/N)$. Suffixes r and i are used to denote the real and imaginary parts of the quantities y_k; thus, for l even, we obtain:

$$X_k(l) = (-1)^{lk+a}(y_k^{er}(l) + W_k^r y_k^{er}(l) - W_k^i y_k^{oi}(l) \tag{3.11}$$

$$X_{N-k}(l) = (-1)^{lk+a}(y_k^{er}(l) - W_k^r y_k^{er}(l) + W_k^i y_k^{oi}(l) \tag{3.12}$$

The corresponding relations for l odd are:

$$X_k(l) = (-1)^{lk+a}(-y_k^{ei}(l) - W_k^i y_k^{er}(l) - W_k^r y_k^{oi}(l) \tag{3.13}$$

$$X_{N-k}(l) = (-1)^{lk+a}(y_k^{ei}(l) - W_k^i y_k^{er}(l) - W_k^r y_k^{oi}(l) \tag{3.14}$$

The cases with k=0 and k=N are peculiar: as the input signal is real, the bandwidth is half that of the other channels, and no frequency translation is required. In most applications, these signals are just discarded, because extremes of the input bandwidth are usually also affected by other ill factors (e.g. roll-off and aliasing in the input analog filter). In the case of k=0, the output signal is just the sum of the odd and even samples, $X_0(l) = y_0^o(l) + y_0^e(l)$. The signal is only the first low-pass filtered 1/2N portion of the input band; it is sampled at twice the Nyquist frequency.

3.1.2 Two-stage Polyphase Filter Bank with overlapping spectrometer

The hole between output channels in a conventional polyphase filterbank (see fig. 3.1) is not acceptable for spectroscopic observations. When a filterbank is used for wide-band spectroscopy, a filterbank with overlapping bands has often been used. In this approach [23], the output data rate of the filter is doubled with respect to the minimum required by the Nyquist criterion, i.e. channel spacing is equal to half the data rate, with a 50% overlap between adjacent channels. This allows the channel filter to be designed with wide transition regions, and each portion of the input band is covered by at least one output channel. The overlapping causes however a waste of resources, and various techniques have been used to delete the overlapped regions from subsequent processing. In this design, a spectrometer composed of a two-stage polyphase filterbank, in which a second FFT is performed in parallel over couples of overlapping regions from the first FFT, is designed. The design automatically deletes the unused portions of each region, providing a seamless, uniform channelization of the input band. The system block schematics is shown in 3.3.

After the analog to digital conversion (ADC), the samples of the input signal are parallelized in a deserializer. Time multiplexing factor can be either 8 or 16, for a bandwidth of 0.5 and 1 GHz, respectively. Digital parallel data are sent to a parallel polyphase digital filter bank (PDFB1), which divides the input bandwidth into 8 or 16 overlapping regions, with a

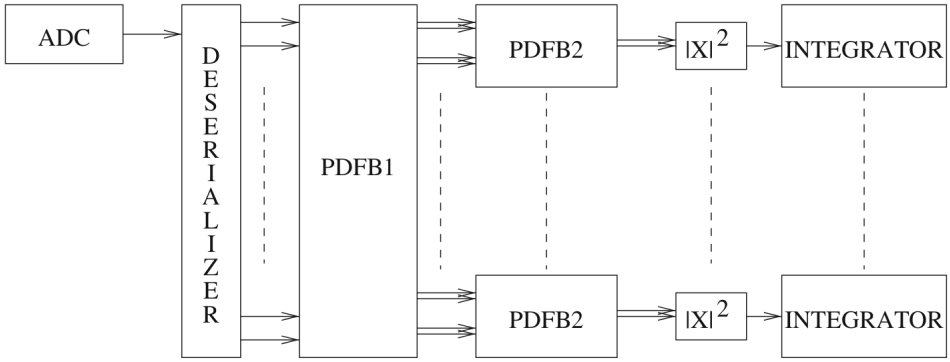

Figure 3.3: *Block diagram of the two-stage polyphase FFT.*

bandwidth of 128 MHz each, and a spacing of 64 MHz. Signals are then analyzed by a serial polyphase digital filter bank (PDFB2) array. PDFB2 outputs are squared, and the total power is integrated in time; thus, we obtain the power spectrum of the input signal. Each PDFB2 block simultaneously computes the spectrum of two PDFB1 channels, and integrates only the central portion of each channel. The first filterbank PDFB1 uses a parallel, decimation-in-time (DIT) FFT architecture, with a FFT length of twice the multiplexing factor (16 points for the 8 channel version), and an output data rate for each channel of 128 MHz. In this way, we achieve an overlapping of 50% between adjacent FFT complex outputs. Only the central 64 MHz of each region is used, thus only this part of the prototype filter needs to be flat, with the stop band beginning at 150% of the Nyquist frequency for the output signal, as shown in fig. 3.4.

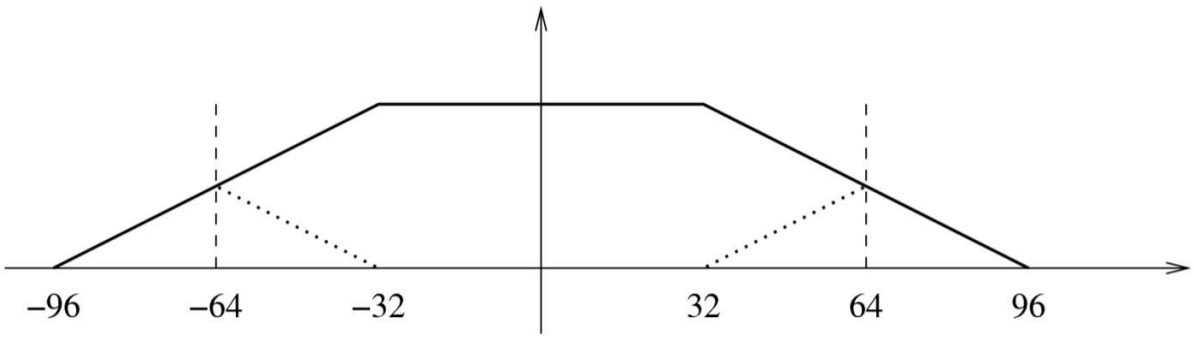

Figure 3.4: *Polyphase filter.*

This drastically reduces the number of taps in the FIR filter architecture: for the 16 channel version, a 64-taps FIR filter has been used with a stopband attenuation of 45 dB. Outputs of the first PDFB are sent in couples to a serial PDFB array. Each PDFB2 block consists of a serial polyphase filter that provides the correct insulation between spectral channels for the next serial decimation-in-frequency FFT engine. The FFT length is 1024 points, of which the central 512 are used, for a total of 4096 spectral points over the input 512 MHz band. The polyphase low-pass filter has 4096 taps; it was designed by extending, in frequency, a smaller FIR filter, computed using the Remez algorithm. It has a passband slightly larger than the channel separation, and an out-of-band rejection of roughly 90 dB. The standard FFT algorithm is able to produce simultaneous spectra from two independent signals because the N-point spectrum of a single signal is calculated in N/2 cycles. The FFT engine provides the two spectra sequentially, with two spectral outputs computed at each clock cycle. In a conventional PDFB, spectra of all the sub-channels are entirely processed and, at the end of the integration, good portions are extracted and stitched together. This wastes a considerable amount of resources, especially memory, for information that is successively discarded. We exploit the parallelism of the FFT engine to discard the unused portions of the spectra as early as possible, thus saving memory and logic resources in the following data processing (correlation, integration). The DIF FFT algorithm produces spectral points in bit reversal order. The two spectral samples computed by the FFT engine at each clock cycle are always spaced exactly by half band, and therefore we have always one sample in the central (good) portion of the spectrum and the other one in the external transition band. Due to the bit reversal order, at each clock cycle, good samples are presented alternately on the two outputs. Therefore, the selection of good portions of the spectra is performed by processing alternately one of the two outputs of the FFT engine for every cycle and discarding the other, as shown in fig. 3.5.

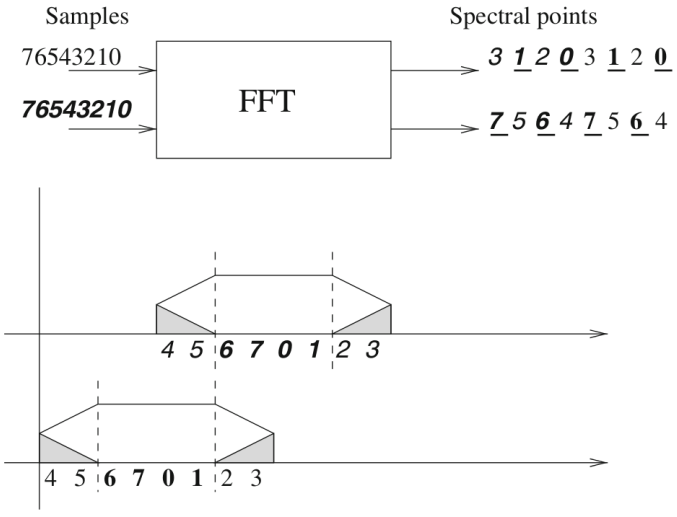

Figure 3.5: *FFT engine.*

3.1.3 An RFI monitoring system based on a wideband digital FFT spectrometer

The infrastructure[24] consists of the wide-band FFT spectrometer (described earlier) operating in piggy-back mode on a copy of the radio astronomical signal, and a Linux-based PC containing the software used for this application. A QT-based program communicates with the spectrometer and with the control software of the antenna: thus, we can retrieve both the spectra and information concerning the telescope status (azimuth, elevation, local oscillator etc). Data are saved and stored in the well-known FITS (Flexible Image Transport System) format, thus a RFI detection algorithm - developed for the Arecibo observatory - is applied. The spectrometer is implemented on the Digital Base Band Converter.

Usually, in radio astronomy, a spectrometer has a conventional configuration, with a single stage polyphase filter bank that splits up the entire input bandwidth into smaller pieces and, whereupon, each channel is squared and summed up for an integer number of FFT cycles. The solution adopted in this approach was to make the two-stage aforementioned described polyphase filter bank. The overflow, in a conventional FFT spectrometer, is a fairly frequent event in the face of uncontrollable radio interferences, particularly with a large number of channels. This is why, in the case of strong and narrow interferences, all of the power is concentrated in a particular channel: the possibility to have an overflow in a certain stage of the FFT engine increases. Due to the possible strong emission like radar or other kinds of radio interferences, the FFT engine could saturate and the entire spectrum goes bad. In this case, instead, the first PFB acts as a "damage limiter", i. e. it distributes the power to different portions of the bandwidth and, if a powerful narrow RFI is present, only the interested sub-band is contaminated and risks being ruined. In other words, that RFI has a negative impact uniquely for the spectrum area containing it, while the rest of the spectrum has no negative consequences. This solution reduces significantly the percentage of unusable data and, in any case, the RFI can be located in a particular spectral zone for a following identification. Clearly, the fact remains that an RFI can be so marked that the first PFB, although in a parallel configuration and with only a few channels, may also saturate.

The control software of the infrastructure has been written in C++ language; it uses a QT 4.8 based framework. Figure 3.6 shows the application GUI.

The application interrogates the antenna's control software - called NURAGHE - via a dedicated server named "external client" that merely makes it possible to retrieve information like azimuth, elevation, local oscillator, etc; the most relevant of them are plotted in the graphical interface.

A QtcpSocket class is used to establish a connection with the NURAGHE server; the string "antennaParameter" is sent to the external client and the received data are parsed. Accordingly with the selected receiver, the corresponding button turns to green (L-band in case of fig. 3.6), and left or right polarization can be chosen. If we push the "START MONITORING" button, apart from the fact that it turns in "STOP MONITORING", a gnuplot script is dynamically created and started up via a process by using a Qprocess class. In order to kill the process, the button must be pushed again. The "Save Data" option must be activated to store the data; in addition, the "Send Data to" option allows us to send spectra and antenna parameters information to a specified client with the corresponding Internet Protocol address. The FITS data converter rewrites the acquired data in a more suitable format for astrophysical purposes. No information is added, just a translation/reorganization of the available data is done in order to compose the final FITS standard format.

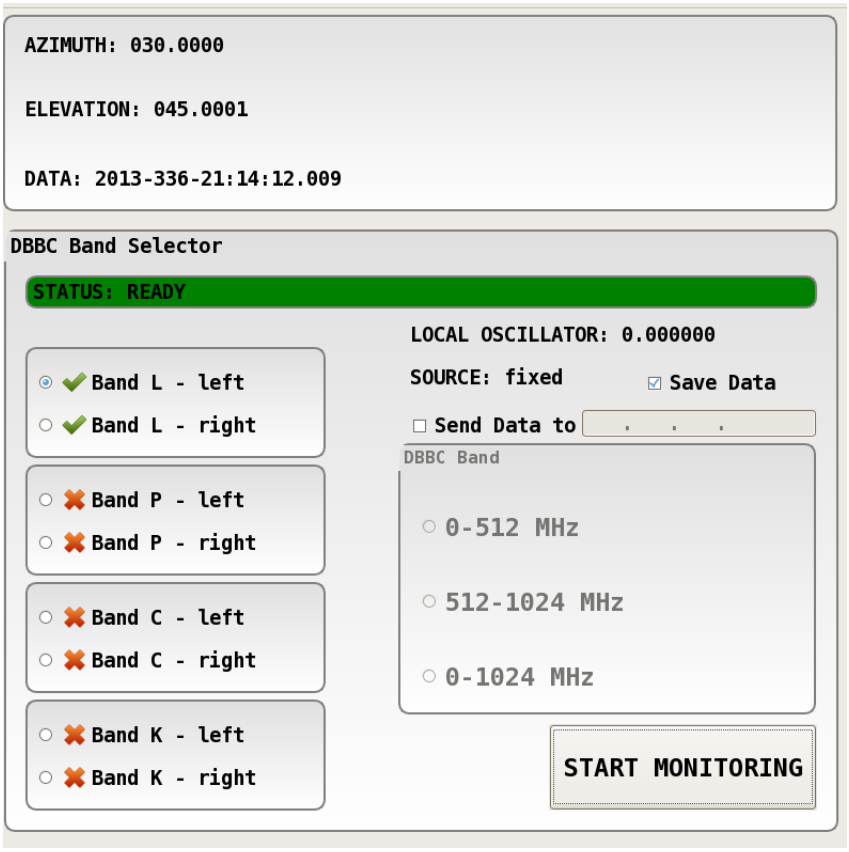

Figure 3.6: *Graphical interface of the RFI application.*

Once data are written in the proper FITS format, we can apply an RFI detection algorithm. We use an algorithm named GALFACTS (G-ALFA Continuum Transit Survey), which is a pipeline able to process the huge amount of spectro-polarimetric data (about 10 TB every 6 observing hours) taken with the Arecibo L-band Feed Array by exploiting the Mock FFT spectrometer. The algorithm detects the presence of an RFI by applying a threshold for each spectral channel; figure 3.7 shows an example with data acquired at SRT.

Data are plotted as time vs frequency RFI flagger for a certain time interval. Each dot represents a sample-time/frequency channel flagged as RFI affected. A percentage of RFI occupancy can also be useful, like shown in fig. 3.8.

The effort spent to make such a system was very useful, over and above the RFI platform, to become familiar with the backends external control mode; indeed, until now, such a technique had never been used. Therefore, this work allow us to figure out the limitations of the external client mode, especially in terms of its feasibility and stability. What we realized is the technical working of this approach with limited spectra rates - of the order of ten dumps in a second -, but the conventional socket connection is not quite efficient; in terms of data rate, demands is ten times greater at least, we understood that this solution could not be good for astronomical purposes.

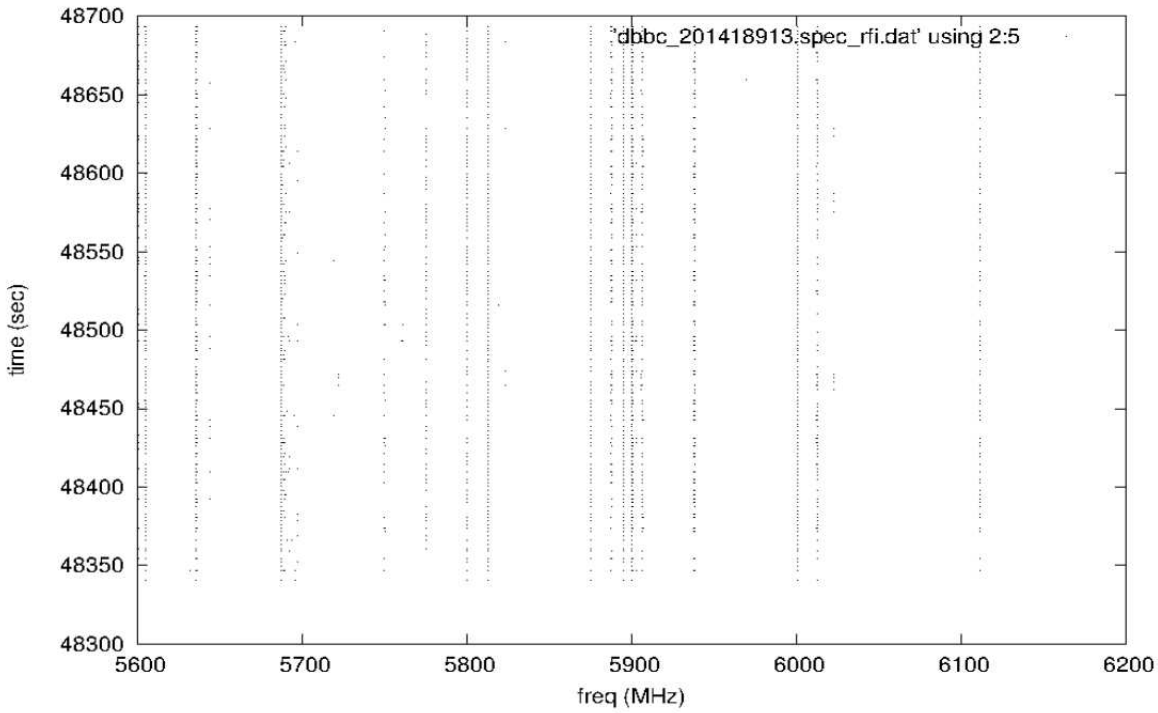

Figure 3.7: *RFI flag plot.*

3.2 Hybrid approach

The SRT monitoring RFI station is, at the moment, the only one of its kind in the world. Figure 3.9 shows a block diagram of the system.

The front-end section consists of a log-periodic antenna, twin rotors (two axes of movement: horizontal, to change the polarization, and vertical for the azimuth orientation) and a RF preconditioning box, all of them are placed on top of a self-supporting tower that is 12 meters high. The back-end is equipped with several devices and radio-frequency instrumentation like a spectrum analyzer and a wide-band receiver. In addition, there are two controllers: the first one is used for RF front-end preconditioning module, while the second is used for the complete movement of the antenna. Finally, a personal computer controlling the entire system is available.

In order to highlight the two different areas, a dotted line is used: the first one is located on the tower, while the second one on the ground, inside of a dedicated infrastructure for RFI monitoring. The front-end equipment is connected by coaxial (low loss) and multi-pole cables to provide supply and all of the control signals. The overall system works 24 hours a day. It monitors, alternately, P, L and S band spectra band. A rotor controller is used to change direction and polarization of the antenna, while the "Box Front-end" (BFE) allow the band selection. These operations can be done simultaneously, either manually or via PC by exploiting both the controllers (via C2 and C3 cable). Once the BFE is configured cor-

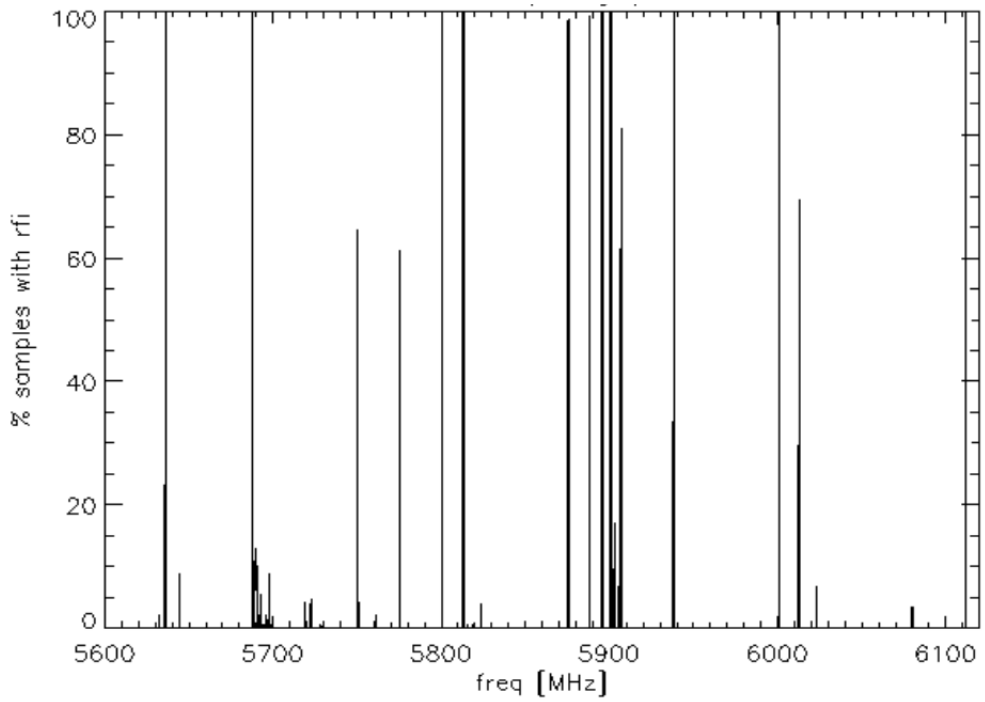

Figure 3.8: *RFI occupancy (example in C band).*

rectly, the RF signal is sent (via the Coax Tower 1), and we can do the proper filtering and signal amplification; thus, the conditioned signal is transferred (Coax Tower 2) to the back-end. Here, the signal is split up and sent to the spectrum analyzer (COAX 3) and to the wide band receiver (COAX 4). Simultaneous acquisitions by both systems is not mandatory, but simplifies the analysis regarding what is being received. The data of signal demodulation -produced by the spectrum analyzer- is sent to the PC (through C1) within which some information (amplitude, frequency, spectrum density, max peak etc.) are displayed and stored for post-processing. The antenna positioning, the setup of the selected BFE channel and spectrum analyzer parameters must be included on the data before its storing. Figure 3.10 shows the control panel of the insfrastructure.

A 64-meter radio telescope has a sensibility unreachable by an RFI station, thus the main goal we focused on has consisted in how these differences can be exploited in concrete terms. A telescope like SRT works on several scientific fronts, both single dish mode and collaborating with other antennas. While during an interferometric observation, the observer cannot do anything even if he sees a RFI, for a single dish observational session things are different. Observers wish to avoid radio interferences as much as they can, and real-time RFI monitoring represents crucial information. If that is the case, a synergy between available systems is desirable, and we describe it in this section.

The first contact in this regard is the data from the DBBC: figure 3.11 shows the ideal L-band receiver bandwidth at SRT, i. e. with the passband with no interferences; a visual verification allows the observer to evaluate the presence of interferences immediately. The

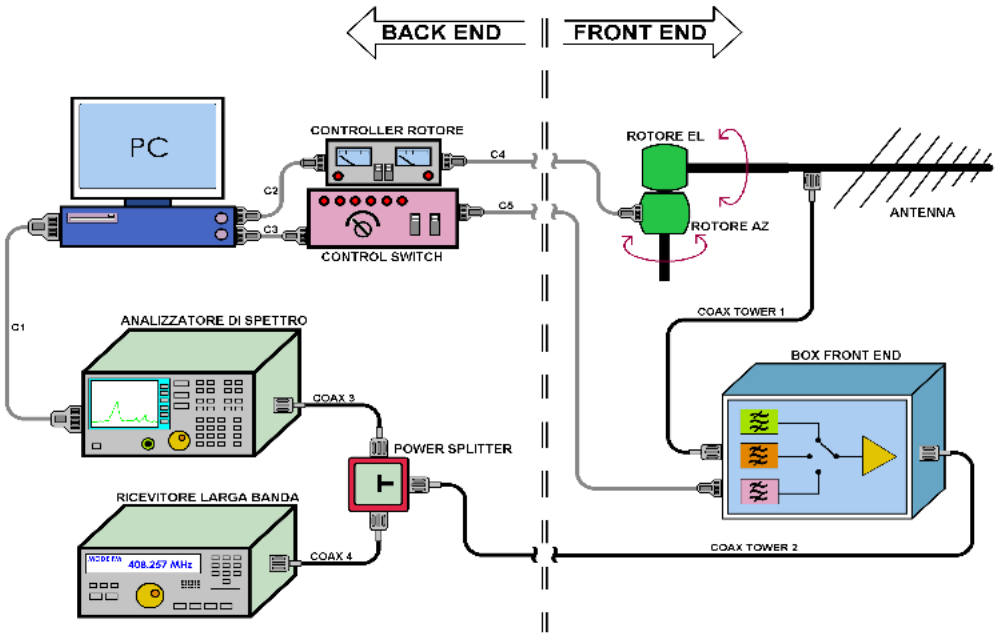

Figure 3.9: *The automatic wide-band radio-frequency monitoring RFI for the SRT.*

uniform passband provided by the spectrometer, as shown, is quite clear: no “interrupts” are present inside the profile, although the spectrum was broken and then built back.

The reference point is the ideal passband for each receiver; the spectrometer runs in real time so that gives clear indications about eventual interferences. Data are plotted in the control room of the telescope and sent to the PC controlling RFI station; the first step in this effort is to establish how great the difference between these data is. Thus, we can draw the appropriate conclusions on the fact that each interference regards strong interference (present in both spectra) or not (only in the DBBC spectra). With this as a starting point, the station checks an RFI database to establish whether or not a certain RFI already exists. If it does not produce positive results, the RFI has to be investigated and identified by a mobile station with the assistance of a spectrum analyzer.

This type of situation can require two types of measurements: the first one whether the DBBC is capable of detecting every detail of the interference; in this case, no additional information have to be reported to the observer. The second is adopted in case the earlier situation does not occur, thus an in-depth analysis has to be carried out by experts in order to investigate the problem and report it as soon as possible.

3.2.1 Results

In this paragraph, we describe a real-time interaction between the two aforementioned systems[25]. The DBBC interacts with the control software of the SRT, called NURAGHE, as

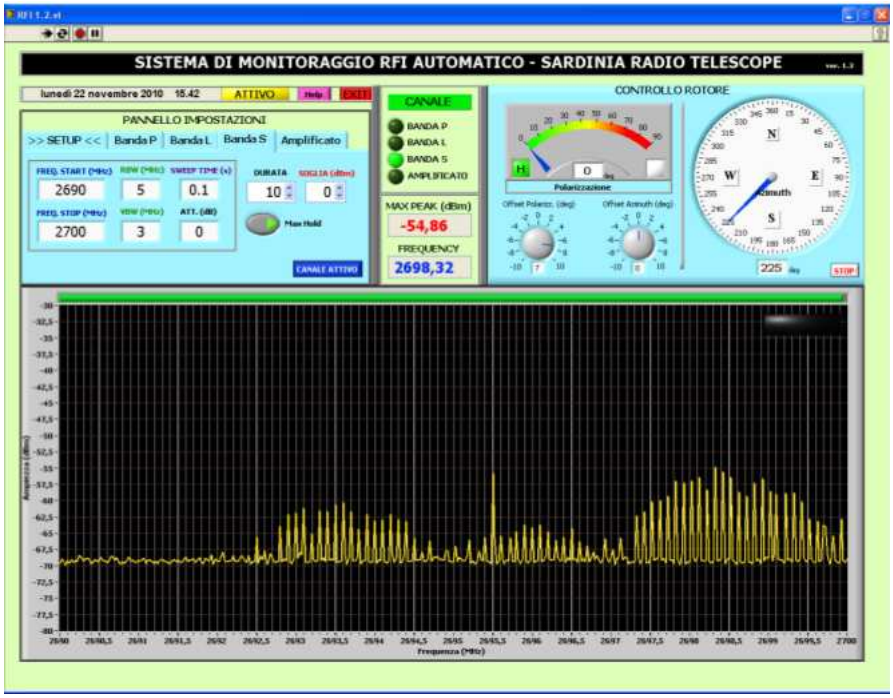

Figure 3.10: *Control panel of the RFI system.*

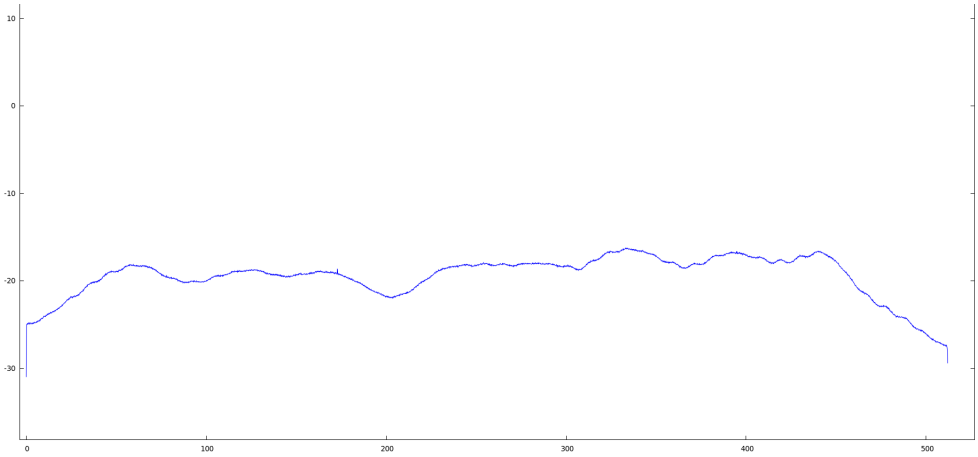

Figure 3.11: *Ideal L-band at SRT.*

external client in piggy-back mode, essentially. NURAGHE is being interrogated once per second in order to get the necessary information: azimuth, elevation, local oscillator etc. The rotor is moved to the same telescope azimuth direction and, automatically, the polarization of the signal is checked (V, H or circular), thus we are sure that the spectra are as coherent as possible. Although the telescope is pointing to the sky, it "captures" the RFI because is able to receive signals from the horizon. That is due to multiple causes: the antenna's side lobes, signals bouncings between the metal structure (quadrupode for example) as well as the land's orography. It is worth noting that, outside of the main beam, the sensibility of the telescope is drammatically reduced (comparable to that of the RFI station), but the telescope

is still able to receive interfering signals from the horizon. It is actually quite difficult to thoroughly forecast the telescope elevation's degrees for which signals from the horizon can be "seen" by the paraboloid; this is mainly due to the dependency between main lobe and the first side lobe when the frequency varies, and the uncertainty of the bouncing effect. The main search regards common "peaks", which can immediately be reported in control room to the astronomer. On this basis, the coordination between the SRT and the RFI monitoring, basically consisting in a real-time comparison of corresponding spectra, can help.

A short comparison test between the two systems was done at the SRT site. The azimuth and elevation of the telescope were 45 and 320 degrees respectively, while the RFI station antenna was, contemporaneously, pointed to the horizon at the same elevation of the telescope. Figure 3.12 shows the plots of the L-band spectra taken, simultaneously, with the two systems.

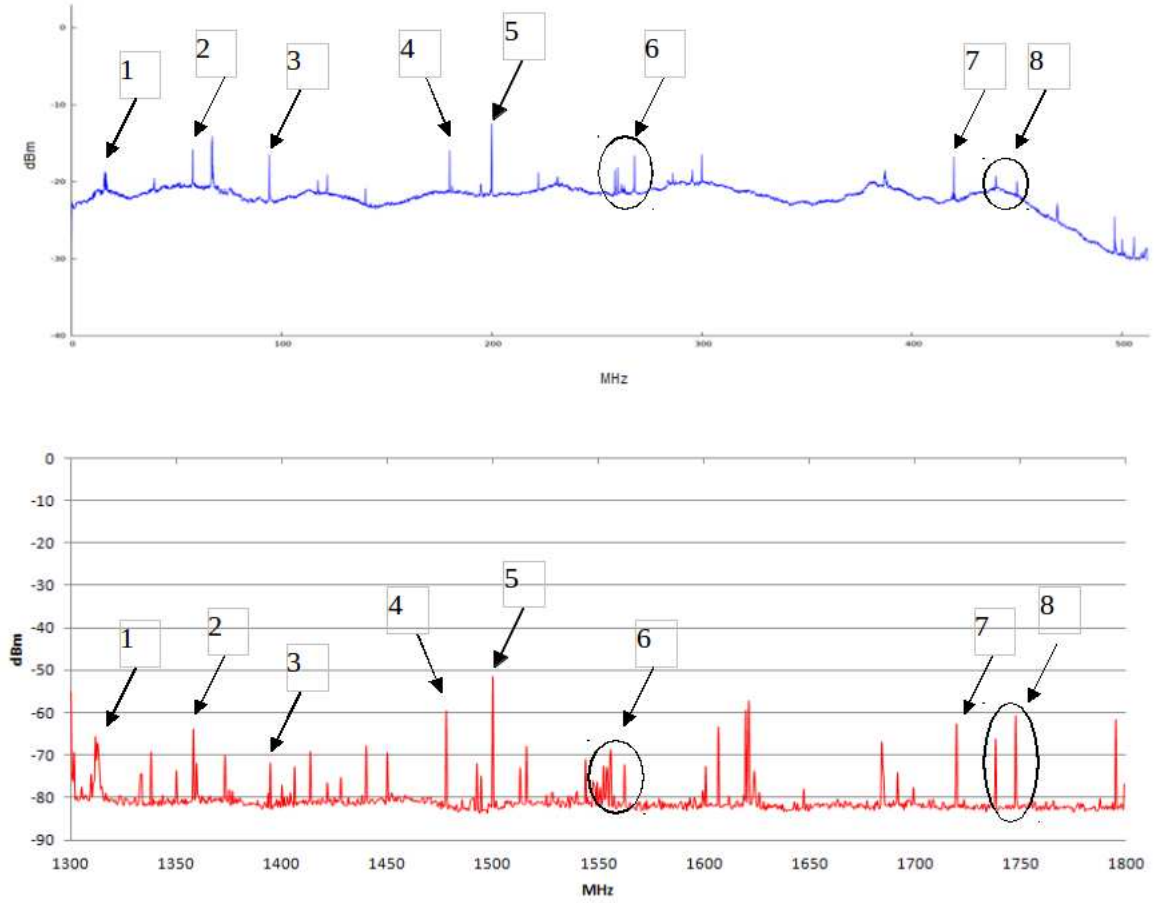

Figure 3.12: *DBBC (upper plot) and RFI station (lower plot) spectra.*

A considerable number of common radio frequencies are easily recognizable. The lower trace is the spectrum taken from the RFI station, while the upper one regards the DBBC. The L-band, which works in the sky frequency range 1300 - 1800 MHz, is first moved on the interval 500 - 1000 MHz and then base-band converted by analog-to-digital converter operating in its second Nyquist window; therefore, the interval 0 - 512 MHz - indicated on the X-axis

of the upper plot - corresponds to the same of the lower plot (1300 - 1800 MHz). Due to the different receiving and conditioning RF chains, the two signal levels have large discrepancies; however, this does not undermine the proper functioning of the entire system. Black arrows (numbered 1 to 8) refer to the detected signals from both systems. Signals numbered 1, 2, 3 regard the carrier and corresponding spurious of a radar placed 70 km from the SRT site. Signals 4, 5, 6 are digital links while 7, 8 are signals coming from cellular phones in the DCS uplink band. As can be clearly noticed, not all signals have simultaneously being seen since they depend on both the position and the type of signal itself. In fact, SRT alone receives some weaks signals, predominantly due to electronic devices with which the telescope is equipped; these signals, always present regardless the telescope's pointing, can be identified as "RF spikes" immediately. On the other hand, the RFI station may has a greater sensibility at the horizon than the telescope, therefore other signals are detected, exclusively, by a log-periodic antenna. For a complete monitoring of the telescope site, the hybrid approach described above is therefore essential, especially during low-frequency single-dish observations.

In general, we wish to avoid the burden due to already known RFIs. Current developing works must necessarily be done to provide a "clever" queried database exploitable to avoid well known interference that can certainly ruin or degrade radio astronomical observations. The goal is to make a dynamic scheduling that deals with the RFI occupancy regarding frequency, the period in the year, the telescope's pointing and so on.

Chapter 4

SARDARA: SArdinia Roach2-based Digital Architecture for Radio Astronomy

SARDARA is the acronym for "SArdinia Roach2-based Digital Architecture for Radio Astronomy". As mentioned in chapter 2, SRT is equipped with a variety of digital platforms that are applicable to a significant amount of scientific studies. However, they present both pros and cons: the Total Power backend is the only backend capable of processing the entire bandwidth (2.1 GHz) and all (up to) 14 IFs, but can be used solely for continuum studies; XARCOS can act as a full-Stokes spectrometer, but 125 MHz is the widest available bandwidth; the DFB can be used as a spectro-polarimeter as well and with a greater instantaneous bandwidth (1 GHz) than XARCOS, but only 4 IFs are available. What is lacking is an infrastructure that can combine the aforementioned characteristics; in particular, the ideal system for SRT should be able to meet the following requirements:

- Up to 14 IFs simultaneously
- Up to 2.1 GHz of bandwidth for each IF
- Full reconfigurability and adaptability for all scientific requirements

To accomplish these goals, as a starting point we chose to use the new ROACH2[26] boards developed by the CASPER[27] consortium (Collaboration for Astronomy Signal Processing and Electronic Research). A Xilinx Virtex 6 FPGA is the centerpiece of the boards, and the available ADCs[28] - with a sampling time of 5 GSample/s - allow us to obtain a bandwidth as large as 2.5 GHz. This fits the requirements listed above perfectly. Moreover, two SFP (Small Form-factor Pluggable)+ mezzanine cards[29] can be used to sent out up to 80 Gbit/sec to recording or post-processing systems. In this chapter, after a brief presentation of the boards, we discuss the peculiarity of the entire infrastructure that has been thought, and in particular how it can be used for various scientific applications, pointing out all of the enhancements compared to the previous approach (dedicated machines for targeted projects). As we will explain, improvements were made in: data processing management, possibility to work with wide uniform bandwidths without waste of resources, an easier and

quicker integration into the control software of the telescope (notoriously one of the major issues) and, finally, the possibility to do different parallel signal processing on the same intermediate frequency signals acquired with the telescope (very important in the case of piggyback research like fast radio burst or search for extraterrestrial life).

4.1 ROACH2 boards

The ROACH2 is a stand-alone FPGA-based board that represents the successor to the original ROACH board we already mentioned in chapter 2. Figure 4.1 shows a block diagram of the board.

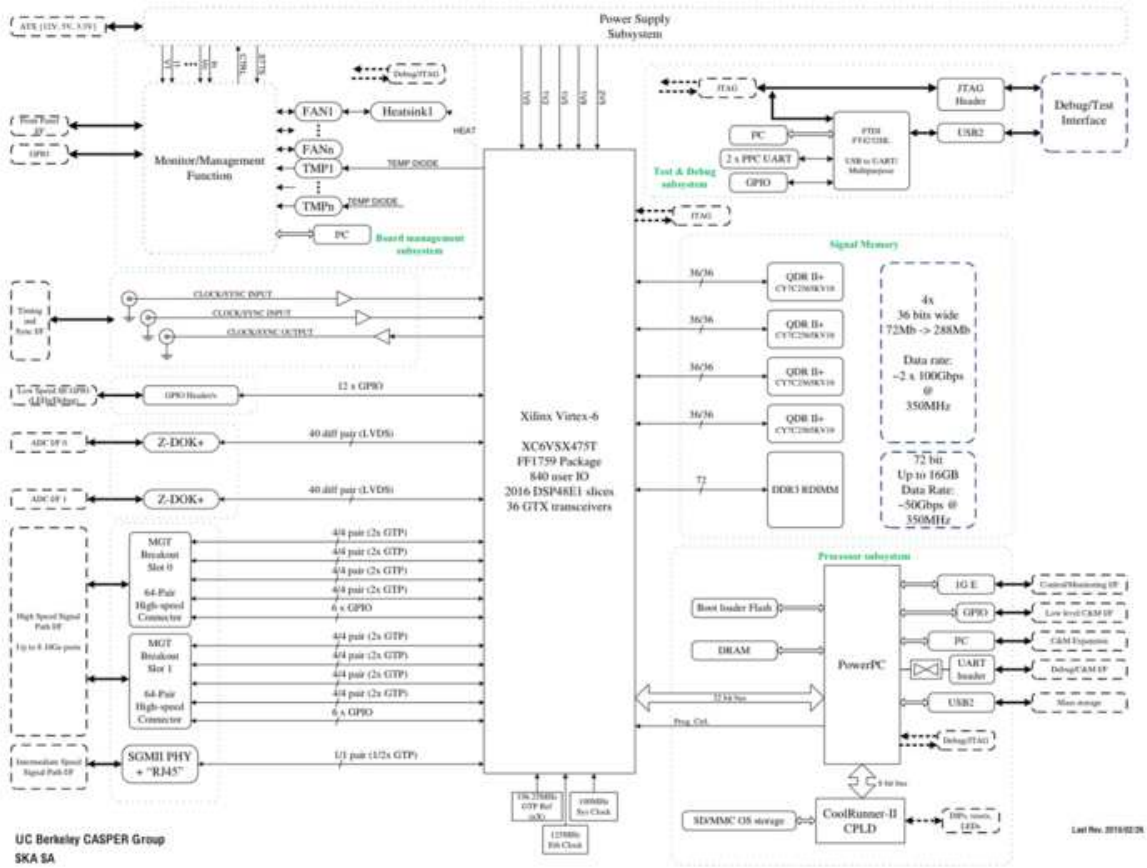

Figure 4.1: *ROACH2's block diagram.*

The ROACH2 has, as a centerpiece, a Xilinx Virtex6 FPGA (ROACH has a Virtex5 one), it maintains all of the aspects that made the ROACH a success, but increases the overall performance in terms of processing power, I/O throughput and memory bandwidth. The PowerPC 440EPx, used to control the board, is the same present on the ROACH but adds an unified JTAG interface provided through a FTDI FT4232H IC. The main features of the board are the following:

- Virtex-6 SX475T FPGA (XC6VSX475T-1FFG1759C)

- PowerPC 440EPx stand-alone processor to provide control functions
- 2 x Multi-gigabit transceiver break out card slots, supporting up to 8x10Ge links which may be CX4 or SFP+
- 4 x 36 * 2M QDR II+ SRAMs connected to the FPGA
- A single 72-bit DDR3 RDIMM slot connected to the FPGA
- 2 x ZDOKs
- An FTDI FT4232H USB to JTAG, serial and IIC

The configuration for our project has two multi-gigabit transceiver mezzanine cards SFP+ with which up to 80 Gbit/sec can be sent out. Concerning high-speed ADCs, we have installed, to the ZDOK connectors, two ADC boards that are able to manage up to 5 GS/s with a representation of 8 bit for each sample. The ADC board has 4 cores that operate in interleaving mode: two for each IF in the 2-inputs mode (maximum bandwidth: 1.25 GHz) and four for each IF in the 1-input mode (maximum bandwidth: 2.5 GHz). The latter mode is the one employed for this thesis.

Figure 4.2 shows a picture of a complete ROACH2. We can notice four available SMA (SubMiniature version A) inputs for each ADC board: two of them accept IFs (although in our case just a single signal is injected) whereas other ones accept the sampling clock (provided by an unexpensive synthesizer) and 1 PPS (Peak Per Second) signals.

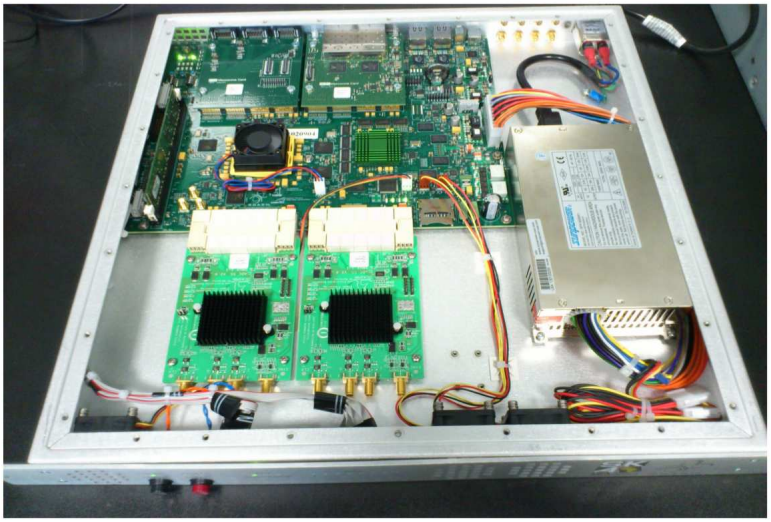

Figure 4.2: *ROACH2.*

The same clock source is sent to both clock inputs via a 2-ways splitter in order to obtain the highest degree of synchronization (especially in the case of polarimetry and pulsar

science); as far as the PPS, on the contrary, two dedicated PPS signals (provided by a proper distributor) can be used.

4.2 SARDARA infrastructure

As the name suggests, the beating heart of the architecture are the ROACH2 boards. They were chosen for different reasons: they are reconfigurable and suitable for the wide required bandwidth (2.1 GHz), moreover we are part of CASPER (Collaboration for Astronomy Signal Processing and Electronic Research), namely a consortium where the motto is "hardware and software are open source" and - this is far from unimportant - the marketing of the boards works well. All of these factors are pointing in the right direction to create the basis for the formation of a multi-purpose platform that goes against the trend compared to the past. Figure 4.3 shows a block diagram of SARDARA.

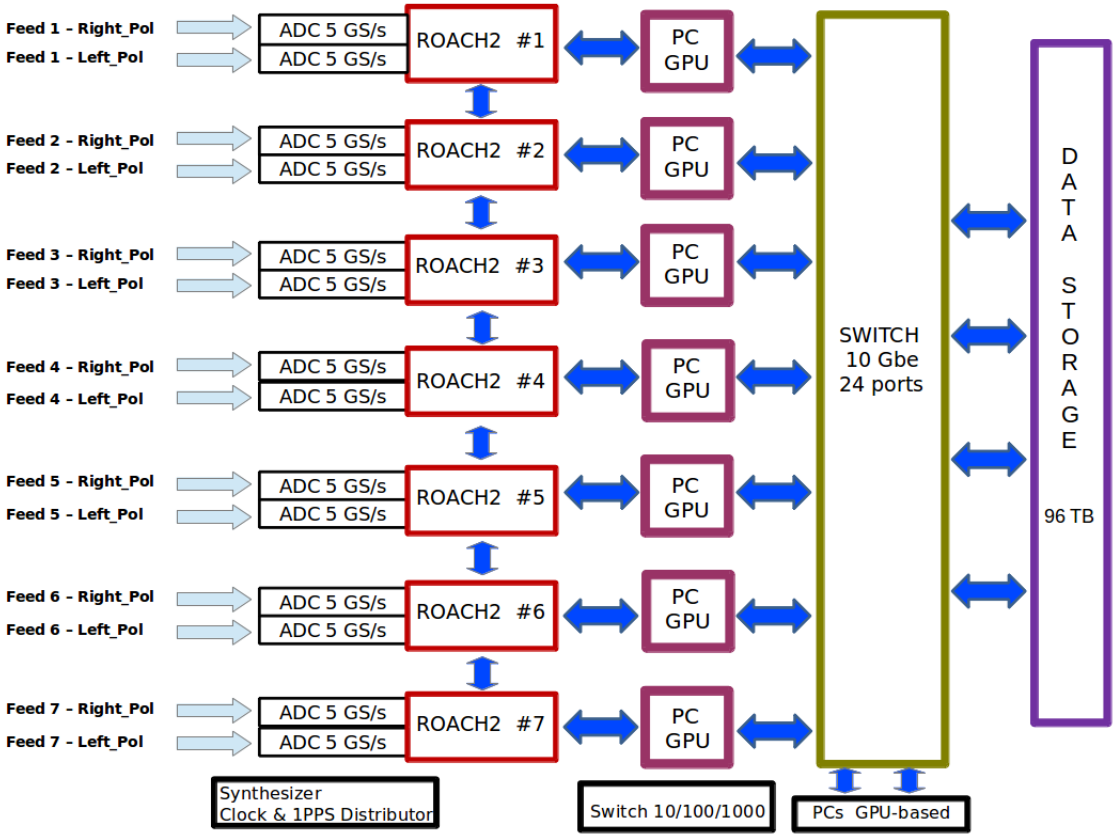

Figure 4.3: *SARDARA's block diagram.*

The whole system consists of eight ROACH2 boards (one of them is a spare), each board being equipped with two 5 GSample/s ADCs. Eight outputs of the mezzanine cards are used (via optical fibers) to connect each ROACH2 board to all of the others and to a GPU-based PC, in which a dual-port SFP+ 10 Gbe is installed. A 24-port SFP+ 10 Gbe is also used to interface PCs with a 96 TB data storage unit. Regardless processing boards that are only the starting point, what is crucial is how these boards can communicate for data exchange and

processing. The basic idea is to make a fully reconfigurable architecture, which is able to cover all of possible scientific requirements a single-dish radio telescope can satisfy. They can be summed up in the following:

- Continuum
- Polarimetry
- Spectro-polarimetry
- Wide and Narrow band spectroscopy
- Pulsar
- Fast Radio Bursts
- Search for ExtraTerrestrial Intelligence

Unfortunately, the current SRT apparatus box does not allow us to install all of the infrastructure shown in fig. 4.3; new building and offices are going to be available at the end of 2016, therefore all of the technological and scientific validation of SARDARA is related to a single chain ROACH2-GPU. Nonetheless, we got very impressive scientific results that we describe in chapter 6.

Over and above that, features that make the concept behind SARDARA innovative are here considered and examinated. They can be summed up in the following:

- An innovative technique for the telescope control software integration
- Possibility to obtain a wideband spectrometer with very high frequency resolution without loss of spectral information
- Possibility to operate, in piggy-back mode, different algorithms for the search for signature's life

In the next sections, the first two items are described in detail, while the following chapter is dedicated to the SETI (Search for ExtraTerrestrial Intelligence) project.

4.2.1 A very fast method for telescope's control software integration

Digital backend integration represents one of the most complicated tasks in the context of a radio telescope control software. As the final stage in the receiving chain, data produced by every backend must include overall information concerning the antenna and the ongoing observation, moreover each backend has its own special features that we must bear in mind.

The control software at Italian radio telescopes is (SRT, Medicina) or will be soon (Noto) based on the framework ALMA Common Software[30] (ACS), namely the one employed at Atacama Large Millimeter Array telescope[31]. Even if a single-dish telescope is completely different from an array of antennas like ALMA (especially for data processing), the versatility of ACS lead us to use it in any case[32]. For instance, besides Italian antennas, it is employed at the Yebes radio telescope[33] as well.

One of the major control software tasks is the so-called FitsWriter, i. e. the component that retrieves information from other ones (in order to generate the header file) and uses the Bulk Data Transfer[34] (BDT) to get the data from each backend and then insert them into the FITS file. However, the main ACS BDT's criticism is the limitation concerning the data rate, currently 80 Mbit/sec; this is absolutely unsuitable in the case of new digital platforms, instead capable of providing up to tens of Gbit/sec (80 in the case of ROACH2 boards). Beyond the kind of infrastructure software that manages the telescope, experience has now taught us that the way a digital backend fully integrated in the control software ACS-based takes a very long time. The reason for its slowness is intrinsically due to the fact that FITS files must contain a lot of information from different components software, therefore a notable effort is needed to ascertain that they are exactly what they should and contain what is expected. Moreover, most modern backends can produce an unmanageable flood of data. Albeit the software controlling the telescope is distributed (it is based on CORBA), a central computer deal with the FITS file finalizer, therefore data produced by the interested backend must be sent to it. This forces us to change the approach we have taken until now by trying, at the same time, to make this job easier and faster than in the past.

The approach conceived for SARDARA follows an opposite trend. In particular, it distinguishes neatly the antenna's parameters and the software controlling the telescope, as if they were two entity acting on their own. The only thing necessary to allow such a independent approach is the overall synchronization of the two systems; this is done via an NTP server available to the telescope site and locked to the MASER.

The following paragraphs describe what happens to the side antenna, side backend and, then, how the overall merging is properly made.

Antenna side

In the case of ordinary ACS backend integration, the control software is fully responsible for everything, which includes the retrieving of data produced by the backend. On the contrary, in this new approach, the control software works independently, i. e. does not care about what the backend does, except start and stop commands, configuration and little else. Basically, the control software gets, at a rate corresponding to the one set as the time integration, all ancillary information traditionally present in a FITS file. The FITS files generated are exactly the final ones except the field that should contain data, filled up with zeroes. Clearly, it is also not easy to retrieve overall information regarding the antenna status when it is often requested. However, as we will see later, the number of different time-stamps is very important just for on-the-fly mappings, and in the case of the K-band receiver, 100 spectra/sec (and, then, 100 different pixel on the sky) is good enough. This value is not an issue for the current control software. Even if in the case of pulsar observations, the dump-time required is notably higher, this technique is perfectly exploitable for pulsar observations as well, although this kind of science is not in on-the-fly mode

This type of solution can be done essentially in different ways: we can exploit an already existing and working backend or not. The former is very useful for backends under development: astronomers can immediately exploit the ongoing development providing, among other things, useful feedback to the developers.

Within a short time, all three Italian radio telescopes (Medicina, Noto, SRT) will have the same control software and the same "main" Total Power backend, also acting as a focus selector platform. It is the best known and time-tested system, as well as the most reliable,

therefore it has been used as a point of reference. The minimum dump time permitted is roughly 1 ms, i. e. up to a thousand of different acquisitions in a second can be registered and stored into a FITS file. As said earlier, 100 dump/sec represents the worst case at the moment at SRT (in particular for the K-band); this means that the maximum timing error is of the order of 0.5 ms in the case of "parallel" acquisition made by another back-end; such a tiny value is perfectly reasonable. This opens up the whole idea of exploiting this opportunity. Essentially, the "secondary" digital backend works independently, data are retrieved by a PC synchronized with the control software, and time-stamps are written just before taking the data. All achieved results during this thesis were obtained with this technique.

Once the backend is well tested and can be considered reliable, it must be fully integrated into the software controlling the telescope. As mentioned earlier, the control software provides all of the ancillar informations regarding the telescope status by filling up a "no-data" FITS file. Figure 4.4 shows an instance of such scenario. Panels on the left show the FITS skeleton in which one can notice all information retrieved by the control software and then written into the file; the panel on the right shows the "absent" spectra.

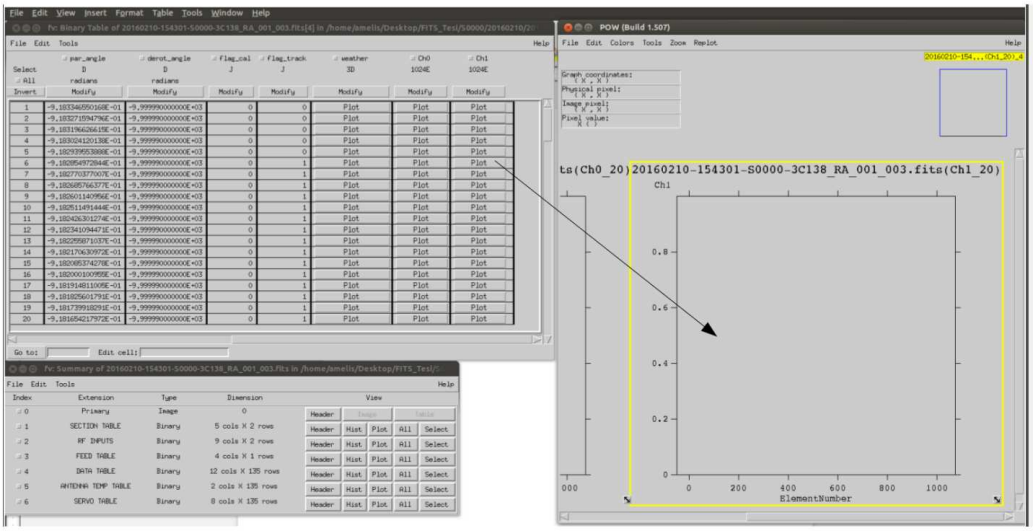

Figure 4.4: *FITS containing only ancillar informations from the telescope (no astronomical data).*

Backend side

The most advantage of this approach compared to the traditional one regards backend management. In fact, the handling and the storing of the data are entirely "on board": all of the complicated and dangerous data exchange between nodes involving the software controlling the telescope are avoided. The high-speed data, coming from ROACH2 boards via optical fiber, have a binary representation and, theoretically, can be immediately stored. However, in order to check the proper working of the data acquisition, they are written in a fictitious FITS file format that contains only the data, i.e. spectral points provided by the spectrometer running in the ROACH2. Figure 4.5 shows such an intermediate FITS file.

In this case, the personality employed consists in a spectrometer that works in a bandwidth 1500 MHz large and provides 4096 channels: the first half correspond to the auto-

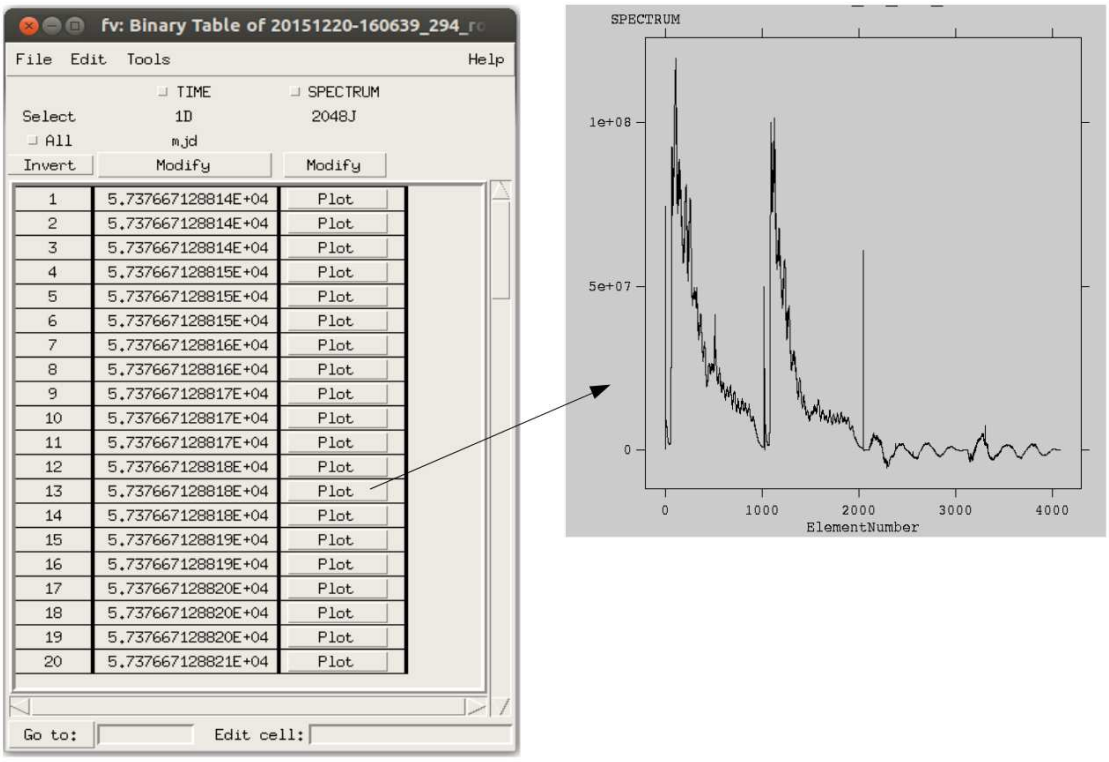

Figure 4.5: *FITS containing only astronomical data.*

correlations of left and right polarization during a C-band observation, while the rest represents cross-correlations. The most important aspect is the time-stamp assigned to the data, and in particular to each spectrum. This is why the time is the unique point of connection between ROACH2s and the rest of the telescope environment. In fact, once the data acquisition starts, the node controlling the corresponding ROACH2 works virtually in full autonomy.

Merging

Incomplete FITS files produced by antenna and backend are, finally, merged in order to get the final FITS files. When we tried to test the merging method, it was not automatical that this solution would have worked, particularly given the subject was never tried before. Usually, although in several ways, the control software acts as coordinator within systems that compose the overall infrastructure. This often represents the only choice in radio astronomy because the concept of time is crucial, especially when more than a single telescope is involved, e.g. for the LEAP or VLBI projects. Single-dish observations, being “home made”, have more degrees of freedom on this matter, therefore we have explored the possibility to maintain the independence of the backend as much as we can. Figure 4.6 shows the first successful experiment; the general working is confirmed also visually.

The algorithm adopted to perform the merge is quite simple: a pipeline software check the time correspondance between FITS files. The time-stamp provided by the control software is related to the start of each dump, while the time assigned to the final FITS must be moved up a half time-period in order to reduce, as far as possible, (even if minimal) in-

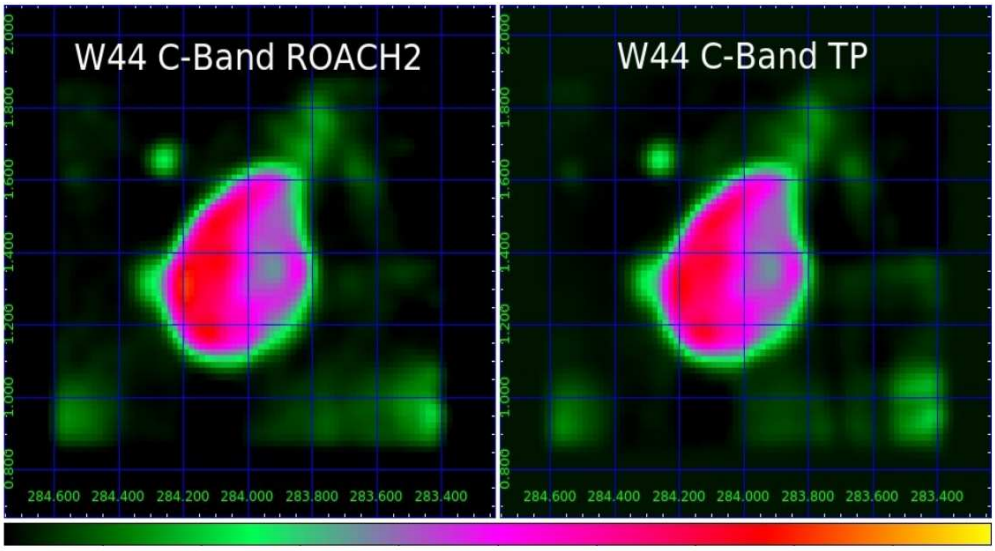

Figure 4.6: *SNR W44 in C band observed, simultaneously, with Total Power and SARDARA. Credits by A. Pellizzoni, E. Egron, N. Iacolina, A. Trois, M. Bachetti on behalf of the team of the project Tender-7*

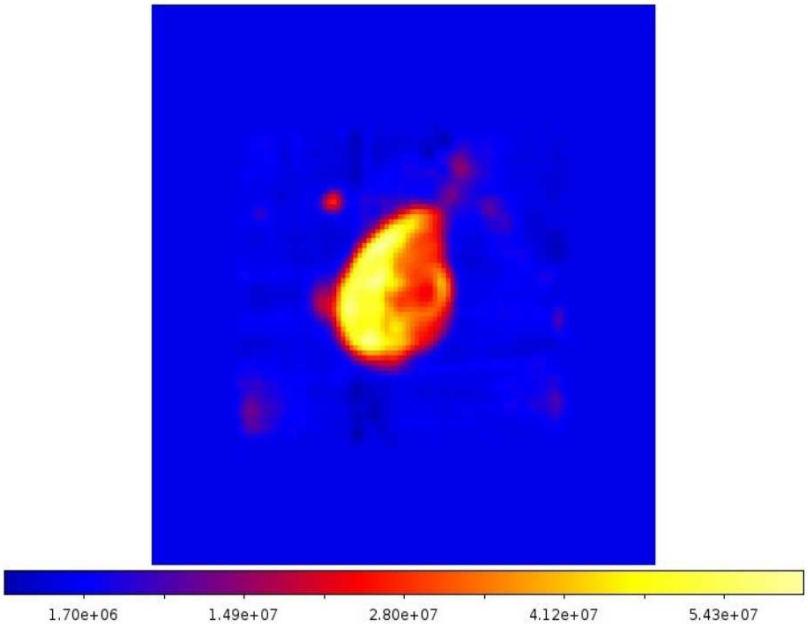

Figure 4.7: *SNR W44 in C band observed with SARDARA that acquires at 9 spectra/sec. Credits by A. Pellizzoni, E. Egron, N. Iacolina, A. Trois, M. Bachetti on behalf of the team of the project Tender-7*

evitable errors. On the other hand, this is a better interpretation because a single sky pixel must be positioned in the centre of an integrated period, not at the beginning.

With regard to figure 4.6, the dump time is 100 spectra/sec, namely the worst case as

already said; on one hand, this demonstrated the global working of the approach proposed. Furthermore, with a reduced dump time the possible committed error increase, however we tried to slow down the dump time up to 9 spectra/sec with no problems whatsoever; figure 4.7 shows the SNR W44 observed with such a scenario.

More generally, this new approach is an authentic manna from heaven for people involved in digital back-ends development. By virtue of the software controlling the telescope, the testing and developing of new systems is almost impossible once a telescope (like SRT) is offered to the international community. In fact, with the precedent technique, the entire availability as well as the functioning of the telescope were strictly necessary: without this, even if just a single part of the telescope is not "active", the FITS file cannot be built. The proposed solution makes it possible to develop a new instrumentation exploiting the piggy-back mode, not only permitting that the telescope be equipped with the most modern technology, but also allowing us to do that in a trasparent and efficient way, by avoiding any waste of the most valuable resource: telescope time.

4.2.2 Wideband lossless high resolution spectrometer

Ideally, in radio astronomy, the optimal backend configuration should be able to acquire and to process, for all of the feeds available by a generic receiver, the entire bandwidth provided and, at the same time, the highest possible frequency resolution of the order of fractions of Hz if required. Actually, very often, a compromise between wide bandwidth and high frequency resolution is a choice that must be made; this is mainly due to limitations in terms of digital signal processing resource available. In order to reach wide instantaneous bandwidths (of the order of a few GHz) provided by most modern receivers, digital boards based on FPGAs are essential. This is why, at present, this technology is the best solution to deal with the huge flood of data required, in accord with the Nyquist thorem. On the other hand, although the resource available on new generation FPGAs are continuously increasing, is not possible to develop overall on-chip wide-band spectrometers with a number of channels beyond a few tens of thousand. Accordingly, we cannot obtain enough accuracy in terms of spectral resolution so as to study sources like, for instance, MASER or more generally the ones in which more features are emitted in a few KHz. In such applications, the so-called "narrow band" approach must, of necessity, be used. In short, a bandwidth's portion is chosen by a digital filter and downconverted in base band; thus, either a spectrometer acting on this reduced bandwidth is directly implemented on FPGA, or an its software implementation is done after that the data are sent to a GPU-based PC.

In order to obtain a wide bandwidth in conjunction with high frequency resolution, the signal can be divided into a relative few number of sub-bands, then properly processed individually (or in a couple) on a dedicated spectrometer on PC or, eventually, in other DSP boards. Finally, all of the partial spectra can be stitched together so as to compose the final spectrum. To do so, the polyphase filter bank technique is one of the best solutions and is almost always being used. However, although the very high efficient channel-to-channel isolation, this technique cannot guarantee a final perfectly uniform channelized bandwidth; namely spectral "holes", even if minimals, are unavoidable.

In this section, we describe how we exploit the SARDARA infrastructure to overtake and to solve this issue permitting, at the same time, wide bandwidth and high frequency resolution.

This work is the natural outcome of the one described in chapter 3 regarding RFI solution.

The need was, in that case, to make a configuration able to achieve a spectrometer stronger from an RFI viewpoint. The adopted solution was to implement a two-stage polyphase filter bank (PFB): the first parallel PFB is responsible for splitting up a wide bandwidth into a certain number of sub-bands, while a set of second serial PFBs by process them. The peculiar features of the entire infrastructure was the forcefullness regarding RFI mitigation (a strong RFI decay just the corresponding sub-band provided by the first PFB, no side effects will result in the other portions of the bandwidth) and the capability to firstly broken up (via the first PFB) and then reconstructs the input signal in the frequency domain with no band's interrupts. In particular, the latter is possible by using a 50% overlapping in the first PFB as well as a digital filter with a proper shape. Moreover, if we employ a proper FFT engine in the second PFB, an automatic selection of the useful bandwidth can be done.

An FPGA implementation of this approach was developed for the DBBC platform, and a maximum of two sub-bands 128 MHz each fit the resource available with a modest number of channels (resolution 125 KHz) as well as a low time-resolution because of the 10 Gbe outputs not available yet. As far as the resource contained in the Xilinx Virtex 6 XC6VSX475T FPGA of the ROACH2 are considerable, they are in any case not sufficient to get the number of channels desired, especially the Block RAM required are neatly not enough.

We are now beginning to see how the SARDARA platform is suitable and exploitable to fulfil this goal. Each ROACH2 is not only connected to the corresponding PC via optical fiber but also with each other ROACH2. This allow us to connect the eight outputs of a certain ROACH2 to the eight PCs simply configurating the FPGAs as a switch: namely, the UDP packets sent by a ROACH2 to another is merely sent out in the proper port of the mezzanine card, in particular the one connected to the corresponding PC. This approach can be applied to whatever ROACH2, therefore the entire system results very versatile and suitable for different applications. An expensive alternative solution would be to insert a 72-port SFP+ 10 Gbe between ROACH2 and PCs, nevertheless the cost of the entire infrastructure would drastically, and uslessly, to grow up. Figure 4.8 shows this scenario. The ROACH2-master implements the parallel PFBs while the ROACH2s-slave get corresponding sub-bands via UDP packets containing the complex samples. Thus, packets are sent to the corresponding node. It is very important to emphasize that whatever ROACH2 can be used both as master and slave indifferently.

We also focus on the achievable improvement for cross-correlations calculation, above all because this feature was not present in the DBBC design. Obviously, if we wish to make a full-Stokes spectrometer, the ROACH2-master must to implement a parallel PFB for each polarization. In a conventional spectropolarimeter, in the case of the J.Mock FFT engine[35] is used, left and right polarization must to be sent to the same engine because, otherwise, it would not make sense to employ an FFT algorithm that accepts two input streams simultaneously. Figure 4.9 shows such a scenario in case of 16 spectral channels.

Samples marked with asterisk represent the right polarization, while capital letters indicate spectral points produced by the FFT. The correlation cannot be done in real time because samples are provided in a order no immediately fruitful. In fact, as shown, the left polarization is provided firstly and, just afterwards, the other polarization is ready; this means that some sort of temporal storing and realignment of the data is necessary, a FIFO (First In First Out) is needed to put the correct order in the data.

Apart from the inevitable final reorder of the spectra due to the bit reversal representation provided by whatever FFT engine, in the case of the proposed solution, spectral points of the two couple of adjacent signals arrive in the correct sequence. Thus, beyond auto-

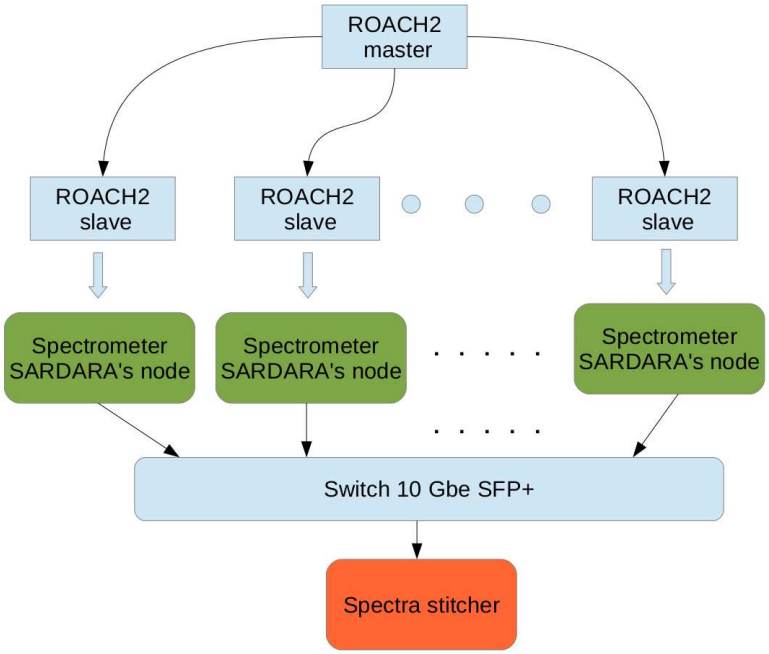

Figure 4.8: *SARDARA's wideband and high resolution configuration.*

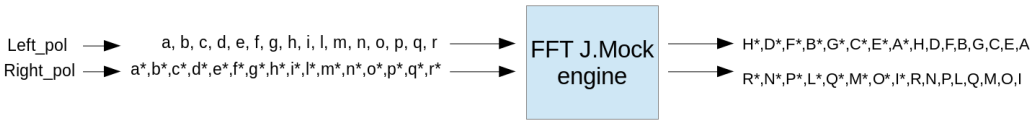

Figure 4.9: *FFT Mock engine for 16 points.*

correlations, cross-correlations can be calculated directly without waste of resource.

As the first PFB has a parallel configuration, the memory usage is almost negligible, therefore only second serial PFBs impact on the BRAM in case of an FPGA implementation.

In case of the SARDARA, the GPU implementation of full-Stokes spectrometers allow us to get a number of channels substantially arbitrary for each sub-band. Thus, we have simulated such a scenario by processing a generic base-band signal with different bandwidth: the number of channels achievable with a single SARDARA node can be plausibly estimated. Essentially, we can figure out which is the maximum bandwidth manageable by a single node, the maximum number of channels achievable and, above all, whether the spectrometer can be done in a real-time implementation by using the available GPUs. On this basis, the feasibility of a wide band "no-holes" high resolution full-Stokes spectrometer has been done. All

achieved results are described in chapter 6.

Chapter 5

SETI: Search for ExtraTerrestrial Intelligence

The SETI project means “Search for ExtraTerrestrial Intelligence”, i. e. the search for evidence of intelligence coming from a possible extraterrestrial civilization. As a consequence, the project does not deal with to figure out whether, in a certain planet, living worms, animals or, more generally, life forms unable to make their lives present in some way. That also includes hypothetical people or alien creatures that have not arrived to a technological level to do that yet. Moreover, in this regard, it is important to pointing out that the only goal of the SETI project is to receive and to recognize artificiality of the acquired signals; the issue of understanding the content of the message, as well as what response should be sent back, could be handled by other (probably politician) people. On the other hand, we need to think about the extraordinary amount of different languages in our planet: how can we “extract” the meaning of a message and what kind of protocol would be suitable in case some sort of response would have sent back? Finally, the enormous distance between habitable planets suggest us that, probably, the message was sent many years ago and, in the meantime, the technological progress of those civilitazions should have reached a greater level; we can see how, for example, the world is rapidly changed after the Second World War.

Up to now, no evidence of life has yet been found, however it is statistically almost impossible that other life forms are not present in the Universe. We can just immagine that there are a hundred billions stars in the Milky Way, as well as hundred billions of galaxyes - similar to the Milky Way - in the Universe: the idea that we are the unique life form is, statistically speaking, completely bizarre. However, we may have “listened” in the wrong way, wrong manner, wrong direction and who know what else.

In this chapter, we present the mathematical approaches to the problem, then the thesis contribution from a hardware/software point of view; the goal is to increase the possibility to find something out there and respond to the question “Are we alone?”.

5.1 Mathematical SETI

From a mathematical viewpoint, SETI researches can be distinguished in two main categories: the ones concerning signals intentionally transmitted by possible extraterrestrial civ-

ilizations and the ones concerning signals unintentionally transmitted. Historically, each SETI research has been done towards the first direction, by exploiting the narrow-band FFT approach; however, recently, the wideband approach based on the Kahrunen-Loeve Transform (KLT)[36]- good for the second option - has been investigated.

5.1.1 Fourier approach

Whatever periodic signal can be described as a linear combination of orthogonal basis functions. These functions, in accordance with the Fourier theory, are sine and cosine. Sine and cosine functions have a certain frequency, phase and amplitude. Let us suppose that these functions can be expressed with $\phi_k(t)$ where t is an independent variable and $k = ..,-1,0,1,2,...$ If we consider $x(t)$ as a generic signal in the time domain, and $X(k)$ that represent various terms regarding the amplitude of the functions, $x(t)$ can be written as follows:

$$x(t) = \sum_{k=-\infty}^{\infty} X(k)\phi_k(t) \tag{5.1}$$

In the discrete case t became nT, where T is fixed a priori while $n = ..,-1,0,1,2,...$ Thus, we can define $x(n)$ and $\phi_k(n)$ as the corresponding discrete representation of $x(t)$ and $\phi_k(t)$, evaluated for $t = nT$. The equation (5.1) can be, therefore, written as follows:

$$x(n) = \sum_{k=-\infty}^{\infty} X(k)\phi_k(n) \tag{5.2}$$

In a realistic case, the number of "samples" must be finite, let us suppose for instance to have N points. The (5.2) can be written as follows:

$$x(n) = \sum_{k=0}^{N-1} X(k)\phi_k(n) \tag{5.3}$$

ϕ can be defined as the following matrix:

$$\phi = \begin{pmatrix} \phi_0(0) & \phi_1(0) & ... & \phi_{N-1}(0) \\ \phi_0(1) & \phi_1(1) & ... & \phi_{N-1}(1) \\ . & . & & . \\ . & . & & . \\ \phi_0(N-1) & \phi_1(N-1) & ... & \phi_{N-1}(N-1) \end{pmatrix}$$

Thus, if we indicate X as $[X(0), X(1), X(2), ..., X(N-1)]^T$, the equation (5.3) can be rewritten in the following compact manner:

$$x = \phi X \tag{5.4}$$

The basis functions contained in the matrix ϕ are well defined, the components of X are the domain of the transformation that represents x. The transformation of the x domain is particularly useful for digital processing: if $x(0), x(1), x(2), ...$ is a sequence of data, this sequence can be transformed in another domain of representation by the sequence $X(0), X(1), X(2), ...$, also named "spectral analysys". This correspond to the analysys of the coefficients $X(k)$ of the Fourier series of $x(t)$, i.e. the spectrum.

The transformation from a domain to another, i.e. the operation to get coefficients of the Fourier series $X(k)$ from $x(t)$, can be obtained by using the "Fourier Transform" F. Let us

suppose that the signal $x(t)$ be periodic of period P; the Fourier series at real coefficients is given by:

$$x(t) = \frac{a_0}{2} + \sum_{k=1}^{\infty} \left[a_k \cos \frac{2\pi k t}{P} + b_k \sin \frac{2\pi k t}{P} \right] \tag{5.5}$$

where $k = 0, 1, 2, ...$ represents the number of cycles in P, thus k/P is the frequency while $a_0, a_1, a_2, ...$ are coefficients of the Fourier series. The series with complex coefficients can be obtained by using the following equations:

$$\cos(\theta) = \frac{1}{2}(e^{j\theta} + e^{-j\theta}) \tag{5.6}$$

$$\sin(\theta) = \frac{1}{2j}(e^{j\theta} - e^{-j\theta}) \tag{5.7}$$

θ can be expressed as $2\pi k t/P$ then, if we put the (5.6) and the (5.7) in the (5.5), we get the following equation:

$$x(t) = \frac{a_0}{2} + \frac{1}{2} \sum_{k=1}^{\infty} \left[a_k (e^{j\theta} + e^{-j\theta}) + \frac{1}{j} b_k (e^{j\theta} - e^{-j\theta}) \right] \tag{5.8}$$

$$x(t) = \frac{a_0}{2} + \sum_{k=1}^{\infty} \left[\frac{1}{2}(a_k - j b_k) e^{j\theta} + \frac{1}{2}(a_k + j b_k) e^{-j\theta} \right] = \sum_{k=1}^{\infty} \frac{1}{2} \left[a_{|k|} - j sign(k) b_{|k|} \right] e^{j\theta} \tag{5.9}$$

Thus, if we define $X(k) = \frac{1}{2}[a_{|k|} - j sign(k) b_{|k|}]$, the (5.9) can be rewritten as follows:

$$x(t) = \sum_{k=-\infty}^{\infty} X(k) e^{\frac{2\pi k t}{P}} \tag{5.10}$$

The equation (5.10) represents $x(t)$ as linear combination of sinusoidal functions with complex coefficients. The following formula allows us to calculate these coefficients:

$$X(k) = \frac{1}{P} \int_{-P/2}^{P/2} x(t) e^{\frac{-j2\pi k t}{P}} dt \tag{5.11}$$

We are dealing with digital systems, thus the equation (5.11) can be expressed more efficiently in a discrete format:

$$X(k) = \frac{1}{N} \sum_{t=0}^{N} x(t) e^{\frac{-2\pi k t}{P}} \tag{5.12}$$

The Fourier transform is then defined as follows:

$$F[x(t)] = X(k) = \frac{1}{N} \sum_{t=0}^{N} x(t) e^{\frac{-2\pi k t}{P}} \tag{5.13}$$

The inverse operator can be used to reconstructs $x(t)$ with the following formula:

$$x(t) = F^{-1}[X(k)] = \frac{1}{N} \sum_{k=0}^{N} X(k) e^{\frac{-2\pi k t}{P}} \tag{5.14}$$

The major issue of the Fourier transform is that requires N*N multiplications and N*N additions, therefore it is fairly inefficient from a computational point of view. In order to reduce the number of required operations, the well-known Fast Fourier Transform (FFT) is usually employed: in fact, the FFT needs only N*logN multiplications.

5.1.2 KLT

The Kahrunen-Loeve Transform (KLT)[37] is an argument of great interest in different fields: signal processing, mathematics, statistics, physics etc. To see why the KLT can, in some areas, be better than FFT[38], we consider an analogy with mechanics. Let us take as an example a book and a reference system composed of three Cartesian axes. In accordance with classic mechanics, all of the book's properties concerning the rotational dynamics can be described by a symmetric 3x3 matrix called the "inertia matrix". As is well known, computing the autocorrelation is a good method for extracting a signal immersed in noise. Let us consider the autocorrelation to be the book itself; eigenvectors of the autocorrelation matrix can then be calculated so as to find the simplest data representation. This is the idea behind the KLT.

Let us consider a random function $X(t)$ also called "stochastic process of the time"; we ask here "is it possible to separate the probabilistic components from its behaviour in time?" and the answer is that it can be done by using the KLT. The starting point of the discussion is the Kahrunen-Loeve expansion of $X(t)$ over the time interval $0 \leq t \leq T$ expressed by the following formula:

$$X(t) = \sum_{n=1}^{\infty} Z_n \phi_n(t) \tag{5.15}$$

Regardless the instrinsic meaning of $\phi_n(t)$ and Z_n , we can say immediately that the first one is time-dependent, while the second is entirely incorrelated than the time. This means that, in general, whatever random function $X(t)$ can be thought as "something" made of two parts: its behavior in time, represented by the functions $\phi_n(t)$, and its behaviour with respect to probability and statistics, which must therefore be represented by another part, the Z_n precisely. This also means that various variables Z_n, which contribute to compose $X(t)$, represent variables totally random. Such a sharp distinction between stochastic contribution ($\phi(t)$) and random contribution (Z_n) is a very important and "original" feature never seen in mathematics. A certain value of Z_n, being not time-tied and absolutely random, for a generic instant t can exist.

$\phi_n(t)$ are the eigenvectors obtained by the following eigen-problem:

$$\int_0^T E\Big\{X(t_1)X(t_2)\Big\}\phi_n(t_2)\,dt_2 = \lambda_n \phi_n(t_1) \tag{5.16}$$

where $E\Big\{X(t_1)X(t_2)\Big\}$ is the autocorrelation of the process $X(t)$ given by:

$$X(t) = \int_0^T E\Big\{X(t_1)X(t_2)\Big\} = \int_{-\infty}^{\infty} dx_1 \int_{-\infty}^{\infty} x_1 x_2 f_{x(t_1)x(t_2)}\big(x_1, x_2\big)\,dx_2 \tag{5.17}$$

Let us suppose that the autocorrelation be function of t_1 and t_2; moreover, we suppose $E\Big\{X(t_1)X(t_2)\Big\} = 0$. The equation (5.16) represents the eigen-problem in which the operator has a symmetric nucleus, therefore eigenvalues are real while eigenvectors are, between

them, orthogonal. The eigenvectors are a complete set, thus $\phi_n(t)$ form an orthonormal basis in the space $L^2(0,T)^3$. If the equation (5.15) is multiplied by one of the $\phi_m(t)$ and integrated, the orthonormality of the eigenvectors can be exploited to get coefficients Z_m :

$$Z_m = \int_0^T X(t)\phi_m(t)dt \tag{5.18}$$

We can show that also the coefficients Z_n are orthogonal from the autocorrelation point of view:

$$E\Big\{Z_m Z_n\Big\} = E\Big\{\int_0^T X(t_1)\phi_m(t_1)dt_1 \int_0^T X(t_2)\phi_n(t_2)dt_2\Big\} \tag{5.19}$$

$$E\Big\{Z_m Z_n\Big\} = \int_0^T dt_1\phi_m(t) \int_0^T dt_2\phi_n(t_2)E\big\{X(t_1)X(t_2)\big\} \tag{5.20}$$

$$E\Big\{Z_m Z_n\Big\} = \lambda_n \int_0^T dt_1\phi_m(t_1)\phi_n(t_1) = \lambda_n\delta_{nm} \tag{5.21}$$

The average value of Z_n is 0, as demonstrates the following equation:

$$E\big\{Z_n\big\} = E\Big\{\int_0^T X(t)\phi_n(t)dt\Big\} = \int_0^T E\big\{X(t)\big\}\phi_n(t)dt = \int_0^T 0\phi_n(t)dt = 0 \tag{5.22}$$

Another property of Z_n is that the variance σ^2_{Zn} is equals to the relative eigenvalue:

$$\sigma^2_{Zn} = E\{Z_n^2\} - E^2\{Z_n\} = E\{Z_n^2\} - 0 = E\{Z_n Z_n\} = \lambda_n\delta_{nm} = \lambda_n \tag{5.23}$$

The standard deviation of each Z_n, around the average, is equal to $\pm\sqrt{\lambda_n}$. Thus, we can get the autocorrelation and the variance in terms of eigenfunctions (eigenvectors); the autocorrelation can be written as follows:

$$E\big\{X(t_1)X(t_2)\big\} = E\Big\{\sum_{m=1}^{\infty} Z_m\phi_m(t_1)\sum_{n=1}^{\infty} Z_n\phi_n(t_2)\Big\} = \sum_{m=1}^{\infty}\sum_{n=1}^{\infty} E\{Z_m Z_n\}\phi_m(t_1)\phi_n(t_2) \tag{5.24}$$

Thus:

$$E\big\{X(t_1)X(t_2)\big\} = \sum_{m=1}^{\infty}\sum_{n=1}^{\infty}\lambda_n\delta_{nm}\phi_m(t_1)\phi_n(t_2) = \sum_{n=1}^{\infty}\lambda_n\phi_n(t_1)\phi_n(t_2) \tag{5.25}$$

$X(t_1)$ has an average value equals to zero, thus if we use the equation (5.25) with $t_1 = t_2 = t$, the following formula can be written:

$$\sigma^2_{X(t)} = E\big\{X(t)X(t)\big\} - E^2\big\{X(t)\big\} = \sum_{n=1}^{\infty}\lambda_n\phi_n^2(t) - 0 = \sum_{n=1}^{\infty}\lambda_n\phi_n^2(t) \tag{5.26}$$

The following equation is fundamental to figure out the KLT:

$$\int_0^T \sigma^2_{X(t)}dt = \sum_{n=1}^{\infty}\lambda_n \tag{5.27}$$

The equation (5.27) means that the overall energy is given by the sum of the eigenvalues. Usually, the eigenvalues are ordered from the higher to the lower, i.e. $\lambda_1 > \lambda_2 > ... > \lambda_n > 0$ where λ_2 is named "dominant eigenvalue".

In addition, the Z_n coefficients are random, with average equals to zero and variance λ_n; the $\lim_{n\to\infty} \lambda_n = 0$, thus we obtain that the random coefficients Z_n become, for n that grows, coefficients with a variance that tends to zero. Morevover, they have average equals to zero, thus if we consider n by tending to ∞, they become deterministic with a value of zero, as shown in fig. 5.1

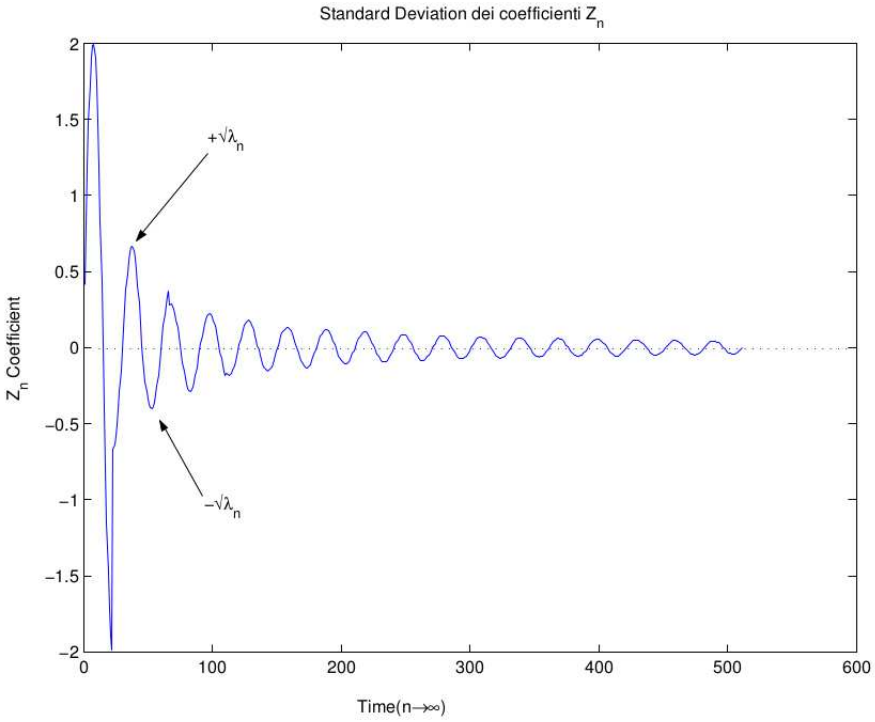

Figure 5.1: *Variance of the coefficients Z_n.*

In a general way, our goal is to find a set of vectors that describes a matrix of autocorrelation got from a certain digital data frame acquired by a radio telescope like SRT. Let us suppose that the data frame has N elements; as a consequence, the matrix of autocorrelation A is of the order N, i.e. $A \in R^{NxN}$. We can rewrite the equation (5.16) in the discrete form:

$$Av = \lambda v \tag{5.28}$$

where λ is the eigenvalue and v is the eigenvector. The autocorrelation and the eigenvalues are linked by the following formula:

$$NA(0,0) = \sum_{i=0}^{N-1} \lambda_i \tag{5.29}$$

where $A(0,0)$ represents the energy of the acquired signal.

If we consider a matrix of order N, we can extract N eigenvalues and N eigenvectors. Each eigenvector has associated an eigenvalue; we can define, as eigenpair, the pair of elements (v_i, λ_i), where v_i is the eigenvector or privileged axis, while λ_i is the eigenvalue that indicates the energy associated to the eigenvector.

The matrix A has N privileged axes that represent the eigenvectors, thus we can decompose the acquired data frame as the sum of eigenvectors weighted by the values of an appropriate vector p. The equation (5.15) can be rewritten as follows:

$$x = V\vec{p} \tag{5.30}$$

where V is the following matrix that contains eigenvectors, while $\vec{p} = [p1, p2, ...pN]$.

$$V = \begin{pmatrix} v_0(0) & v_1(0) & ... & v_{N-1}(0) \\ v_0(1) & v_1(1) & ... & v_{N-1}(1) \\ . & . & & . \\ . & . & & . \\ v_0(N-1) & v_1(N-1) & ... & v_{N-1}(N-1) \end{pmatrix}$$

Consequently, the equation (5.15), in the discrete case, can be written as:

$$x(t) = \sum_{i=0}^{N-1} V_i(t) p_i \tag{5.31}$$

where the weights p, in analogy with the equation (5.18), can be obtained by the following formula:

$$p_i = \sum_{k=0}^{N-1} V_i^T(k) x(k) \tag{5.32}$$

In other words, weights are obtained via a projection of the acquired data on the matrix of transformation given by the eigenvectors. In the context of this thesis, we are dealing with the use of the KLT for reveal possible alien signals, therefore we are not interested about the reconstruction of the original signal. Hence, the KLT algorithm that we have used is partially truncated to facilitate the heavy digital signal processing required.

5.2 Hardware and Software implementation

In this section, we explain the strategies adopted for applying mathematical algorithms earlier examined and, in particular, the hardware-software architecture employed.

5.2.1 KLT algorithm

The FFT algorithm divides, in a certain number of pieces, the overall energy contained in the acquired signal; therefore, we can estabilish a threshold to determine whether, in a certain channel, a stronger signal is present. The KLT algorithm adopted[39] uses a different approach: it considers all the energy of the signal instead of the amplitude of a particular channel. Figure 5.2 shows the algorithm's functioning step by step.

The "autocorrelation vector" block performs the autocorrelation of the data provided by the ROACH2 board and gives, as output, a vector "[0, 1, 2, ...N-1,...,2N-1]". This vector allows us the calculation of the autocorrelation matrix in the following block. The matrix has a particular structure: it is symmetric and with constant elements on each diagonal; usually, such a kind of matrix is named "Toeplitz matrix". For instance, with a vector $[edcbabcde]$, the matrix A has the following structure:

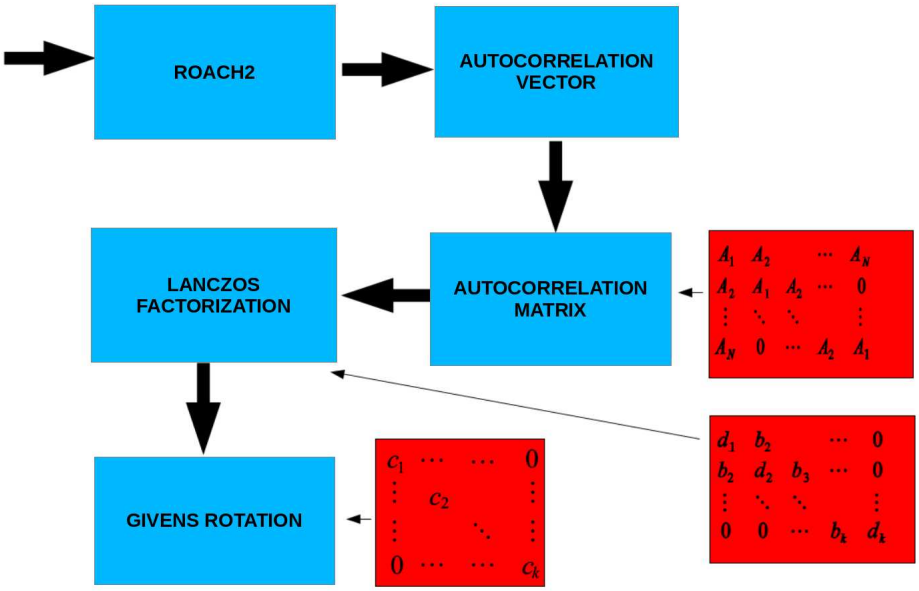

Figure 5.2: *Block diagram of the adopted algorithm.*

$$A = \begin{pmatrix} a & b & c & d & e \\ b & a & b & c & d \\ c & b & a & b & c \\ d & c & b & a & b \\ e & d & c & b & a \end{pmatrix}$$

The "Lanczos factorization" block reduces the matrix A - which is of order N - so as to makes the calculation of the eigenvalues less complex. The output of this block is a square matrix (tridiagonal) of order $k << N$. The last block, named "Givens Rotation", extracts the eigenvalues from the aforementioed tridiagonal matrix by exploiting the algorithm known as "Givens rotation". This algorithm provides a diagonal matrix - of order k - that contains the k greater approximated eigenvalues of the matrix A.

Essentially, the goal is to get the privileged axes that describe the acquired signals in the best possible way; this correspond to perform the calculation of eigenvectors/eigenvalues of the autocorrelation matrix of these signals. Once we get the eigenvalues and the eigenvectors, a specific energy evaluation can be done by SETI experts.

5.2.2 Implementation in SARDARA

Since SETI research is often conducted in piggyback mode only, a dedicated conditioning module is employed at the level of the intermediate frequencies. In particular, it acts as frequency compensation mechanism that is necessary for keeping the chosen bandwidth stable even when a Doppler tracking system is activated, or in case the chosen bandwidth changes completely during the observation; Figure 5.3 shows a block diagram of this scenario.

The intermediate frequency signals are beaten by a tunable tone generated by the synthesizer "Valon 5009"[40] so as to compensate possible Doppler tracking programs as said

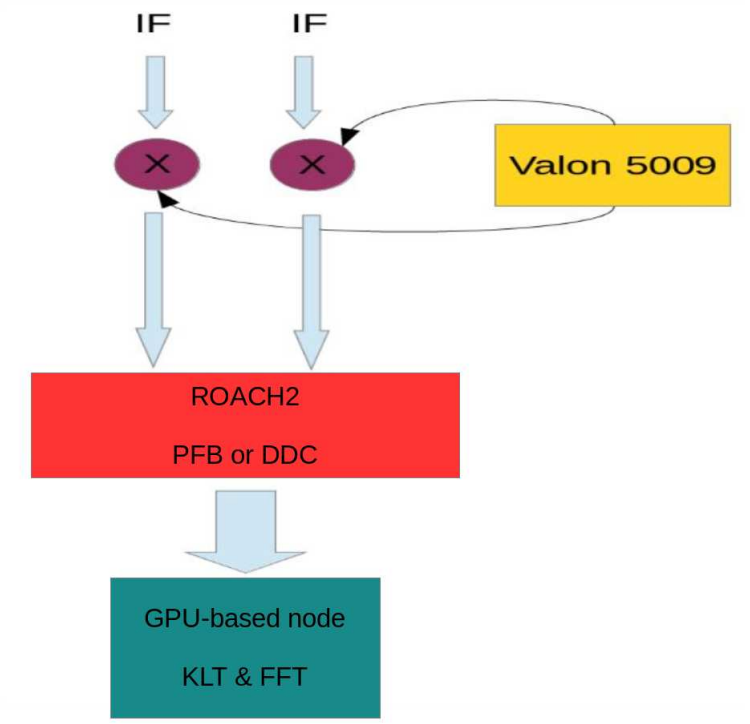

Figure 5.3: *Block diagram for piggyback SETI.*

earlier. Astronomers, in fact, can observe a particular known source, therefore the Doppler correction is needed to keep a particular narrow-band emission in a certain channel, usually the central one of the entire bandwidth of interest. Moreover, in the case of the observer moves the band for observing another portion of the spectrum, the synthesizer can be used to keep the precedent sub-band. Clearly, if the band is moved in a totally different area, the ongoing SETI search ought to be stopped and a new one - starkly different - must begin.

The KLT algorithm is really heavy from a computational point of view, in the next chapter we discuss numerically all of these aspects. At any case, the acquired bandwidth with SARDARA (up to 2.1 GHz) must be reduced in order to store only a portion in base-band mode. We have two possibilities to do that: we can implement the polyphase filter bank or, alternately, the digital down conversion; we have decided to use the second option. In particular, the acquired signal is beaten with a complex mixer that turn it into a complex form - i.e. with a real and an imaginary part - and a decimating filter is applied to the signal. As a consequence, the complex signal is base-band converted with the center of the chosen bandwidth that corresponds to zero. Figure 5.4 shows these steps graphically.

Finally, the signal is sent to a SARDARA node within which the KLT and the FFT are performed. The signal's format is already ready for the FFT engine, because there are several architecture that are able to perform the FFT both for real and complex signals. On the contrary, the KLT algorithm accepts only real signals, therefore a choice must be made: we can use the absolute value of complex number or, alternately, we keep the real part of the signal. However, in the latter case, a filter is mandatory so as to avoid aliasing phenomena. In order to simplify the system as much as possible, we have decided to use the first solution. As regards the maximum bandwidth that can be used for a real time implementation, the bot-

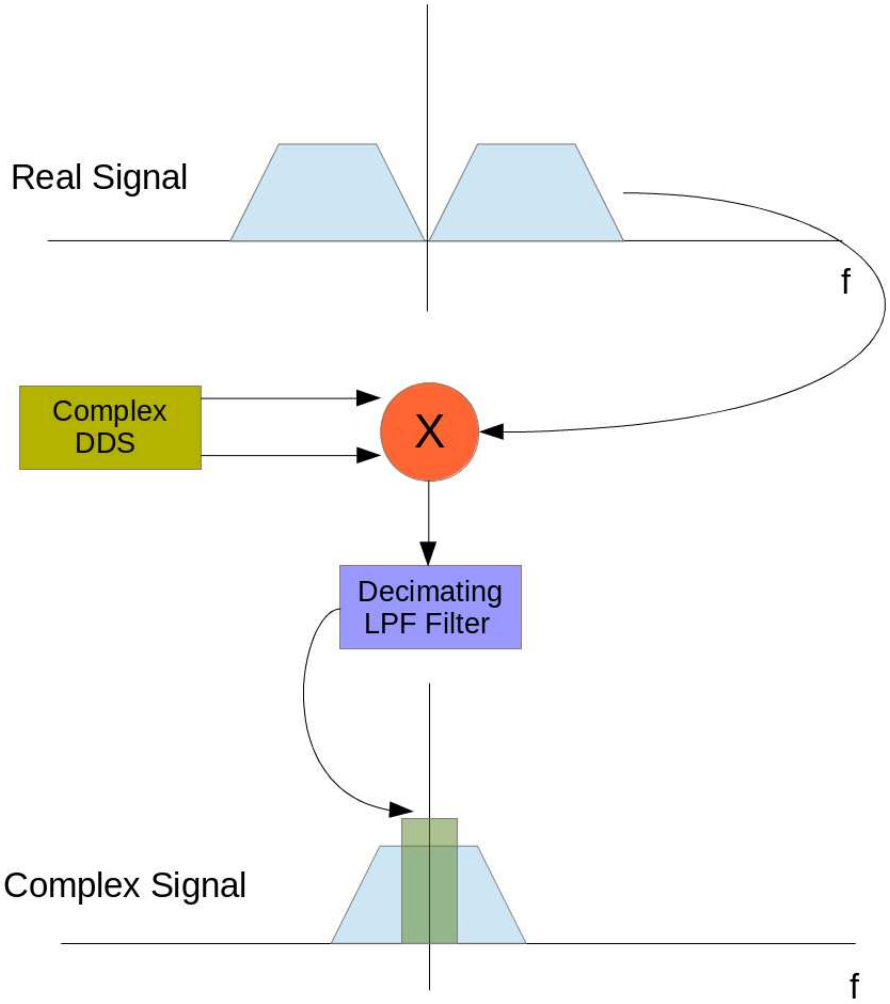

Figure 5.4: *Digital Down Conversion.*

tleneck is represented by the KLT engine. Once we have figure out what is the "sustainable" real time data rate for which a SARDARA node work properly with the KLT, we can estimate the number of FFT channels necessary to do SETI, i.e. the one that allows us an adequate resolution of a fraction of Hz. All these tests and measurements are presented in chapter 6.

5.2.3 Brief conclusions

The SETI infrastructure presented is a new thing entirely. Although several studies about KLT have been performed by many people, a platform that implements the KLT and, in parallel, the FFT on data taken by a radio telescope, was totally lacking. There is a lot of work to do again, however, this is an important starting point for SETI people.

Future development is being discussed about new algorithms potentially interesting. The BAM (Bordered Autocorrelation Method)[41], for instance, is an alternative numerical technique for evaluating the KLT in the case of stationary processes, that may be less heavy from a computational point of view and, by virtue of the BAM, the KLT succeeds in extract-

ing a tone embedded in the noise while the FFT utterly fails. Another important algorithm for SETI is the relativistic KLT[42]. Both the KLT and the BAM KLT can be used for "fixed" source, namely they work just for habitable planets; however, we can receive signals from alien spaceships as well. In this case, the relativistic KLT is the best solution and it will be investigated in a near future, as well as well-known algorithms like Wavelet.

Chapter 6

Experimental Results

In this chapter, we describe all the results we have been achieved. Three main parts are presented. First, scientific observations conducted at SRT by adopting, in different observing mode, the SARDARA backend. Then, simulations conducted to figure out the performance of SARDARA in terms of instantaneous uniform bandwidth, in conjunction with high frequency resolution. Finally, the SARDARA performance for the search for extraterrestrial intelligent life forms.

6.1 Scientific results of SARDARA

SARDARA is a multi-purpose instrument that is applicable to a significant amount of scientific studies. As said earlier, it is able to meet requirements never satisfied before at Italian facilities. In particular, no current instrument provides a spectrometer with an instantaneous bandwidth up to 2.5 GHz and, with regard to polarimetric science, SARDARA is the first digital spectropolarimeter fully operational at SRT.

In the next sections, we outline the achieved results in the following scientific fields: imaging, polarimetry, spectroscopy and, finally, pulsars.

6.1.1 Imaging

One of the most important kind of science with SRT is the on-the-fly mapping of extended sources. It consists in performing the data acquisition with continuity (sampling time of a few tens ms) at constant speed (typically a few degrees/min), repeatedly scanning the sky in both right ascension (RA) and declination (DEC) directions (each passage is called "subscan"). Figure 6.1 shows a spectacular example of this observing mode.

Supernova remnants (SNRs) correspond to the final stage of a massive star's life. They are typically bright (10-100 Jy at 1 GHz) extended sources (0.5-1 deg) well suited to perform the "first light" of SARDARA . Integrated fluxes are typically available in literature up to 5-10 GHz, while SNR spatially resolved fluxes are largely unexplored above this frequency range. 3C157 (also named IC443) is one of the best-studied Galactic SNR. The large structure of the source extends over 0.75 deg and shows evidence of interactions with both atomic and molecular clouds[43].

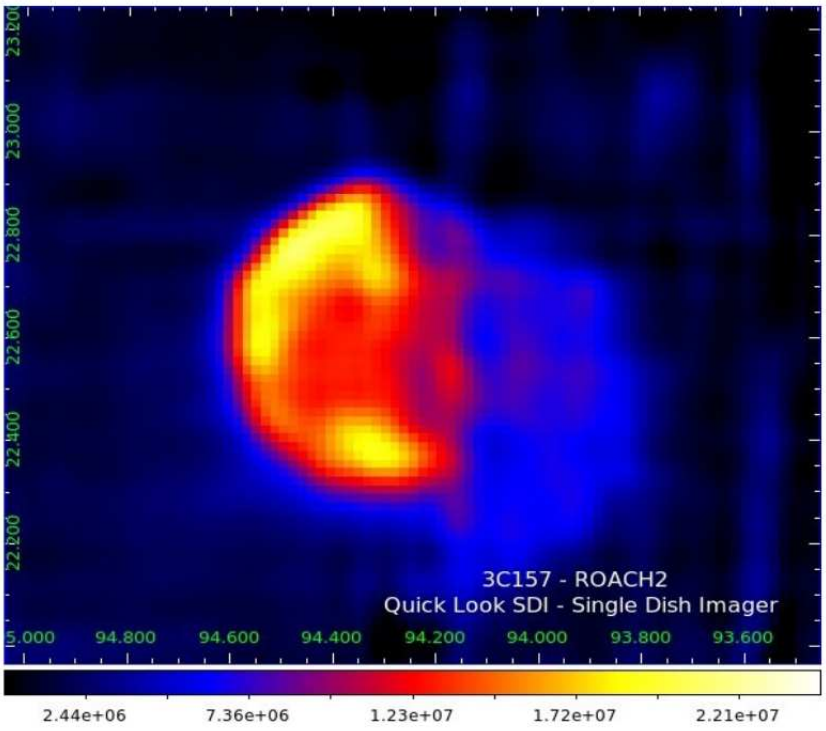

Figure 6.1: *On-the-fly map of the SuperNova Renmant 3C157. Credits: A. Pellizzoni, E. Egron, N. Iacolina, A. Trois, M. Bachetti on behalf of the team of the project Tender-7*

Image analysis is based on SRT Single Dish Imager (SDI)[44], a state-of-the-art imaging data analysis software optimized for OTF scans, including automated baseline subtraction techniques and RFI rejection ([45], [46]).

Each map's pixel represents the overall received energy for the corresponding sky area. The adopted configuration provides a bandwidth of 1,500 MHz divided into 1,024 spectral channels for both polarizations, thus all of the channels are "collapsed" in a single one in order to achieve the entire power. The employed receiver is the mono-feed C-band (5.7 - 7.7 GHz), the RFI situation was quite good but no ideal; however, is it possible to exclude all of the affected channels, thus the resulting energy corresponds to the real one.

6.1.2 Polarimetry

As said earlier, SARDARA is the first spectropolarimeter ever used at SRT, thus we didn't know much about this matter and relative issues. This is why, after seeing the proper working of the system for the imaging mode, a decision was taken to face the polarimetric mode. The ad-hoc tool adopted for all of the observations is named SCUBE (Single-dish Spectral-polarimetry Software)[47].

The main issue in polarimetric observations is the calibration between left and right polarizations: they have to be phased correctly so as to get cross-correlations and, finally, calculates the Stokes parameter. At the beginning, due to an asynchronous initialization of the ADC samplers of SARDARA, a spurious phase shift between left and right circular polarization was present. The shift causes a rotation of the observed polarization angle by an amount

that increases linearly with the frequency. The RL-shift is corrected in SCUBE by mean of a polarization synthesis, as shown in Fig. 6.2. In general, the RL-shift is of the order of 0.1 Deg/MHz, i.e. too small to cause significant depolarization at sub-channel level.

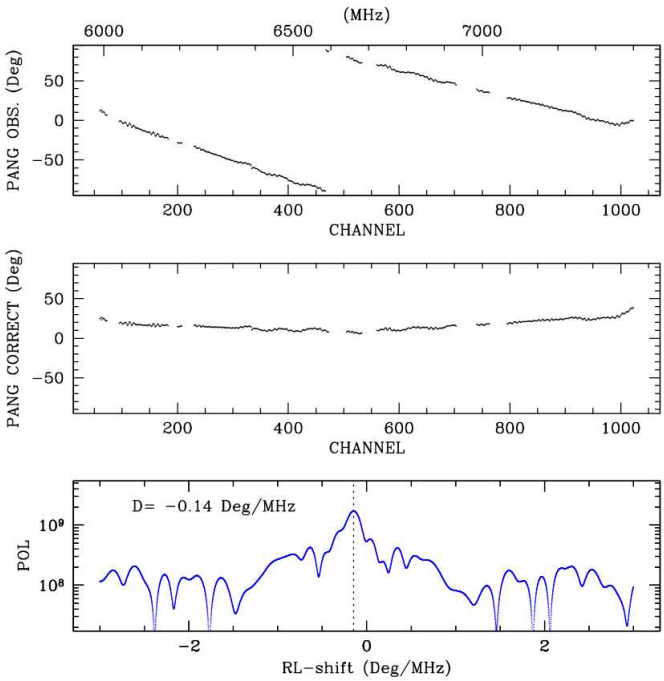

Figure 6.2: *Calibration of the phase shift between the R and L polarizations. Top: observed polarization angle. Middle: corrected polarization angle. Bottom: polarization synthesis. The peak polarization is found at a RL- shift of -0.14 Deg/MHz. .*

Fig. 6.3 and fig. 6.4 show, respectively, total intensity and polarization observations of the 3C129[48] galaxy cluster obtained, with the Sardinia Radio Telescope, by using the C-band receiver.

Imaging is performed in SCUBE by subtracting the base-line from the calibrated telescope sub-scans and by projecting the data in a regular 3-dimensional grid with a resolution of 42"/pixel, which is enough in our case to sample the beam FWHM (Full Width at Half Maximum) with four cells.

The polarization imaging of Stokes parameters Q and U has been performed following the same procedures used for the total intensity imaging: baseline subtraction, gridding, and SWT (Stationary Wavelet Transform, also known as Undecimated Wavelet Transform) stacking. In colours we show the polarized intensity ($P = \sqrt{U^2 + Q^2}$), corrected for the bias, introduced when combining the Stokes Q and U images that we assumed to have an equal noise Gaussian statistics with a measured standard deviation $\sigma_{Q,U} = 0.5$ mJy/beam. The peak polarized intensity is 70 mJy/beam. Critical dynamical range issues are not present with the polarization image, thus no deconvolution was required. Polarization is detected for both 3C129 and 3C129.1 with a global fractional polarization of 0.27 and 0.075, respectively. In 3C129, the polarization angle of the radiation electric field (not corrected for the Faraday rotation effect) is perpendicular to the tail along its entire length. The fractional polarization increases, by going from 0.05 in the head of the radio source, up to 0.67 at the end of the tail.

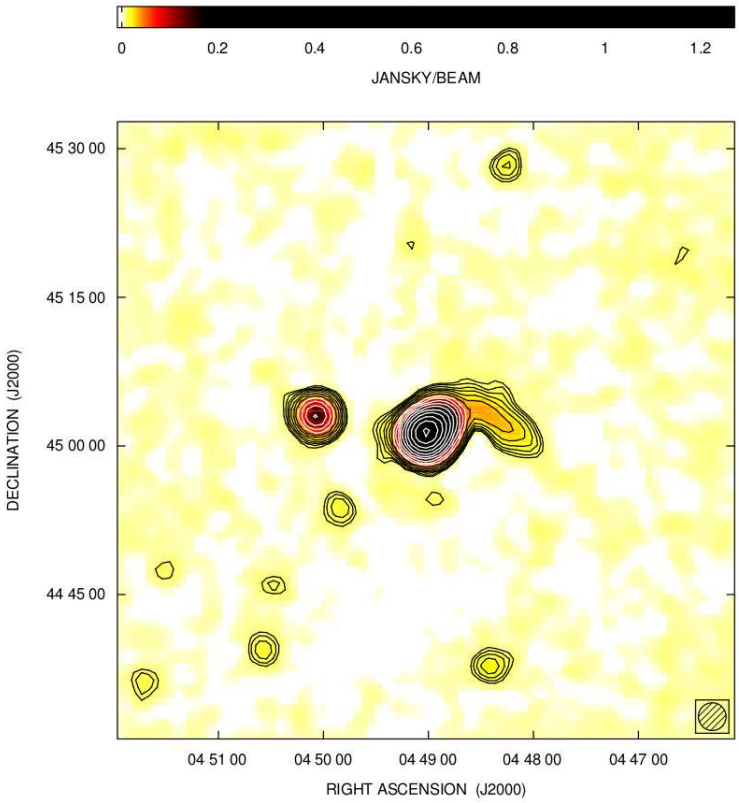

Figure 6.3: *SRT total intensity dirty image of the 3C129 galaxy cluster resulting from the spectral average of the bandwidth between 6000 and 7200 MHz. Credits: M. Murgia, F. Govoni, E. Carretti, on behalf of the team of the project Tender-7.*

6.1.3 Spectroscopy

The scientific detailed analysis of emission/absorption spectral lines (i.e. line profiles, intensity line ratios, etc.) requires high-frequency resolution, well below the one employed for studies outlined in previous sections (e.g., the 1.4-MHz spectral imaging). In this case, a configuration with 16,384 channels was used, with different bandwidths for two different targets. Figure 6.5 shows the first observation, i.e. the spectrum of the 22-GHz water maser source observed in NGC4258[49], taken with the SRT in conjunction with SARDARA on October 24, 2015. The total bandwidth is 1.5-GHz wide, split into 16,384 channels, yelding a full velocity coverage (only a portion of it is shown in the figure) and a channel spacing of 20450 and 1.2 km/s, respectively. The frame of the velocity reported in the x-axis is Heliocentric.

The spectrum shows the redshifted high-velocity features (red, in a velocity range of 1200-1350 km/s), the weaker blueshifted high-velocity features (blue; around -500 km/s), and the systemic velocity features (from 400 to 600 km/s). The systemic velocity of the galaxy is 448 km/s.

The three groups of lines is a distinctive characteristic of masers associated with accretion disks orbiting around supermassive black-holes in Active Galactic Nuclei (AGN). The combination of single-dish monitoring and high-angular resolution maps (in particular taken

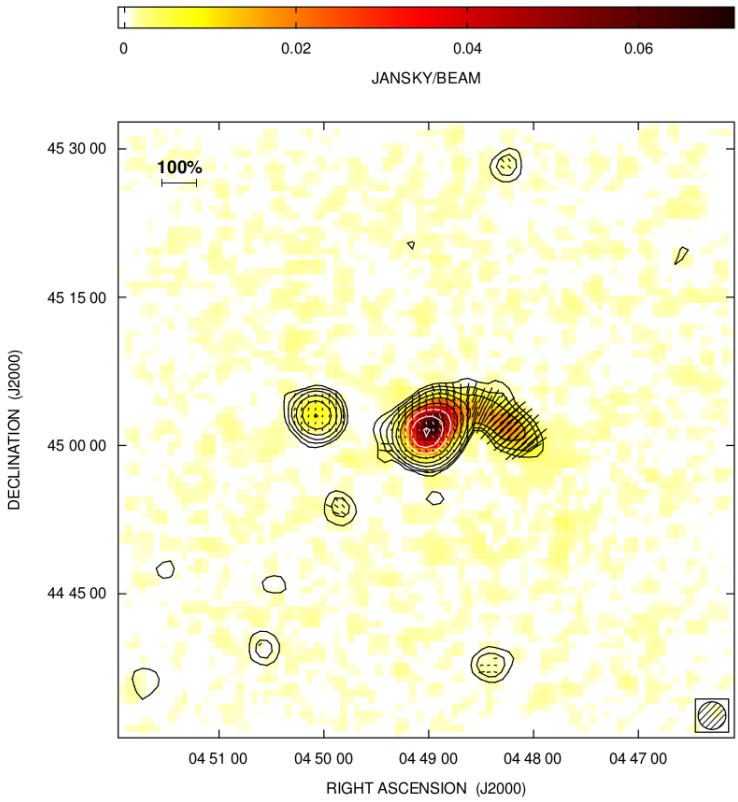

Figure 6.4: *SRT linearly polarized intensity image of the 3C129 galaxy cluster resulting from the spectral average of the bandwidth between 6000 and 7200 MHz. Credits: M. Murgia, F. Govoni, E. Carretti, on behalf of the team of the project Tender-7.*

with Very Long Baseline Interferometry - VLBI - arrays) of the maser lines allow us to shape the rotation curve of the accretion disk, to derive the distance to the host galaxy, and to estimate the black hole mass, as now successfully done for a number of galaxies, like NGC4258 and UGC3789[50], the best studied and the most recent case, respectively.

As mentioned earlier, spectroscopic images (typically referred to as “cubes”) can be also produced by using SARDARA. M31[51], also known as Andromeda Galaxy, is a spiral galaxy approximately 780 kiloparsecs from Earth. Andromeda is the largest galaxy (roughly 220,000 light years across) of the Local Group. The latter also contains the Milky Way, the Triangulum Galaxy as well as about 44 other smaller galaxies. The insterstellar medium in M31 contains about $7.2x10^9$ solar masses of neutral hydrogen (HI), thus a spectral line at a rest frequency of 1420.4 HMz is produced. We observed M31 on September 16, 2015 with SRT; the aim was to test spectral imaging capabilities of SARDARA. Two on-the-fly maps of a field-of-view of about 5x5 degrees were obtained along the RA and DEC directions. We acquired a bandwidth of 300 MHz, starting at 1250 MHz and with 16,384 spectral channels of 18.3 kHz in width. Data reduction was performed with the SCUBE software package; RFI were excised using an automated procedure, thus we corrected for bandpass and removed the scan baseline. The raw counts were calibrated to Jansky/beam by using the well-known calibrator 3C286. Finally, we combined two scans along RA and DEC in a single spectral cube. A continuum

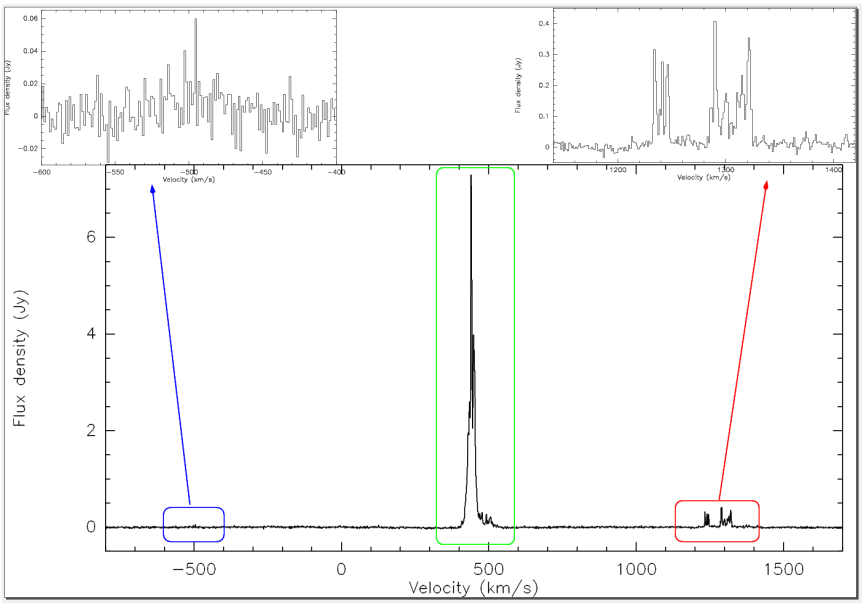

Figure 6.5: *22-GHz water maser source observed in NGC4258 taken with the SRT in conjunction with SARDARA. Credits: A. Tarchi, P. Castangia, on behalf of the team of the project Tender-7.*

subtracted moment-0 image of the HI emission is presented in Fig. 6.6. Colors indicate the Doppler shift of the HI line, caused by the rotation of the M31 galaxy disk. The NE (North East) tip of the disk has a receding radial velocity of about 200 km/s, with respect to the systemic velocity and, therefore, appears red-shifted while the SW (South West) tip is blue-shifted by the same amount.

6.1.4 Pulsars

As said earlier, pulsars[52] are highly-magnetized and rapidly-rotating neutron stars, whose detected signal appears as a periodic sequence of pulses. Their observations require wide frequency bands (some hundreds of MHz), but the frequency-dependent signal's dispersion effect (due to the interstellar medium) imposes the subdivision of the frequency band into narrow frequency channels (fraction of MHz). Moreover, since the period of the most interesting pulsars is of the order of milliseconds, sampling times of the order of few tens of microseconds are mandatory. The computational resources for pulsars are dramatically higher than the ones required for other celestial objects; hence, astronomers often need to use ad-hoc digital backends.

We present two test pulsars. Figure 6.7 shows a 30-minute long observation of $PSRB0355+54$. The observation was performed at C-band with a central frequency of 6700 MHz and a bandwidth 1100-MHz wide.

Figure 6.8 shows a 30-minute long folding mode observation of $PSRB0329+54$. It was performed at L-band with a central frequency of 1550 MHz and a bandwidth 500-MHz wide. The blank horizontal lines indicate that the corresponding frequency channels were strongly affected by RFI, thus they have been removed. With regard to the wobbly baseline, some

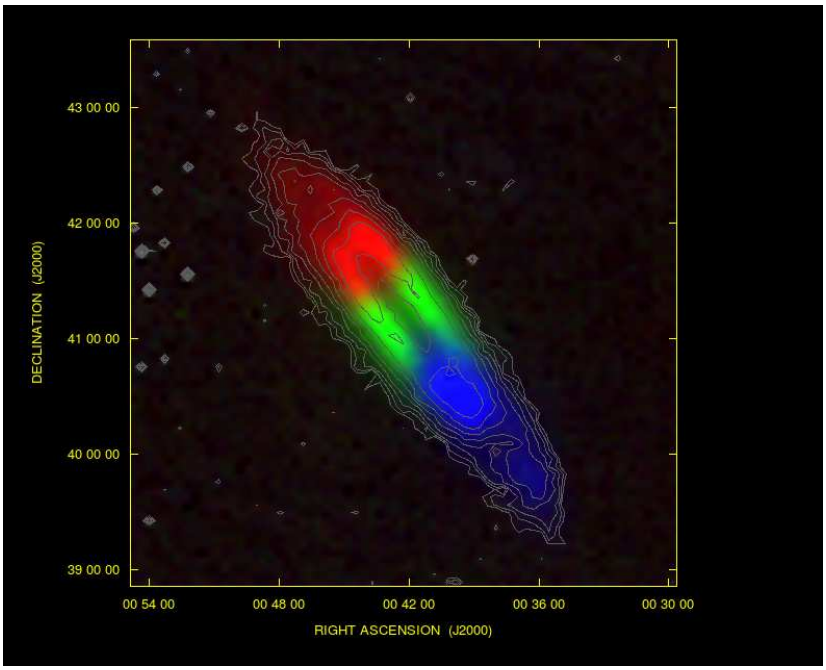

Figure 6.6: *Andromeda galaxy (M31) taken with the SRT in conjunction with SARDARA. Credits: M. Murgia, P. Castangia, A. Tarchi, F. Govoni, on behalf of the team of the project Tender-7.*

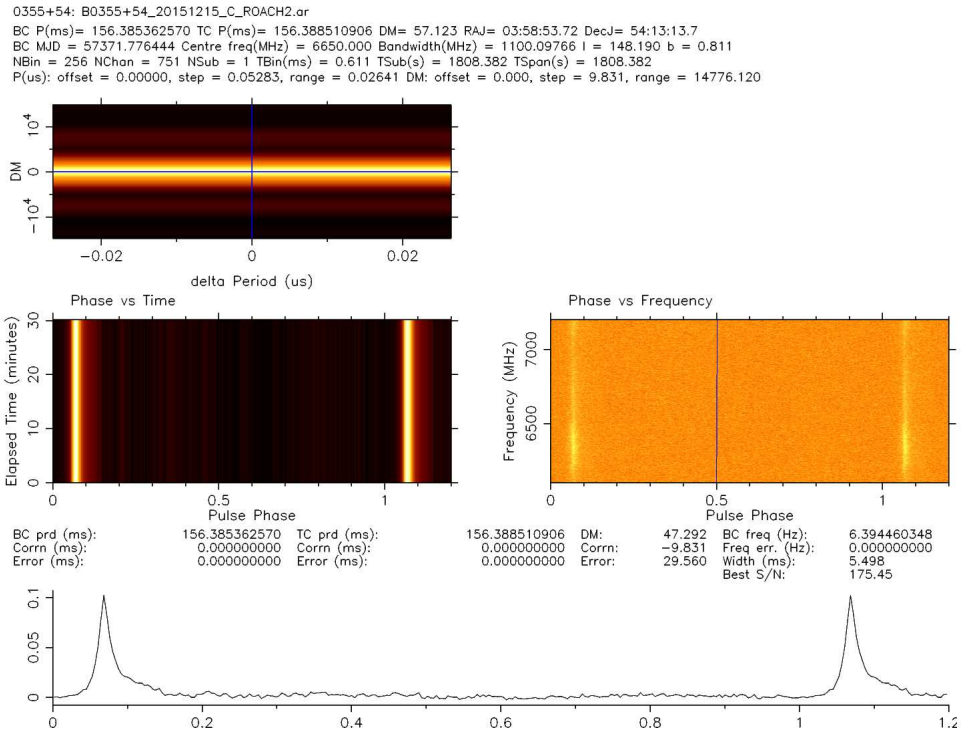

Figure 6.7: *Pulsar B0355+54 observed in C-band with the SRT in conjunction with SARDARA. Credits: M. Pilia, A. Trois, on behalf of the team of the project Tender-7.*

time-domain RFI are still present; however, they can be removed with dedicated RFI excision techniques.

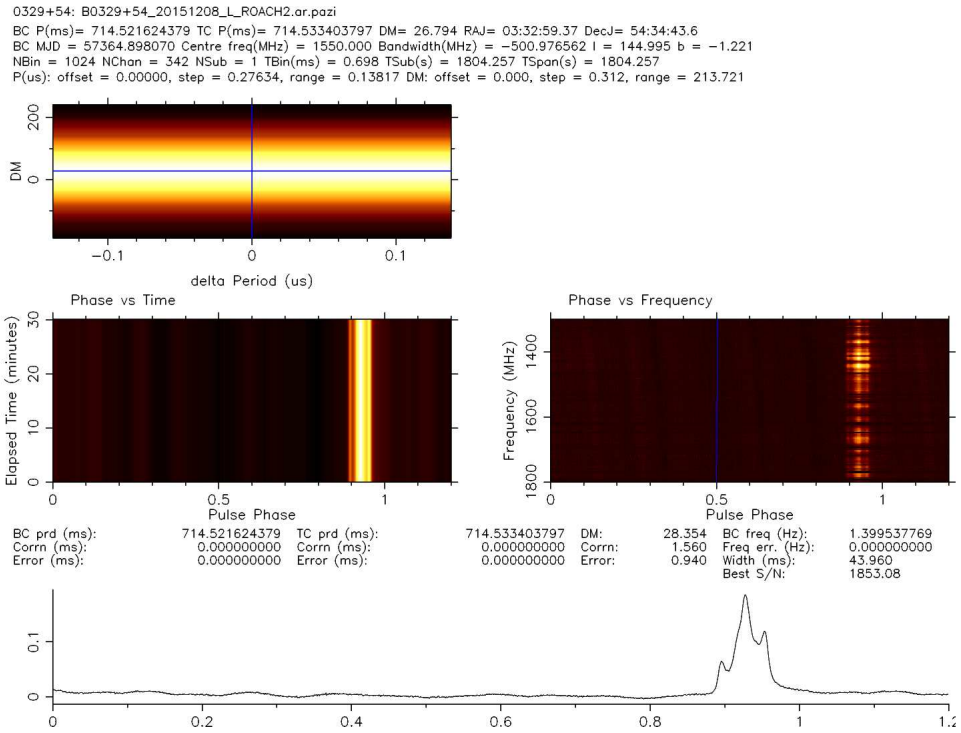

Figure 6.8: *Pulsar B0329+54 observed in L-band with the SRT in conjunction with SARDARA. Credits: M. Pilia, A. Trois, on behalf of the team of the project Tender-7.*

In both cases, the dump-time was 1908 spectra/sec. Raw data were converted into a standard FITS format - suitable for pulsar analysis (psrfits) - by exploting an ad-hoc software. These observations show the capability to produce high-quality pulsar data with SARDARA; further upgrades are ongoing development to improve both temporal and frequency resolution.

6.2 Wideband high-resolution spectrometer

In this section, we present the results regarding the feasibility study for a wideband high-resolution spectrometer. The main goal was to figure out - by using a single SARDARA node - which is the maximum bandwidth that can be managed in a real-time processing and, simultaneously, how many FFT channels can be achieved by exploiting all the resources of the chain ROACH2-GPU node.

Firstly, we have evaluated which was the maximum bandwidth - provided by a ROACH2 board - that a SARDARA node can be able to manage in base-band mode, i.e. the maximum flood of data for which the node can operate without loss of packets. We have conducted several tests and, apparently, the system works correctly up to 200-MHz. However, the ongoing development PFB (described in chapter 3) would provide, in this case, two adjacent bands 100-MHz wide each, thus the real operational bandwidth would be 100-MHz wide. In fact, the implemented overlapping reduces the good bandwidth to 50 MHz for each incoming

stream, for a total of 100 MHz precisely. A single ROACH2 board is able to sent out 8 stream 10 Gbe, while SARDARA is equipped with 8 nodes; therefore, theoretically, a spectrometer with a uniform bandwidth 800-MHz wide can be made.

Secondly, we needed to figure out the number of FFT channels that each node is capable to provides - regardless the real-time at the beginning - both with a pure FFT or with a polyphase filter bank configuration.

The polyphase filter bank, as already mentioned, provides an improved channel-to-channel isolation[53]; if we use more phases, we get a better isolation. We have done several tests - shown in tab 6.1 - with pure FFT (no PFB), PFB with two phases, PFB with four phases and, finally, PFB with eight phases. We have exploited only a single GPU, thus, theoretically, we can consider the following numbers as half of the ones actually achievable.

Table 6.1: *FFT channels with a SARDARA node (only one GPU was used)*

————	PFB 8	PFB 4	PFB 2	No PFB
Channels	262,144	1,048,576	2,097,152	16,777,216

The following step was to figure out whether the overall system could operate in a real-time mode; we set the ROACH2 so as to get the aforementioned bandwidth 200-MHz wide. Firstly, we wrote data on the node, afterwards we post-processed them: this is needed to figure out the time required for the processing itself. We have done an acquisition long 50 seconds; the tab 6.2 shows the corresponding processing time:

Table 6.2: *Time required to process 50 seconds of base-band data (bandwidth: 200-MHz wide).*

————	PFB 8	PFB 4	PFB 2	No PFB
Channels	262,144	1,048,576	2,097,152	16,777,216
Time (seconds)	20	17	18	16

The achieved numbers speak for themselves: a single GTX 980 Ti GPU is capable to perform an FFT processing more quickly whether compared to the time necessary to get the base-band data. Finally, we have made some real-time tests and, essentially, the achieved results have not changed significantly.

In the case of spectroscopic science - the only one that needs such a large number of spectral channels - the spectral isolation is absolutely crucial. Often, astronomers must investigate celestial regions that have very narrow-band emissions; thus, the percentage of energy that can falls into the adjacent channels must be reduced as much as possible. However, a polyphase filter bank with 4 phases, if well designed, can guarantee a channel-to-channel isolation up to 90 dB; this value is absolutely sufficient for all applications.

Hence, all things considered, we can exploit the SARDARA infrastructure to build a very efficient spectrometer, with a uniform bandwidth up 800-MHz wide, in conjunction with up 8 million of spectral channels, i.e. with a spectral resolution less than 100 Hz.

6.3 SETI

The results that we achieved for the parallel implementation of the KLT and the FFT is partially related to those of the previous chapter with regards to the FFT solution. In fact, we have seen that up to 16 million of channels - although without PFB implementation - can be obtained for 200 MHz of bandwidth, therefore there is no reason to check its feasibility from a technical point of view. Clearly, at this stage of the developing, the maximum achievable bandwidth cannot be greater than 16 MHz; this is why the frequency resolution needed for the SETI protocol is of the order of the Hz[54].

For the KLT, unfortunately, a real-time system still remain an ambition. The tests on field demonstrated that a real-time CPU implementation is absolutely unsuitable. In particular, we have calculated the eigenvalues by using data sets of 2048 point. The algorithm seems working properly but the required time is not suitable for a real-time uses even with very small bandwidth. The estimated time for one second of data was - in the case we use a bandwidth 16-MHz wide - approximately 15 minutes. This suggest us to investigate the GPU implementation as the only possible solution; unfortunately, there was not sufficient time to do that during this PhD.

Anyway, we have seen the proper working of the algorithm and, although not in real-time yet, an infrastructure with which we can perform SETI research - both with FFT and KLT - is going to be shortly operative at the Sardinia Radio Telescope.

Figure 6.9 shows an on-field test; the ROACH2 board provided a bandwidth of 50-MHz wide. We were pointing the sky with the SRT in conjunction with the C-band receiver and, in addition to the noise, we injected a tone at 335 MHz and amplitude 6 dBm. For graphical reasons, we made a calculation FFT with “only” 1 million channels.

Figure 6.10 and 6.11 show the eigenvalues - given in parallel by the KLT algorithm - for two subsequent set of 2048 samples from the aforementioned signal.

The dominant eigenvalue is absolutely evident; in the case of simple noise, it is absent. However, the analysis of the results given by the KLT engine go beyond this thesis and, more generally, it must be deeply analyzed by radio astronomical SETI experts.

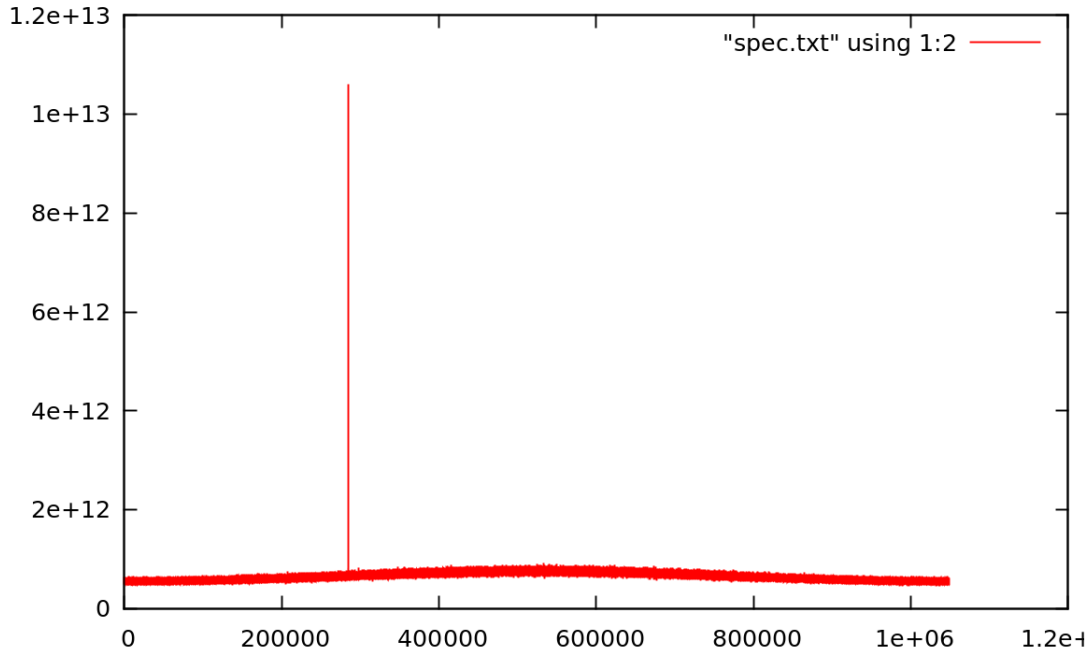

Figure 6.9: *FFT with 1 million channels of the following signal: bandwidth 50-MHz wide acquired in C-band and with injected a tone at 335 MHz-6dBm.*

Figure 6.10: *Eigenvalues provided by the KLT engine for 2048 samples in the case of a signal with bandwidth 50-MHz wide and an injected tone at 335 MHz-6dBm.*

Figure 6.11: *Eigenvalues provided by the KLT engine for the subsequent 2048 samples than the ones used for the plot shown in figure 6.10 .*

Chapter 7

Conclusions

The goal of this thesis was to develop a multi-purpose digital platform, suitable for single dish Italian radio telescopes, and in particular for the 64-m Sardinia Radio Telescope (SRT). This new platform had to be developed with a different strategy compared to that of previous approach (dedicated backends for each different observing mode).

The first step was to figure out what backends were employed at Italian radio telescopes, as well as pros and cons of each (chapter 2). In addition, we have studied one of them (the Digital Base Band Converter) in order to make an innovative RFI (Radio Frequency Interference) system (chapter 3); it is currently used at SRT as monitoring of the intermediate frequencies being observed. In particular, we used a two-stage polyphase filter bank (PFB) design as a possible precursor for new generation spectrometers.

Once we had a full picture of the overall state of the art, we understood that the ideal system for SRT had to be able to meet following requirements:

- Up to 14 IFs simultaneously
- Up to 2.1 GHz of bandwidth for each IF
- Full reconfigurability and adaptability for all scientific requirements

The SARDARA (SArdinia Roach2-based Digital Architecture for Radio Astronomy) was then born (chapter 4).

Features that make the concept behind SARDARA innovative are the following:

- An innovative technique for the integration of new digital backends into the control software of Italian radio telescopes
- Possibility to obtain a wideband spectrometer with very high-frequency resolution with a uniform passband
- Possibility to operate, in piggy-back mode, different algorithms for the search for signature life

Digital backends integration represents one of the most complicated tasks in the context of a radio telescope control software. As the final stage in the receiving chain, data produced

by every backend must include overall information concerning the antenna and the ongoing observation, moreover each backend has its own special features that we must bear in mind. The approach conceived for SARDARA follows an opposite trend. In particular, it distinguishes neatly the antenna parameters and the software controlling the telescope, as if they were two entity acting on their own. In particular, the proposed solution makes it possible to develop a new instrumentation exploiting the piggy-back mode, not only permitting that the telescope be equipped with the most modern technology, but also allowing us to do that in a trasparent and efficient way, by avoiding any waste of the most valuable resource: telescope time.

Results we have been achieved, both with SARDARA itself and by exploiting this new approach, are shown in chapter 6 for several scientific observations of well-known celestial sources. The observing modes investigated were: imaging, spectro-polarimetry, spectroscopy and, finally, pulsars. All of them given us very impressive never seen before results.

With regards to the second point, very often a compromise between wide bandwidth and high frequency resolution is a choice that must be made; this is mainly due to limitations in terms of digital signal processing resource available. When a high-resolution is needed, the so-called "narrow band" approach must, of necessity, be used. The adopted solution was to implement a two-stage polyphase filter bank (PFB): the first parallel PFB is responsible for splitting up a wide bandwidth into a certain number of sub-bands, while a set of second serial PFBs by process them. If we use a 50% overlapping in the first PFB, as well as a digital filter with a proper shape, and contemporaneously we adopt a proper FFT engine for the second PFB, an automatic selection of the useful bandwidth can be done: therefore, we are able to avoid spectral holes between sub-bands and, thereafter, stitch together all of them. We have seen that, with the SARDARA infrastructure, we can build a spectrometer with a uniform bandwidth 800-MHz wide with up 8 million of spectral channels, corresponding to a spectral resolution of less than 100 Hz.

Finally, with regards to the SETI project (chapter 5), we have investigated the KLT together with the traditional FFT approach. Since SETI research is often conducted in piggy-back mode only, a dedicated conditioning module was employed at the level of the intermediate frequencies. In particular, it acts as a frequency compensation mechanism that is necessary for keeping the chosen bandwidth stable even when a Doppler tracking system is activated, or in case the chosen bandwidth changes completely during the observation.

The KLT algorithm is really heavy from a computational point of view, therefore the entire acquired bandwidth with SARDARA (up to 2.1 GHz) must be reduced in order to store only a portion of it in base-band mode. The results that we achieved for the parallel implementation of the KLT and the FFT are very different. A real-time implementation of the FFT, with a bandwidth 16-MHz wide and 16 million of channels, worked. On the contrary, for the KLT, a real time system requires a lot of work again. At the moment, the base-band data must be written on disk and post-processed.

Anyway, an innovative infrastructure with which we can perform SETI research - both with FFT and KLT -is going to be shortly operative at the Sardinia Radio Telescope and, in a near future, at the other Italian radio telescopes.

Bibliography

[1] http://www.evlbi.org/ [cited at p. 8]

[2] D. Perrodin, R. Concu, A. Melis et al.: LEAP project at SRT: hardware and software implementation, OAC Internal Report n.39, 2014. [cited at p. 8]

[3] http://www.med.ira.inaf.it/ [cited at p. 8]

[4] http://www.noto.ira.inaf.it/ [cited at p. 9]

[5] http://www.srt.inaf.it/ [cited at p. 10]

[6] I. Prandoni, M. Murgia, A. Tarchi, and the AV team: The Sardinia Radio Telescope: From a Technological Project to a Radio Observatory. Astronomy & Astrophysics, in prep. [cited at p. 10]

[7] P. Bolli, A. Orlati, L. Stringhetti, A. Orfei, S. Righini, R. Ambrosini, M. Bartolini, C. Bortolotti, F. Buffa, M. Buttu, A. Cattani, N. D'Amico, G. Deiana, A. Fara, F. Fiocchi, F. Gaudiomonte, A. Maccaferri, S. Mariotti, P. Marongiu, A. Melis, C. Migoni, M. Morsiani, M. Nanni, F. Nasyr, A. Pellizzoni, T. Pisanu, M. Poloni, S. Poppi, I. Porceddu, I. Prandoni, J. Roda, M. Roma, A. Scalambra, G. Serra, A. Trois, G. Valente, G. P. Vargiu and G. Zacchiroli: Sardinia Radio Telescope: General Description, Technical Commissioning and First Light. Journal of Astronomical Instrumentation, Vol. 4, Nos. 3 & 4 (2015) 1550008 (20 pages) [cited at p. 10]

[8] Carlo Migoni, Andrea Melis, Antonella Fara et al.: VLBI observations with the Sardinia Radio Telescope: Hardware & Software implementation. OAC Internal Report n.42, 2014. [cited at p. 11]

[9] G. Valente; T. Pisanu; P. Bolli; S. Mariotti; P. Marongiu; A. Navarrini; R. Nesti; A. Orfei; J. Roda: The dual-band LP feed system for the Sardinia Radio Telescope prime focus , published in SPIE Proceedings Vol. 7741, Millimeter, Submillimeter, and Far-Infrared Detectors and Instrumentation for Astronomy V. [cited at p. 11]

[10] A. Orfei, L. Carbonaro ; A. Cattani ; A. Cremonini ; L. Cresci ; F. Fiocchi ; A. Maccaferri ; G. Maccaferri ; S. Mariotti ; J. Monari ; M. Morsiani ; V. Natale ; R. Nesti ; D. Panella ; M. Poloni ; J. Roda ; A. Scalambra ; G. Tofani: A Multi-Feed Receiver in the 18 to 26.5 GHz Band for Radio Astronomy. IEEE Antennas and Propagation Magazine (Volume:52 , Issue: 4) [cited at p. 11]

[11] http://www.med.ira.inaf.it/ManualeMedicina/English/8.1 [cited at p. 15]

[12] http://www.med.ira.inaf.it/ManualeMedicina/English/8.1 [cited at p. 15]

[13] G. Comoretto, A. D'Ambrosi, R. Nesti, A. Russo, F. Palagi: A modular multichannel spectrometer - design study, Arcetri Technical Report 4/2006 [cited at p. 15]

[14] A. Melis, C. Migoni, R. Concu, G. Comoretto, P. Castangia, P. Marongiu, A. Poddighe, A. Tarchi, G. Valente: Installation, cabling and testing of the XARCOS spectropolarimeter on the Sardinia Radio Telescope. OAC Internal Report n. 29, 2013. [cited at p. 16]

[15] Andrea Melis, Carlo Migoni, Gianni Comoretto, Paola Castangia, Silvia Casu, Andrea Tarchi, Andrea Orlati, Sergio Poppi & SRT Astrophysical Validation Team: Integration of the digital full-Stokes spectrometer XARCOS into the control software of Sardinia & Medicina radio-telescopes, OAC Internal Report n.52, 2015 [cited at p. 17]

[16] Gino Tuccari, Giovanni Comoretto, Andrea Melis, Salvo Buttaccio: The DBBC environment for millimeter radioastronomy, Proceeding of SPIE 2012 - Millimeter, Submillimeter and Far-Infrared Detectors and Instrumentation for Astronomy VI, Amsterdam, Netherlands. [cited at p. 17]

[17] Grant Hampson and Andrew Brown: A 1GHz Pulsar Digital Filter Bank and RFI Mitigation System, Australia Telescope National Facilty - CSIRO [cited at p. 19]

[18] Alessandro Corongiu: Design of a tool for managing pulsar observations with the Sardinia Radio Telescope, OAC Internal Report n. 35, 2014. [cited at p. 20]

[19] https://casper.berkeley.edu/wiki/ROACH [cited at p. 20]

[20] C.G. Bassa, G.H. Janssen, R. Karuppusamy, M. Kramer, K.J. Lee, K. Liu, J. McKee, D. Perrodin, M. Purver, S. Sanidas, R. Smits, B. W. Stappers : LEAP: the large European array for pulsars, Instrumentation and Methods for Astrophysics (astro-ph.IM), 2015. [cited at p. 21]

[21] Harris, Fredric J. Multirate signal processing for communication systems. Upper Saddle River, NJ: Prentice Hall PTR. ISBN 0-13-146511-2 (2004) [cited at p. 25]

[22] G. Comoretto, A. Russo, G. Tuccari: A 16 channel FFT multiplexer, Arcetri Technical Report 1-2009 [cited at p. 27]

[23] Giovanni Comoretto, Andrea Melis, Gino Tuccari: A wideband multirate FFT spectrometer with highly uniform response, Experimental Astronomy, 2011, Volume 31, Number 1, Pages 59-68. [cited at p. 28]

[24] A. Melis, R. Concu, A. Trois, C. Migoni, R. Ricci, M. Bartolini: An RFI monitoring system based on a wide-band digital back-end for the Sardinia Radio Telescope, OAC Internal Report n.36, 2014 [cited at p. 31]

[25] Andrea Melis, Francesco Gaudiomonte, Massimo Barbaro, Raimondo Concu, Carlo Migoni, Alessio Trois, Giuseppe Valente :An RFI monitoring system based on a hybrid configuration for radioastronomy. Proceeding of SPIE 2014 - Millimeter, Submillimeter and Far - Infrared Detectors and Instrumentation for Astronomy VI, Montreal, Canada [cited at p. 35]

[26] https://casper.berkeley.edu/wiki/ROACH2 [cited at p. 39]

[27] https://casper.berkeley.edu/ [cited at p. 39]

[28] https://casper.berkeley.edu/wiki/ADC1x5000-8 [cited at p. 39]

[29] https://casper.berkeley.edu/wiki/SFP%2B [cited at p. 39]

[30] G. Chiozzi, B. Jeram, H. Sommer, A. Caproni, M. Plesko, M. Sekoranja, K. Zagar, DW Fugate, P. Di Marcantonio, R. Cirami: The ALMA common software: a developer-friendly CORBA-based framework, Proceedings of SPIE - The International Society for Optical Engineering - September 2004 [cited at p. 43]

[31] Alwyn Wootten, A. Richard Thompson, : The Atacama Large Millimeter/submillimeter Array, Instrumentation and Methods for Astrophysics (astro-ph.IM), Proceedings of the IEEE Volume 97, Issue 8, Aug. 2009 Page(s):1463 - 1471 [cited at p. 43]

[32] A. Orlati, M. Buttu, A. Melis, C. Migoni, S. Poppi, S. Righini: The control software for the Sardinia Radio Telescope, Software and Cyberinfrastructure for Astronomy II. Proceedings of the SPIE, Volume 8451, article id. 84512M, 12 pp. (2012) [cited at p. 43]

[33] http://www.oan.es/rt40m/index [cited at p. 43]

[34] R. Cirami, P. Di Marcantonio, G. Chiozzi, B. Jeram: Bulk data transfer distributer: a high performance multicast model in ALMA ACS, Proc. SPIE 6274, Advanced Software and Control for Astronomy, 62741E (27 June 2006) [cited at p. 44]

[35] J. Mock: "JFFT: A tool for generating synthesizeable verilog for streaming FFTs and polyphase filter banks", http://www.naic.edu/ phil/hardware/pdev/fpga/gx/jfft/src/fftt.c [cited at p. 49]

[36] C. Maccone: The KLT (Karhunen-Loeve Transform) to extend SETI searches to broad-band and extremely feeble signals. Acta Astronautica 67 (2010) 1427â1439 [cited at p. 54]

[37] F. Schilliro', S. Pluchino, S. Montebugnoli: La KL Transform: considerazioni generali sulle metodologie di analisi ed impiego nel campo della Radioastronomia, IRA Internal Report 416-08 [cited at p. 56]

[38] C. Maccone: Mathematical SETI, a 724-pages book published by Praxis-Springer in the fall of 2012. ISBN, ISBN-10:3642274366| ISBN-13:978-3642274367 [cited at p. 56]

[39] P. Pari: Rilevazione di segnali tramite trasformata KLT nel progetto SETI, Thesis at Universita' degli Studi di Bologna, Facolta' di Matematica, Fisica e Scienze Naturali, 2003. [cited at p. 59]

[40] http://valontechnology.com/5009 [cited at p. 60]

[41] C. Maccone: A simple introduction to the KLT and BAM-KLT, chapter 17 of Mathematical SETI, a 724-pages book published by Praxis-Springer in the fall of 2012. ISBN, ISBN-10:3642274366| ISBN-13:978-3642274367 [cited at p. 62]

[42] C. Maccone: KLT of radio signals from relativistic spaceships in uniform and decelerated motion, chapter 11 of Mathematical SETI, a 724-pages book published by Praxis-Springer in the fall of 2012. ISBN, ISBN-10:3642274366| ISBN-13:978-3642274367 [cited at p. 63]

[43] Snell R.L., Hollenbach D., Howe J.E. et al. 2005, ApJ, 620, 758 [cited at p. 65]

[44] A. Pellizzoni, E. Egron, N. Iacolina et al., in prep. [cited at p. 66]

[45] E. Egron, A. Pellizzoni, N. Iacolina et al., Astronomical Validation Report 6 in prep. [cited at p. 66]

[46] E. Egron, A. Pellizzoni, N. Iacolina et al., Astronomical Validation Report 7 in prep. [cited at p. 66]

[47] M. Murgia, F. Govoni: Single-dish Spectral-polarimetry Software, in prep. [cited at p. 66]

[48] M. Murgia , F. Govoni , E. Carretti , A. Melis , R. Concu , A. Trois , A. Possenti , et al.: Sardinia Radio Telescope wide-band spectral-polarimetric observations of the 3C129 galaxy cluster. Astronomy & Astrophysics, in prep. [cited at p. 67]

[49] Bragg, A. E., Greenhil, L. J., Moran, J. M., et al., 2000, ApJ, 535, 73 [cited at p. 68]

[50] Braatz, J. A., Reid, M .J., Humphreys, E. M.L., et al., 2010, ApJ, 718, 657 [cited at p. 69]

[51] Spencer A. Wolfe, D. J. Pisano, Felix J. Lockman, Stacy S. McGaugh, Edward J. Shaya : Discrete clouds of neutral gas between the galaxyes M31 and M33, Nature 497, 224-226 (09 May 2013) [cited at p. 69]

[52] Lorimer & Kramer: Handbook of pulsar astronomy, Cambridge University press, 2005 [cited at p. 70]

[53] Jayanth Chennamangalam: CASPER Memo 41, The Polyphase Filter Bank Technique, 2014. [cited at p. 73]

[54] D. Werthimer, D. Ng, Stuart Bowyer, Chuck Donnely : The Berkeley SETI Program: SERENDIP III and IV Instrumentation, ASP Conference series, vol.74, 1995. [cited at p. 74]

List of Publications

Published papers

- P. Bolli, A. Orlati, L. Stringhetti, A. Orfei, S. Righini, R. Ambrosini, M. Bartolini, C. Bortolotti, F. Buffa, M. Buttu, A. Cattani, N. D'Amico, G. Deiana, A. Fara, F. Fiocchi, F. Gaudiomonte, A. Maccaferri, S. Mariotti, P. Marongiu, A. Melis, C. Migoni, M. Morsiani, M. Nanni, F. Nasyr, A. Pellizzoni, T. Pisanu, M. Poloni, S. Poppi, I. Porceddu, I. Prandoni, J. Roda, M. Roma, A. Scalambra, G. Serra, A. Trois, G. Valente, G. P. Vargiu and G. Zacchiroli: *Sardinia Radio Telescope: General Description, Technical Commissioning and First Light.* in *Journal of Astronomical Instrumentation, Vol. 4, Nos. 3 & 4 (2015) 1550008 (20 pages)*

Conference papers

- Gino Tuccari, Giovanni Comoretto, Andrea Melis, Salvo Buttaccio: *The DBBC environment for millimeter radioastronomy.* in *Proceeding of SPIE 2012 - Millimeter, Submillimeter and Far-Infrared Detectors and Instrumentation for Astronomy VI* , Amsterdam, Netherlands.

- A. Orlati, M. Buttu, A. Melis, C. Migoni, S. Poppi, S. Righini: *The control software for the Sardinia Radio Telescope.* in *Proceeding of SPIE 2012 - Software and Cyberinfrastructure for Astronomy II* , Amsterdam, Netherlands.

- M. Buttu, A. Orlati, G. Zacchiroli, M. Morsiani, F. Fiocchi, F. Buffa, G. Maccaferri, G.P. Vargiu, C. Migoni, S. Poppi, S. Righini and A. Melis: *Diving into the Sardinia Radio Telescope minor servo system.* in *Proceeding of SPIE 2012 - Millimeter, Submillimeter and Far-Infrared Detectors and Instrumentation for Astronomy VI* , Amsterdam, Netherlands.

- R. Ambrosini, A. Bocchinu, P. Bolli, F. Buffa, A. Cattani, N. D'Amico, G.L. Deiana, A. Fara, F. Fiocchi, F. Gaudiomonte, A. Maccaferri, S. Mariotti, P. Marongiu, A. Melis, G. Melis, C. Migoni, M. Morsiani, M. Nanni, F. Nasir, R. Nesti, A. Orfei, A. Orlati, F. Perini, C. Pernechele, S. Pilloni, T. Pisanu, M. Poloni, S. Poppi. I. Porceddu, S. Righini, J. Roda, A. Sacalambra, M.R. Schirru, G. Serra, L. Stringhetti, A. Trois, A. Tuveri, G. Valente, G. Vargiu, G. Zacchiroli: *The Sardinia Radio Telescope: overview and status.* in *International Conference on Electromagnetics in Advanced Applications* ,09 Settembre 2013, Torino, Italy.

- Andrea Melis, Giuseppe Valente, Andrea Tarchi, Massimo Barbaro, Raimondo Concu, Alessandro Corongiu, Francesco Gaudiomonte, Carlo Migoni, Giorgio Montisci, Sergio Poppi, Alessio Trois: *An infrastructure for multi back-end observations with the Sardinia Radio Telescope.* in *Proceeding of SPIE 2014 - Millimeter, Submillimeter and Far - Infrared Detectors and Instrumentation for Astronomy VI* , Montreal, Canada.

- Andrea Melis, Francesco Gaudiomonte, Massimo Barbaro, Raimondo Concu, Carlo Migoni, Alessio Trois, Giuseppe Valente: *An RFI monitoring system based on a hybrid configuration for radioastronomy.* in *Proceeding of SPIE 2014 - Millimeter, Submillimeter and Far - Infrared Detectors and Instrumentation for Astronomy VI* , Montreal, Canada.

- M. Murgia, G. Bianchi, P. Bolli, G. Comoretto, D. Dallacasa, M. Z. Farooqui, F. Gaudiomonte, L. Gregorini, F. Govoni, K.-H. Mack, M. Massardi, A. Mattana, A. Melis , J. Monari, L. Mureddu, G. Naldi, F. Paonessa, F. Perini, A. Poddighe, I. Porceddu, I. Prandoni, G. Pupillo, M. Schiaffino, F. Schilliro', G. Serra, A. Tibaldi, T. Venturi, G. Virone and A. Zanichelli: *Sardinia Aperture Array Demonstrator.* in *Proceeding of SPIE 2014 - Millimeter, Submillimeter and Far - Infrared Detectors and Instrumentation for Astronomy VI* , Montreal, Canada.

- G. Valente, G. Serra, F. Gaudiomonte, A. Ladu, T. Pisanu, P. Marongiu,A. Corongiu, A. Melis, M. Buttu, D. Perrodin, G. Montisci, G. Mazzarella, E. Egron, N. Iacolina, C. Tiburzi, V. Vacca: *A multifeed S-band cryogenic receiver for the Sardinia Radio Telescope primary focus.* in *Proceeding of SPIE 2012 - Millimeter, Submillimeter and Far-Infrared Detectors and Instrumentation for Astronomy VI*, Amsterdam, Netherlands.

- Isabella Prandoni, Andrea Melis, Carlo Migoni, Delphine Perrodin, Marta Burgay, Federica Govoni, Matteo Murgia, Alberto Pellizzoni, Simona Righini, Andrea Tarchi, Marco Bartolini, Pietro Bolli, Marco Buttu, Paola Castangia, Silvia Casu, Raimondo Concu, Alessandro Corongiu, Nichi D'Amico, Elise Egron, Antonietta Fara, Francesco Gaudiomonte, Daria Guidetti, Maria Noemi Iacolina, Fabrizio Massi, Francesco Nasyr, Alessandro Orfei, Andrea Orlati, Tonino Pisanu, Sergio Poppi, Ignazio Porceddu, Alessandro Ridolfi, Roberto Ricci, Carlo Stanghellini, Caterina Tiburzi, Alessio Trois, Valentina Vacca, Giuseppe Valente, Alessandra Zanichelli: *The SRT in the Context of European Networks: Astronomical Validation and Future Perspectives.* in *Proceeding of Science, 12th European VLBI Network Symposium and Users Meeting*, 7-10 October 2014, Cagliari, Italy

- P. Bolli, G. Comoretto, D. Dallacasa, M. Z. Farooqui, D. Fierro, F. Gaudiomonte, F. Govoni, A. Lingua, P. Marongiu, A. Mattana, A. Melis, J. Monari, M. Murgia, L. Mureddu, G. Naldi, F. Paonessa, F. Perini, T. Pisanu, A. Poddighe, I. Porceddu, I. Prandoni, G. Pupillo, S. Rusticelli, M. Schiaffino, F. Schilliro', G. Serra, G. Tartarini, A. Tibaldi, T. Venturi, G. Virone, A. Zanichelli: *Sardinia Array Demonstrator: Instrument Overview and Status.* in *International Conference on Electromagnetics in Advanced Applications*, 2015

- P. Bolli, M. Z. Farooqui, F. Paonessa, A. Tibaldi, G. Virone, F. Gaudiomonte, G. Serra, M. Schiaffino, G. Addamo, D. Dallacasa, D. Fierro, F. Govoni, A. Lingua, P. Marongiu, A. Mattana, A. Melis, J. Monari, M. Murgia, L. Mureddu, G. Naldi, F. Perini, O. A. Peverini, T. Pisanu, A. Poddighe, I. Porceddu, I. Prandoni, G. Pupillo, S. Rusticelli, F. Schilliro',

G. Tartarini, T. Venturi, A. Zanichelli: *Sardinia Aperture Array Demonstrator: electromagnetic analysis and measurements.* in *ESA Antenna Workshop on Antennas and RF Systems for Space Science, Noordwikj*, The Netherlands, October 2015.

- M. Pilia, A. Trois, , A. P. Pellizzoni, M. Bachetti, , G. Piano, A. Poddighe, E. Egron, M. N. Iacolina, A. Melis, R. Concu, A. Possenti, and D. Perrodin: *Data Reduction of Multi-wavelength Observations.* in *25th Annual Astronomical Data Analysis Software and Systems (ADASS) conference*, Rydges Worls Square in Sydney, Australia. October 2015.

Not yet Submitted papers

- M. Murgia , F. Govoni , E. Carretti , A. Melis , R. Concu , A. Trois , A. Possenti , et al.: *Sardinia Radio Telescope wide-band spectral-polarimetric observations of the 3C129 galaxy cluster.* in *Astronomy & Astrophysics*
- I. Prandoni, M. Murgia, A. Tarchi, and the AV team: *The Sardinia Radio Telescope: From a Technological Project to a Radio Observatory.* in *Astronomy & Astrophysics*
- A. Melis, R. Concu, P. Pari, C. Maccone, G. Valente, M. Barbaro et al.: *A real-time KLT implementation for radio-SETI applications.* in *Proceeding of SPIE 2016 - Millimeter, Submillimeter and Far - Infrared Detectors and Instrumentation for Astronomy VI*